Photoelectron Spectroscopy
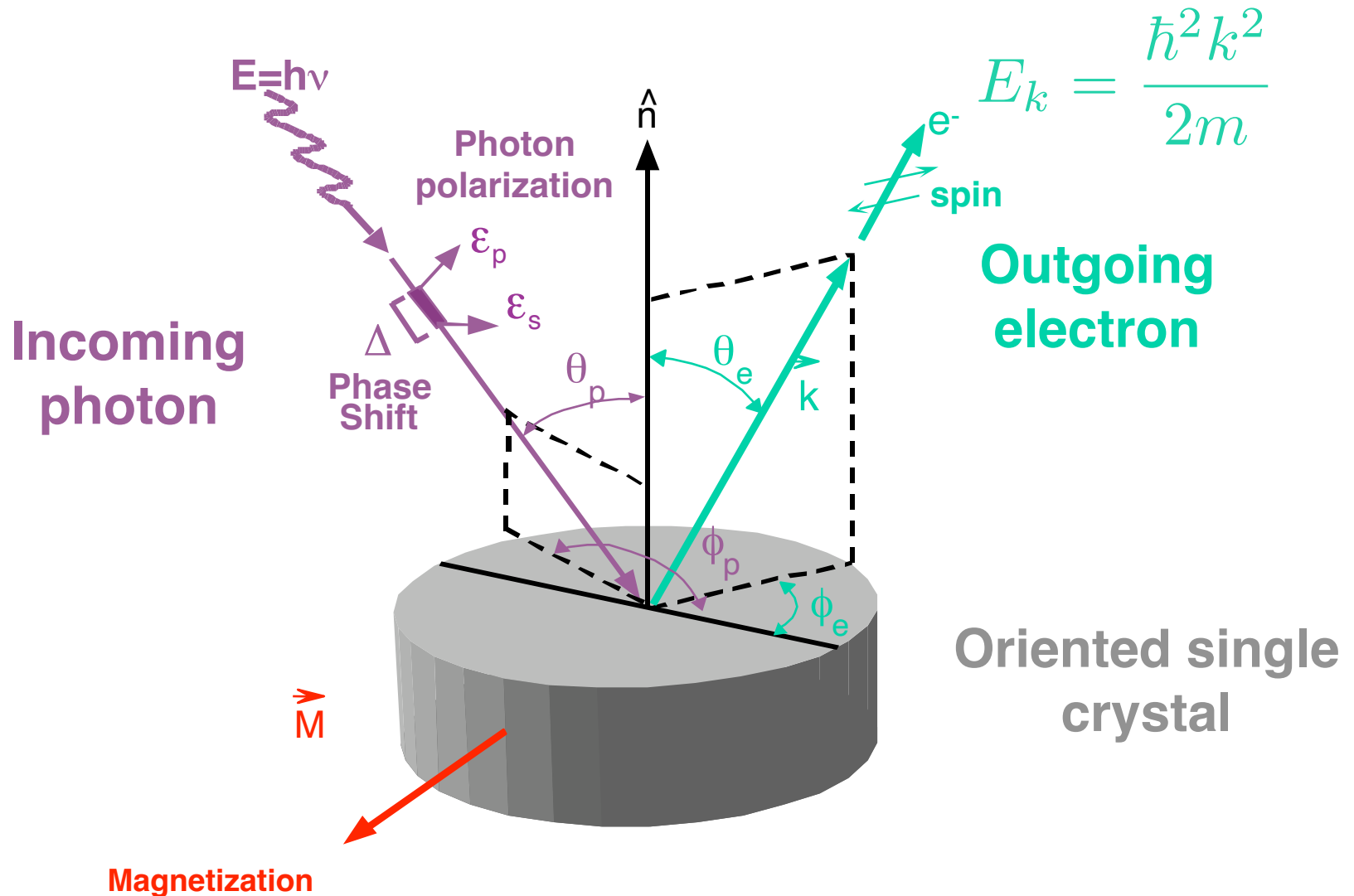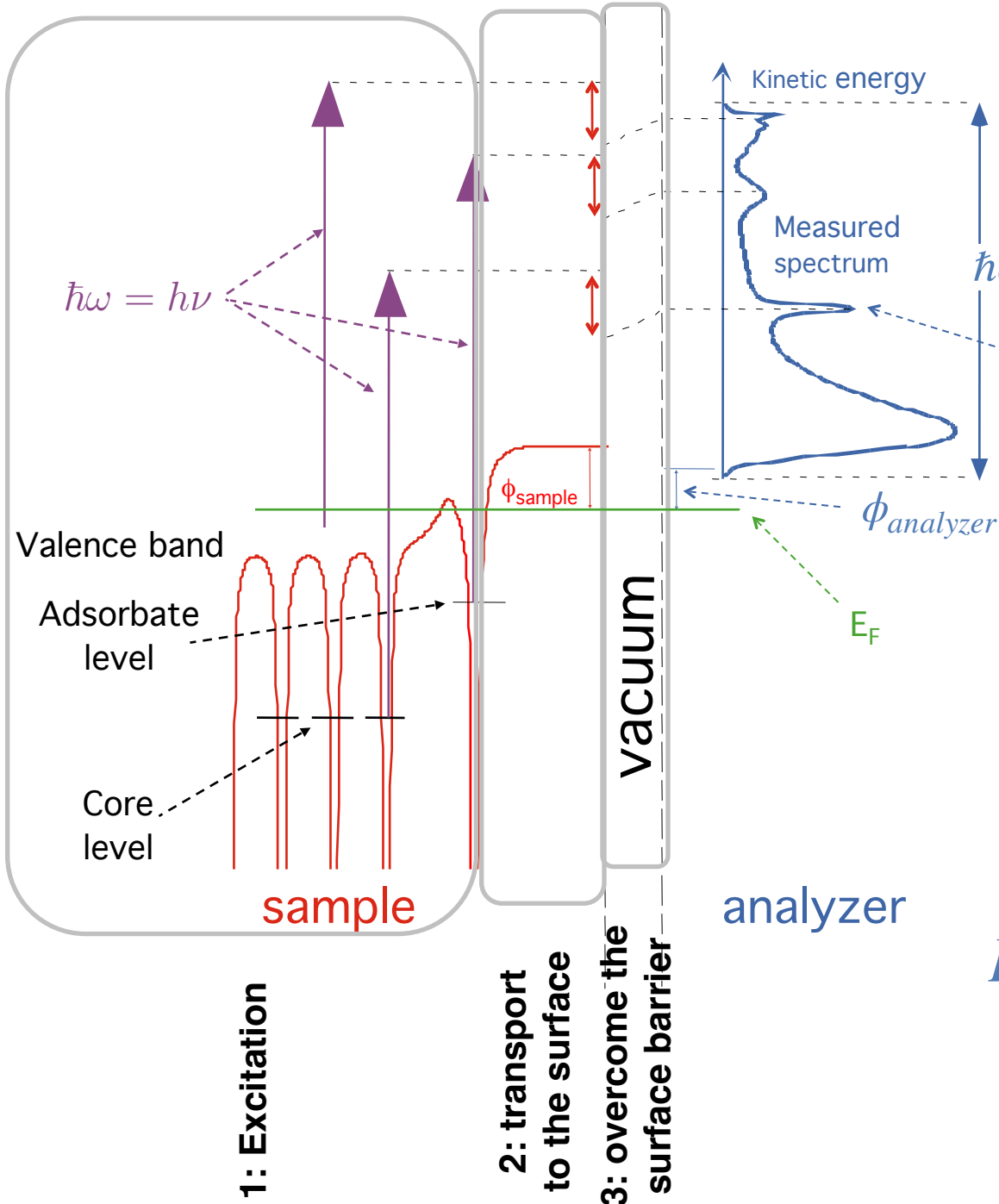
G. Paolucci
Elettra - Sincrotrone Trieste

The photoemission experiment

The "three step model"

$\hbar\omega = h\nu$

Kinetic energy

Measured spectrum

$\hbar\omega - \phi_{sample}$

$\hbar\omega - E_b - \phi_{analyzer}$

ϕ_{sample}

$\phi_{analyzer}$

Valence band

Adsorbate level

Core level

E_F

sample

vacuum

analyzer

1: Excitation

2: transport to the surface

3: overcome the surface barrier

The electron must overcome the sample work function ϕ_{sample} in order to reach the vacuum; afterwards its energy is changed by the difference in work function between the analyzer and the sample. So:

$$E_k^{meas} = \hbar\omega - E_b - \phi_{analyzer}$$

Schematial representation of the three step model. The numbers denote:
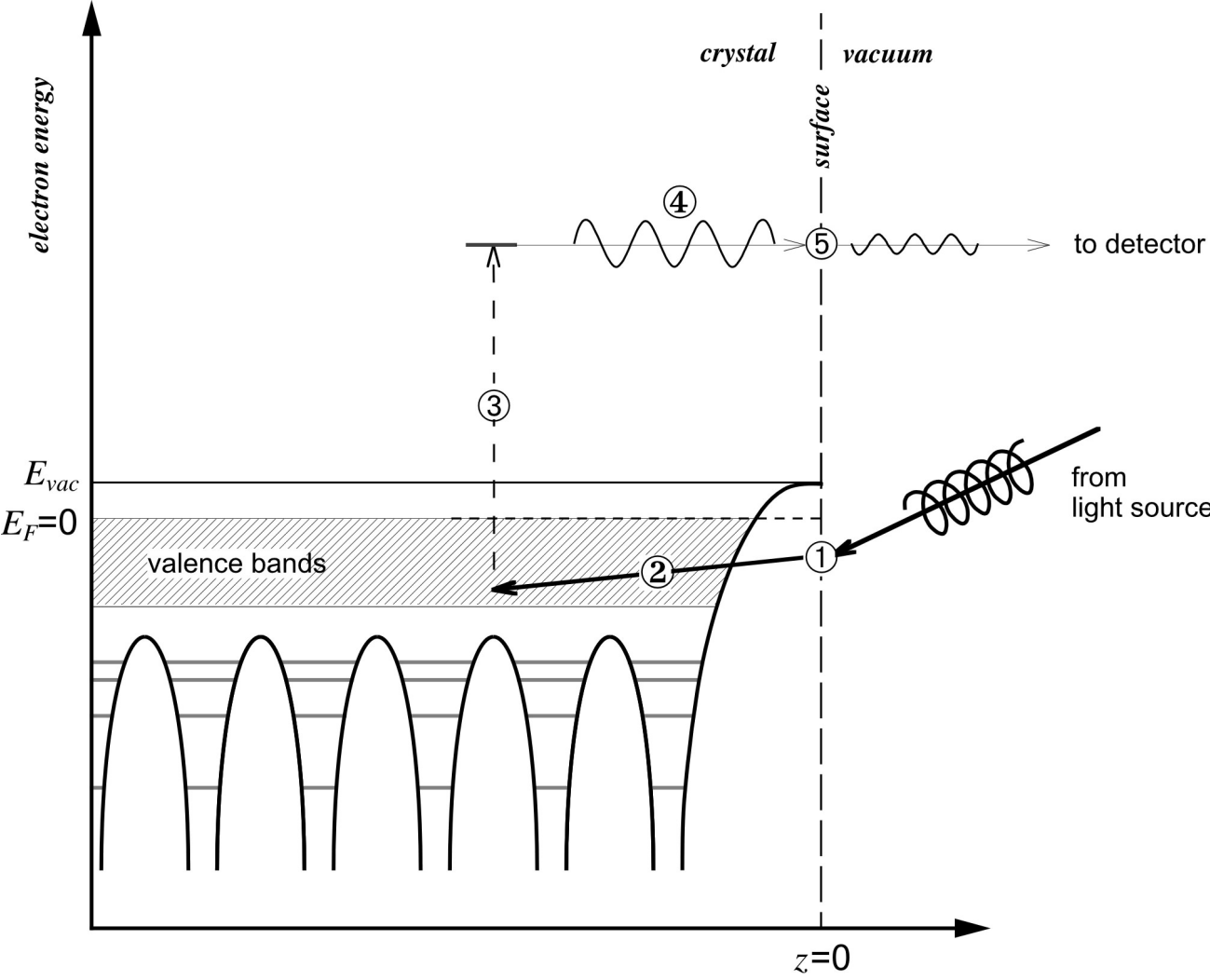1) refraction of the electromagnetic wave at the surface
2) penetration of the photon into the solid
3) photoexcitation
4) propagation of the photoelectron to the surface,
5) diffraction of the electron wave at the surface.

The total photoemission intensity from species i is obtained by integrating:

$dN_i \propto$ (no. of atoms of species i at xyz)

$\times$(photon flux at x,y,z)

incoming flux & absorption coefficient

$\times$(differential cross-section of relevant level of species i)

$\times$(probability of no loss escape of electrons from x,y,z)

electron mean free path

$\times$(acceptance solid angle of electron analyzer)

$\times$(detection efficiency)

relevant for the choice of photon energy!

species i at xyz
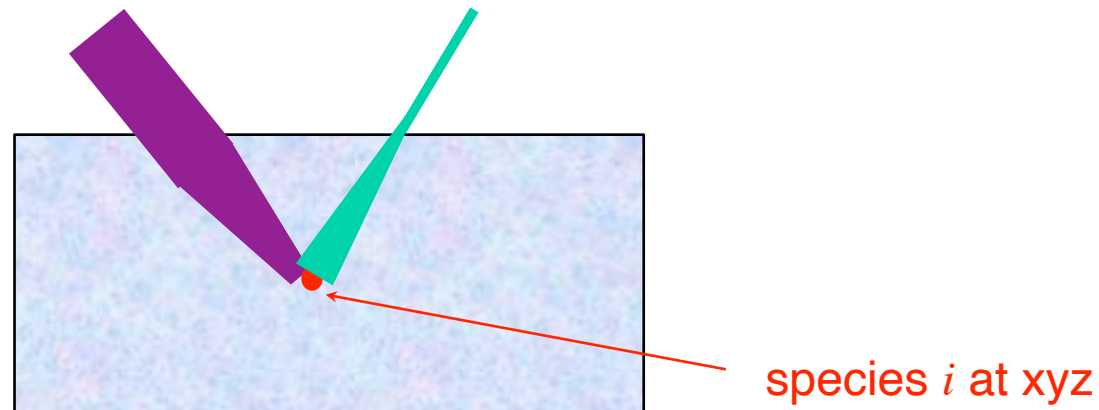
# The incoming photons

> UV to soft x-rays (hν ~10 to ~1500 eV
> or λ ~ 1240 to ~ 5 Å)

- Laboratory sources (relatively cheap) use characteristic transition lines:

    – noble gas discharge (e.g. HeI$_\alpha$=21.22 eV)

    – LASER sources (few tens eV)

    – solid target emission lines (Al K$_\alpha$=1428 eV; Mg K$_\alpha$=1253 eV

- Synchrotron radiation (expensive!) gives tunable, polarized and bright radiation

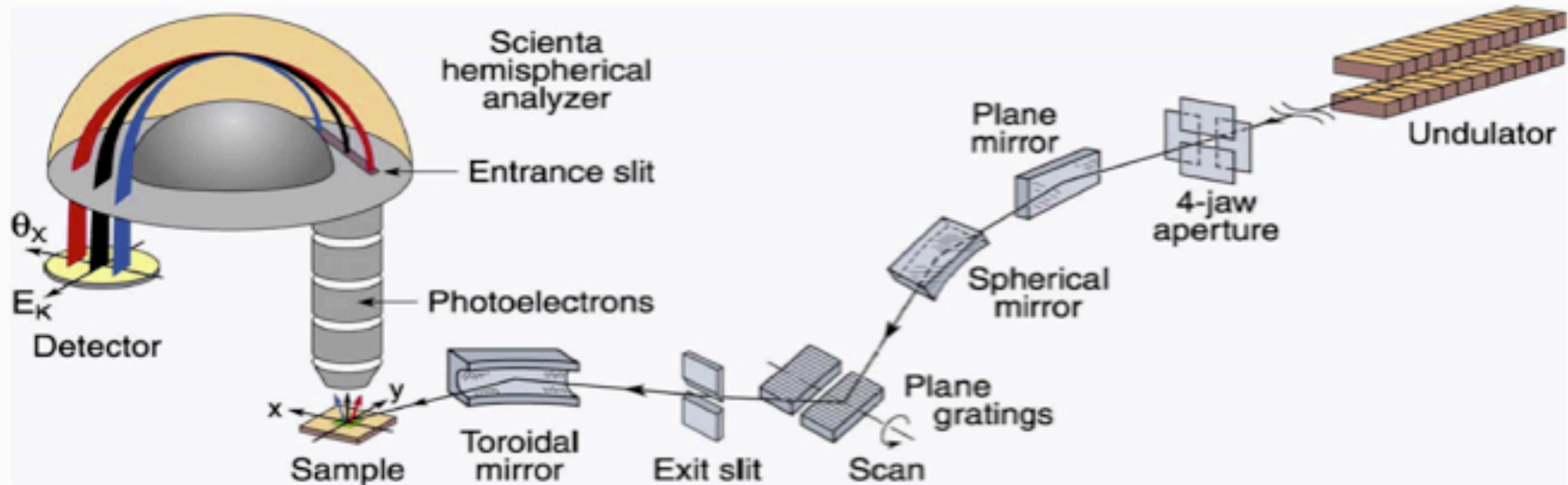# The spherical electron energy analyser
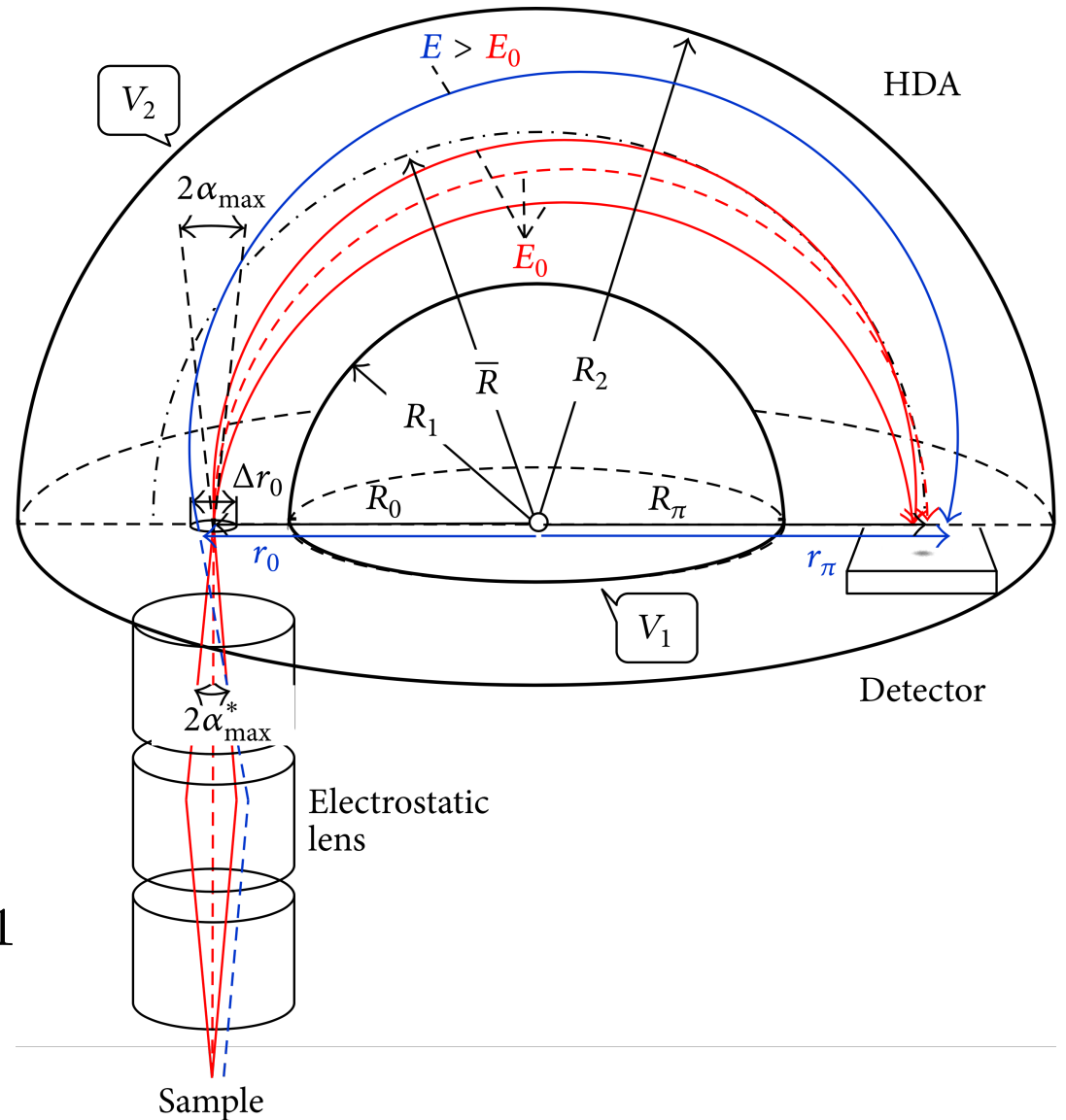
The pass energy E_0 is the energy at which electrons follow a circular trajectory

$$E_0 = \frac{2\Delta V}{R_0}\left(\frac{1}{R_1} - \frac{1}{R_2}\right)^{-1}$$
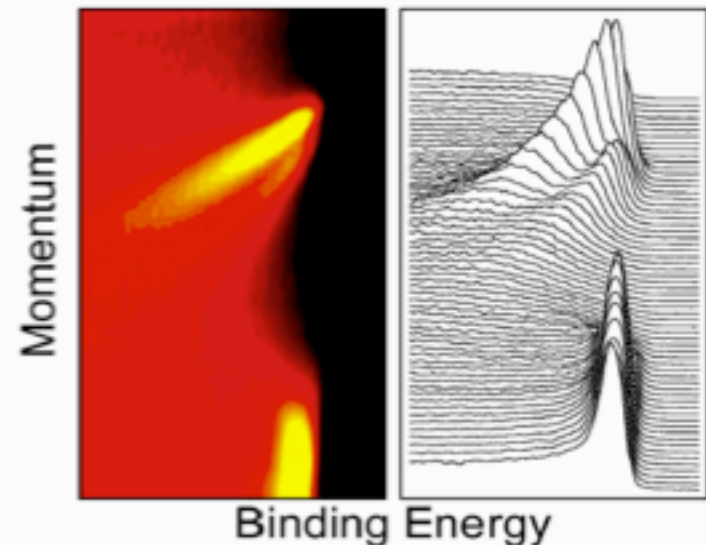
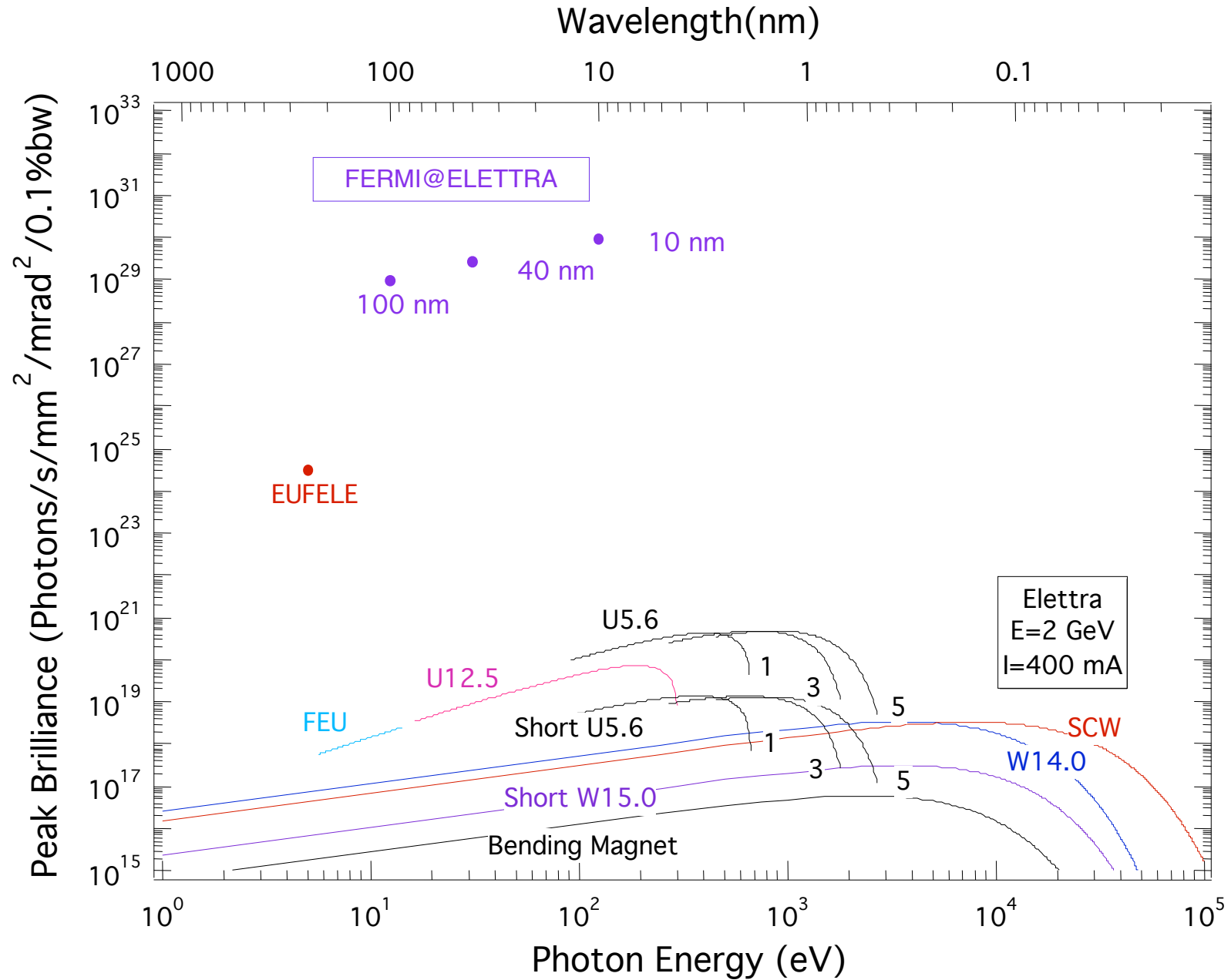# Position sensitive detection

State-of-the-art

courtesy of A. Damascelli

Photon sources at Elettra

The "three step model"
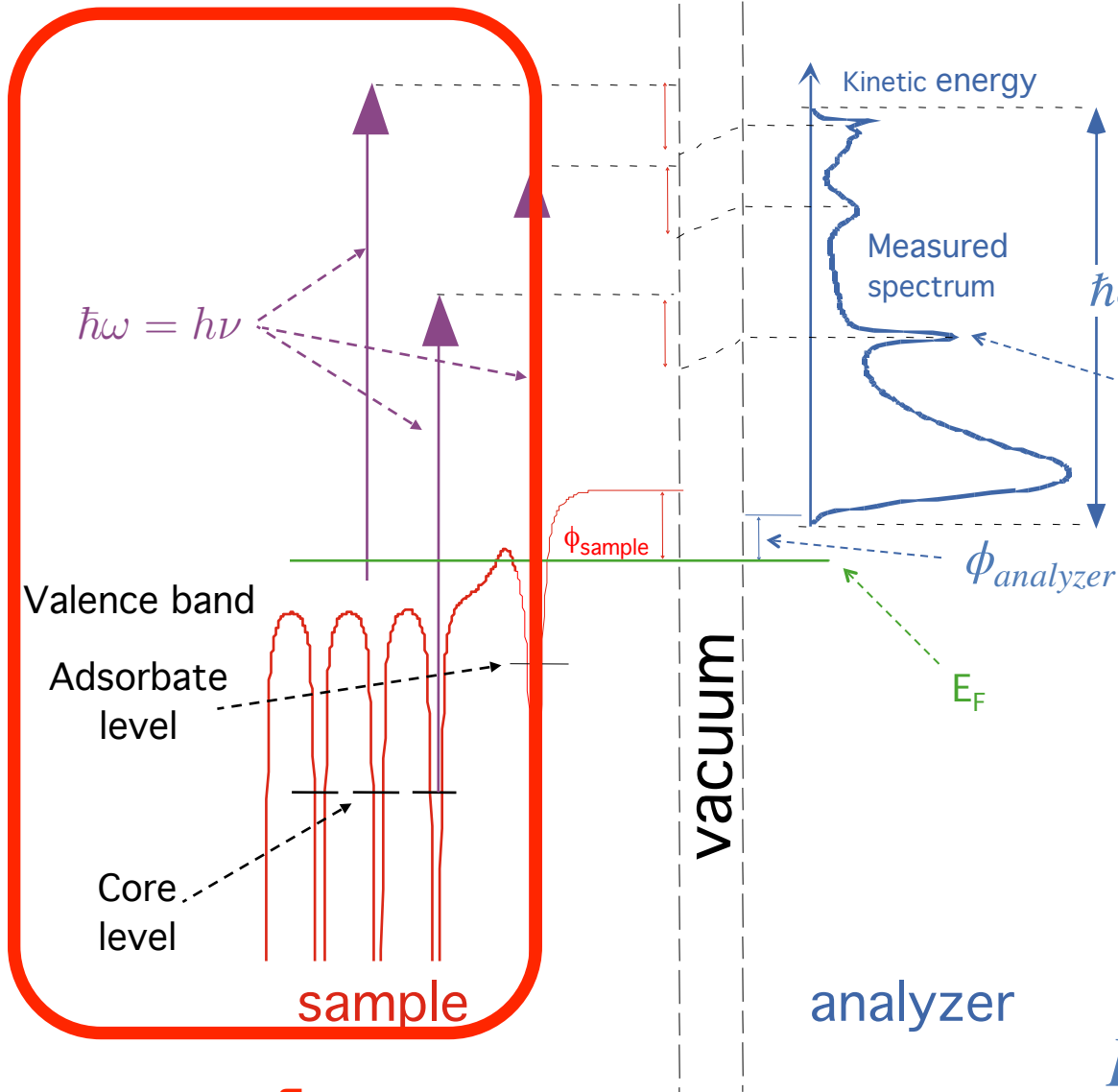
Kinetic energy

Measured spectrum

$\hbar\omega - \phi_{sample}$

$\hbar\omega - E_b - \phi_{analyzer}$

$\hbar\omega = h\nu$

ϕ_{sample}

$\phi_{analyzer}$

E_F

Valence band

Adsorbate level

Core level

sample

analyzer

vacuum

1: Excitation

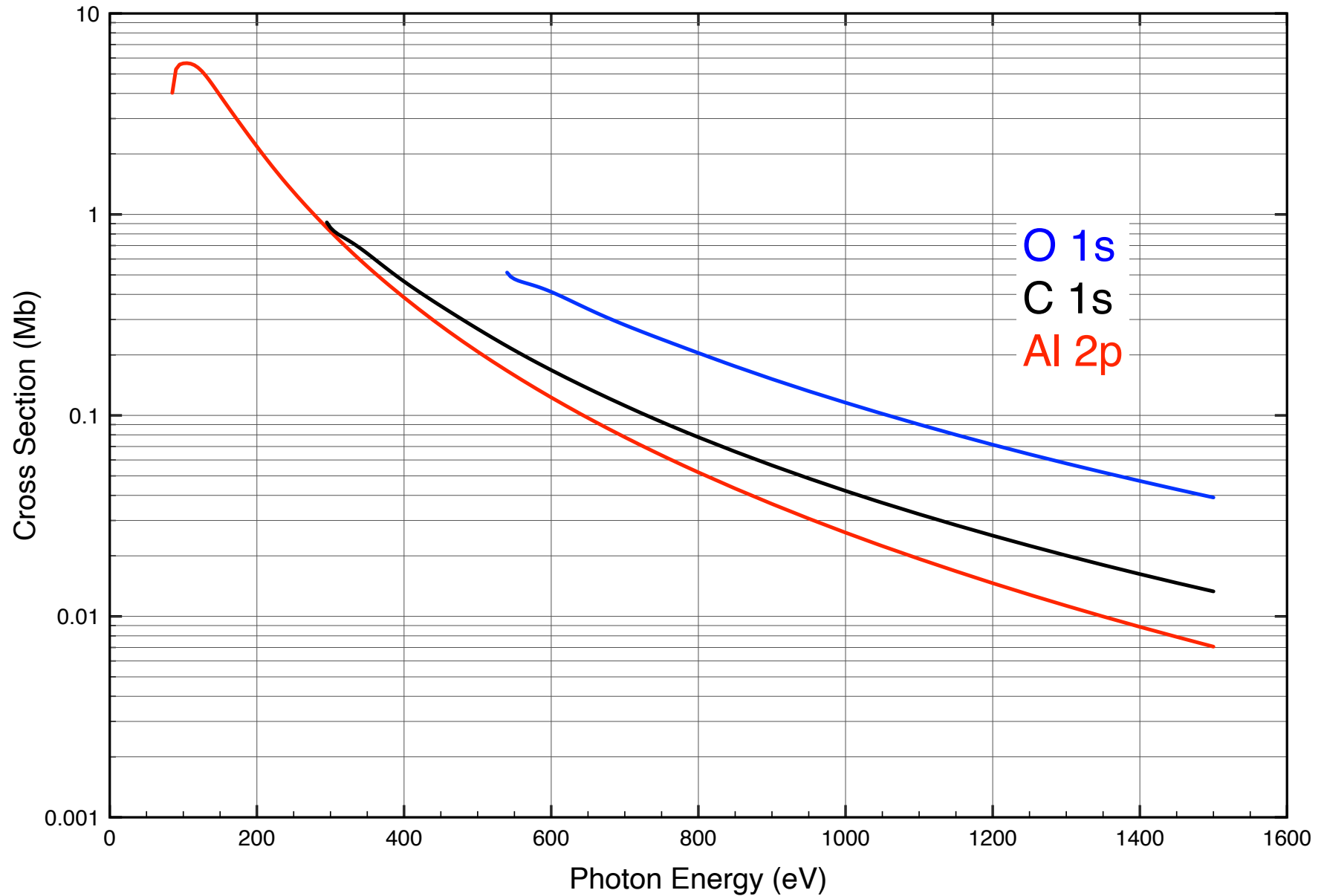The electron must overcome the sample work function ϕ_{sample} in order to reach the vacuum; afterwards its energy is changed by the difference in work function between the analyzer and the sample. So:

$$E_k^{meas} = \hbar\omega - E_b - \phi_{analyzer}$$

Photoemission atomic cross section

Step 1: photoexcitation

The single particle Hamiltonian of an electron in an external electromagnetic field is:

$$H = \frac{1}{2m}\left(\vec{p} + e\frac{\vec{A}\,(\vec{r},t)}{c}\right)^2 - e\phi\,(\vec{r},t) + V(\vec{r})$$

where the electric and magnetic fields are given by:

$$\vec{E} = -\vec{\nabla}\phi - \frac{1}{c}\frac{\partial \vec{A}}{\partial t}$$

$$\vec{B} = \vec{\nabla} \times \vec{A}$$

Step 1: photoexcitation

When no external charges or currents are present, is is customary to define vector and scalar potentials in the so called "transverse gauge":

$$\vec{\nabla} \cdot \vec{A} = 0$$
$$\phi = 0$$

which, inserted into Maxwell's equations give that the vector potential satisfies the equation:

$$\nabla^2 \vec{A} - \frac{1}{c^2} \frac{\partial^2 \vec{A}}{\partial t^2} = 0$$

Step 1: photoexcitation

By expanding the hamiltonian, we can write the Schrödinger equation:

$$\left[\frac{1}{2m} p^2 + \frac{e}{2mc} \left(\vec{p} \cdot \vec{A} + \vec{A} \cdot \vec{p} \right) + \boxed{\frac{e}{2mc^2} A^2} + V(\vec{r}) \right] \psi = E\psi$$

≈ 0

The square term in the vector potential can be neglected

Moreover because of the transverse gauge we have that

$$\left[\vec{p}, \vec{A} \right] = 0$$

So:
$$\left[\frac{1}{2m} p^2 + \frac{e}{2mc} \left(\vec{p} \cdot \vec{A} + \vec{A} \cdot \vec{p} \right) + \frac{e}{2mc^2} + V(\vec{r}) \right] \psi = E\psi$$

$\Downarrow$

$$\left[\frac{1}{2m} p^2 + \frac{e}{mc} \vec{A} \cdot \vec{p} + V(\vec{r}) \right] \psi = E\psi$$

Step 1: photoexcitation

Which means that we can write the hamiltonian in the form

$$H = H_0 + H_1$$

in which H_1 is the perturbation due to the external electromagnetic field, given by:

$$H_1 = \frac{e}{mc}\overrightarrow{A}\cdot\vec{p} = -\frac{ie\hbar}{mc}\overrightarrow{A}\cdot\overrightarrow{\nabla}$$

Since the vector potential satisfies the wave equation, it can be expressed as a superposition of plane waves:

$$\overrightarrow{A} = \sum_{\omega}\overrightarrow{A}_{\omega}e^{-i(\vec{q}\cdot\vec{r}-\omega t)} + c.c.$$

Step 1: photoexcitation

From the expression for the vector potential

$$\vec{A} = \sum_{\omega} \vec{A}_{\omega} e^{-i(\vec{q}\cdot\vec{r} - \omega t)} + c.c.$$

and reminding that in our gauge

$$\vec{E} = -\frac{1}{c}\frac{\partial \vec{A}}{\partial t}$$

we get immediately

$$\vec{E} = \sum_{\omega} \frac{i\omega}{c} \vec{A}_{\omega} e^{-i(\vec{q}\cdot\vec{r} - \omega t)} + c.c.$$

Step 1: photoexcitation

The Fermi golden rule gives the transition probability per unit time from a the initial state i to the final state f as:

$$W_{f,i} = \frac{2\pi}{\hbar} \left| \left\langle f \left| H_1 \right| i \right\rangle \right|^2 \delta \left(E_f - E_i - \hbar\omega \right)$$

$$= 2\pi\hbar \left(\frac{e}{mc} \right)^2 \left| \vec{A}_\omega \cdot \left\langle f \left| e^{i\vec{q}\cdot\vec{r}} \vec{\nabla} \right| i \right\rangle \right|^2 \delta \left(E_f - E_i - \hbar\omega \right)$$

The oscillating term is in the second order approximation

$$e^{i\vec{q}\cdot\vec{r}} = 1 + i\vec{q}\cdot\vec{r} - \frac{(\vec{q}\cdot\vec{r})^2}{2} + O\left((\vec{q}\cdot\vec{r})^3 \right)$$

The modulus of the wave vector, |q| is given by $2\pi/\lambda$. For example at 100 eV its value is $|q|_{(\hbar\omega=100eV)} \approx 0.05 \text{Å}^{-1}$: the scalar product is negligible in the region where the wave functions are significantly $\neq 0$

Step 1: photoexcitation

We can therefore write the transition probability in the **dipole approximation** as:

$$W_{f,i} \simeq 2\pi\hbar \left(\frac{e}{mc}\right)^2 \left| \vec{A}_\omega \cdot \left\langle f \left| \vec{\nabla} \right| i \right\rangle \right|^2 \delta\left(E_f - E_i - \hbar\omega\right)$$

$$= \frac{2\pi}{\hbar} \left(\frac{e}{mc}\right)^2 \left| \vec{A}_\omega \cdot \left\langle f \left| \vec{p} \right| i \right\rangle \right|^2 \delta\left(E_f - E_i - \hbar\omega\right)$$

Step 1: photoexcitation

Since $|f\rangle$ and $|i\rangle$ are eigenstates of the unperturbed hamiltonian and:

$$\left[\vec{p}, H_0\right] = -i\hbar\,\overrightarrow{\nabla} V\left(\vec{r}\right)$$

$$\left[\vec{r}, H_0\right] = i\hbar\frac{\vec{p}}{m}$$

we can write

$$\overrightarrow{M}_{f,i} = \left\langle f\left|\vec{p}\right|i\right\rangle \qquad \longleftarrow \quad \text{dipole velocity}$$

$$= -\frac{1}{E_f - E_i}\left\langle f\left|\left[\vec{p}, H_0\right]\right|i\right\rangle$$

$$= \frac{i\hbar}{\omega_{f,i}}\left\langle f\left|\overrightarrow{\nabla} V\left(\vec{r}\right)\right|i\right\rangle \qquad \longleftarrow \quad \text{dipole acceleration}$$

$$= im\omega_{f,i}\left\langle f\left|\vec{r}\right|i\right\rangle \qquad \longleftarrow \quad \text{dipole length}$$

We define the photoionization cross section:

$$\sigma\left(\hbar\omega\right) = \frac{P\left(\hbar\omega\right)}{I\left(\hbar\omega\right)}$$

where *P(ℏω)* is the number of photons absorbed by one atom per unit time at photon energy $\hbar\omega$ (phot•s^{-1}) and *I(ℏω)* is the incident photon flux (phot•s^{-1}×cm^{-2})

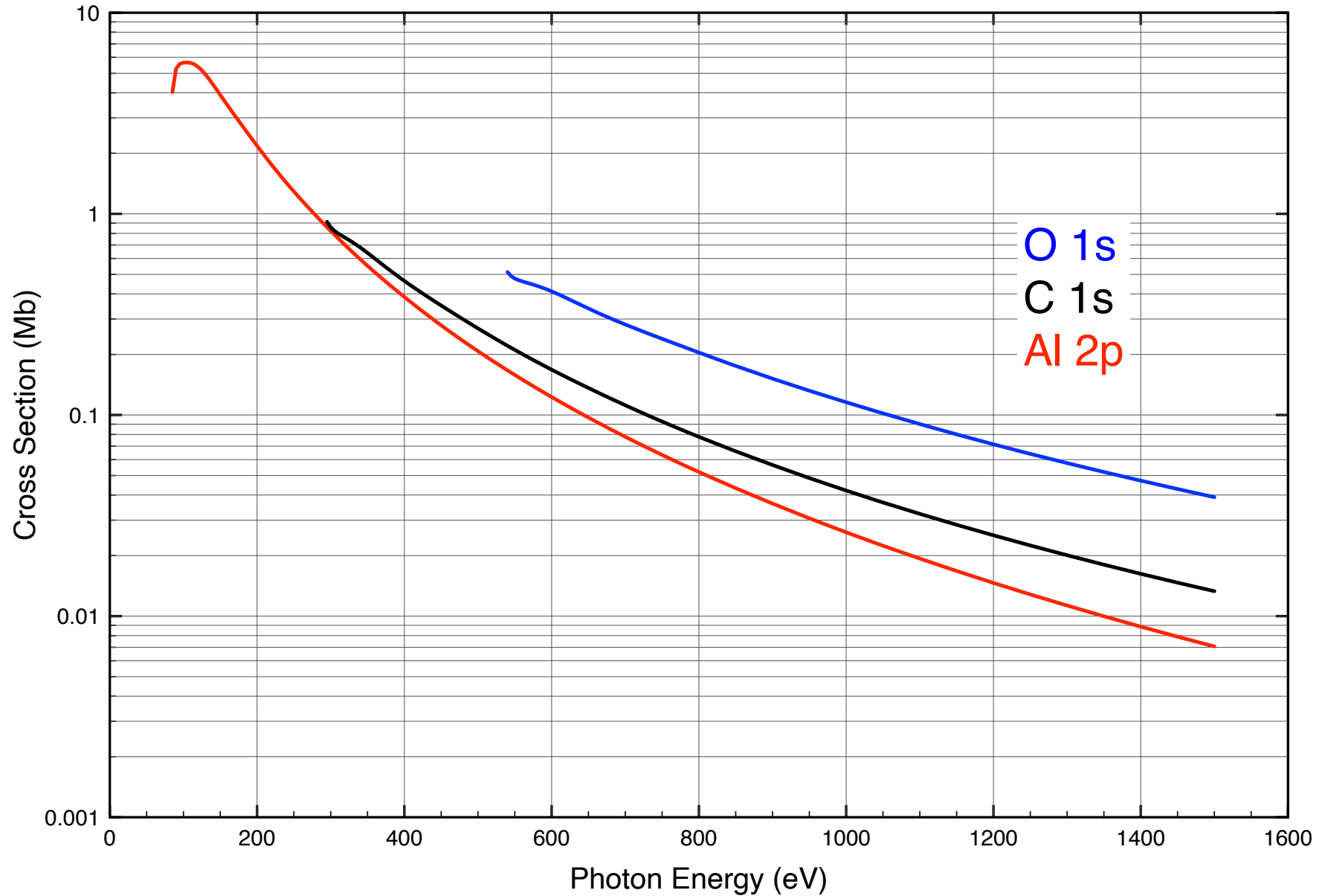For a medium with *n* atoms per unit volume and photons traveling a distance *dx*

$$\frac{dI}{I} = -n\sigma dx$$

or

$$I\left(x\right) = I_0 e^{-n\sigma x}$$

σ is generally measured in Megabarn (Mb, 1Mb=10^{-18}cm^2)

Photoemission atomic cross section

For a spherically symmetric system (isolated atom) the initial and final states can be expressed as product of a radial and angular part:

$$\Psi_i\left(\vec{r}\right) = R^i_{l_i}(r)\, Y_{L_i}\left(\hat{r}\right)$$

$$\Psi_f\left(\vec{r}\right) = 4\pi \sum_L Y^*_L\left(\hat{k}_f\right) i^{-l} e^{i\delta_l} R^f_l(r)\, Y_L\left(\hat{r}\right)$$

The Ψ_f can also be written as

$$\Psi_f\left(\vec{r}\right) = e^{-i\vec{k}_f\cdot\vec{r}} + f\left(E_f, \vec{k}_f\right) \frac{e^{i\vec{k}_f\cdot\vec{r}}}{r}$$

For spherically symmetric systems (free atoms) the well known selection rules ($\Delta l=\pm 1$) apply.

One can write the intensity for emission at a given angle γ from the polarization of the beam in the following form

$$\frac{d\sigma_{nl}(\hbar\omega)}{d\Omega} = \frac{\sigma_{nl}(\hbar\omega)}{4\pi}\left[1 + \beta P_2\left(\cos(\gamma)\right)\right]$$

$$P_2\left(\cos(\gamma)\right) = \frac{3\cos^2(\gamma) - 1}{2}$$

This term controls the weight of $\Delta l =+1$ and $\Delta l =-1$ channels

-1≤β ≤ 2

At $\gamma=54.7°$ (magic angle) $P_2=0$: the measurement is independent of β

For $l=0$ (s levels) $\beta\equiv 2$

For $l=0$ (s levels) $\beta \equiv 2$

$$\frac{d\sigma_{nl=0}\left(\hbar\omega\right)}{d\Omega} = \frac{\sigma_{nl=0}\left(\hbar\omega\right)}{4\pi}\left(\cos\left(\gamma\right)\right)^2$$
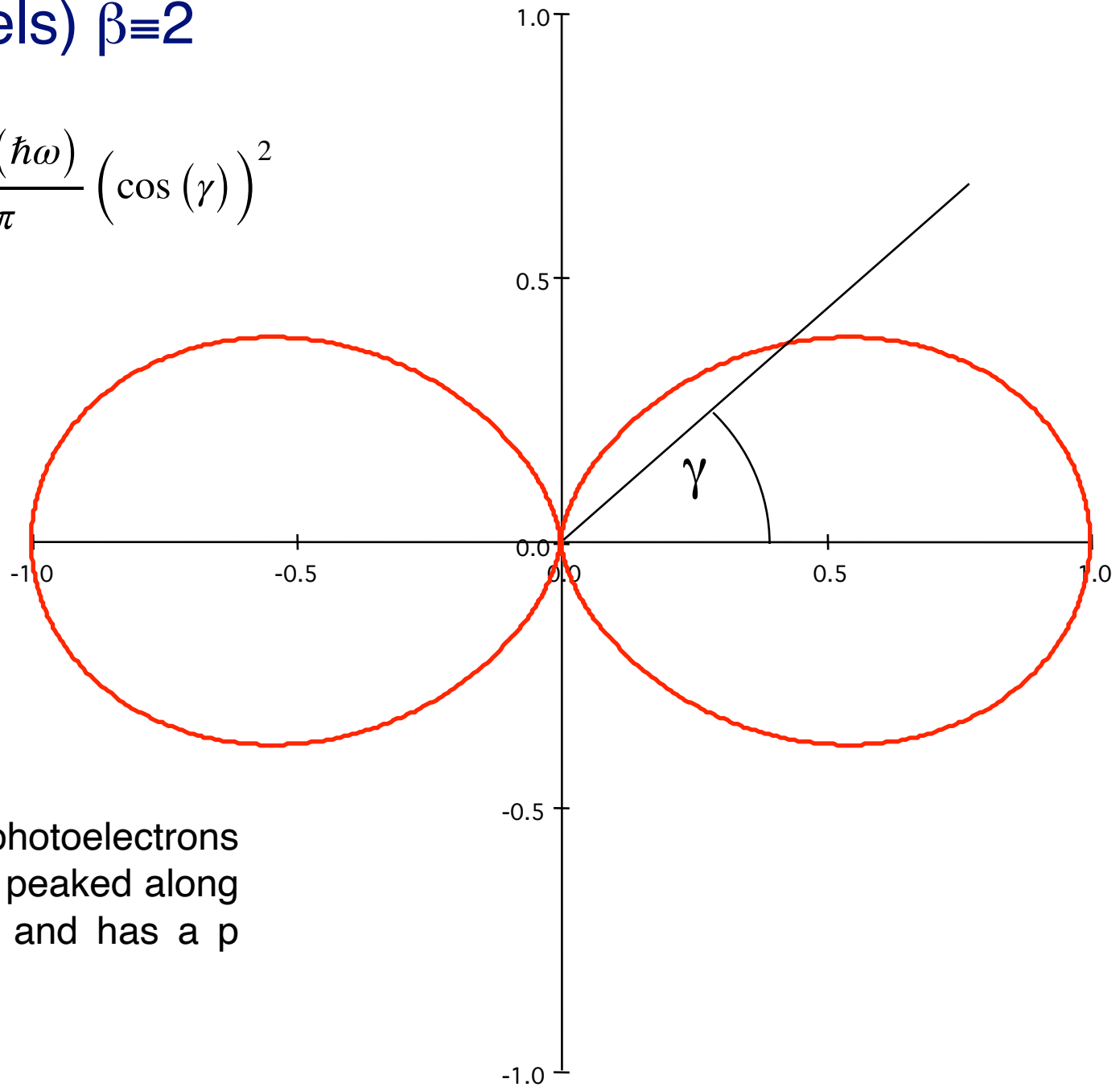
The angular pattern of photoelectrons emitted from an s level is peaked along the polarisation direction and has a p level like shape

Example: the Ag 4d level
(from J.J. Yeh: "Atomic calculation of photoionization cross sections and asymmetry parameters",Gordon Breach)

Ag4d

— σ

— β
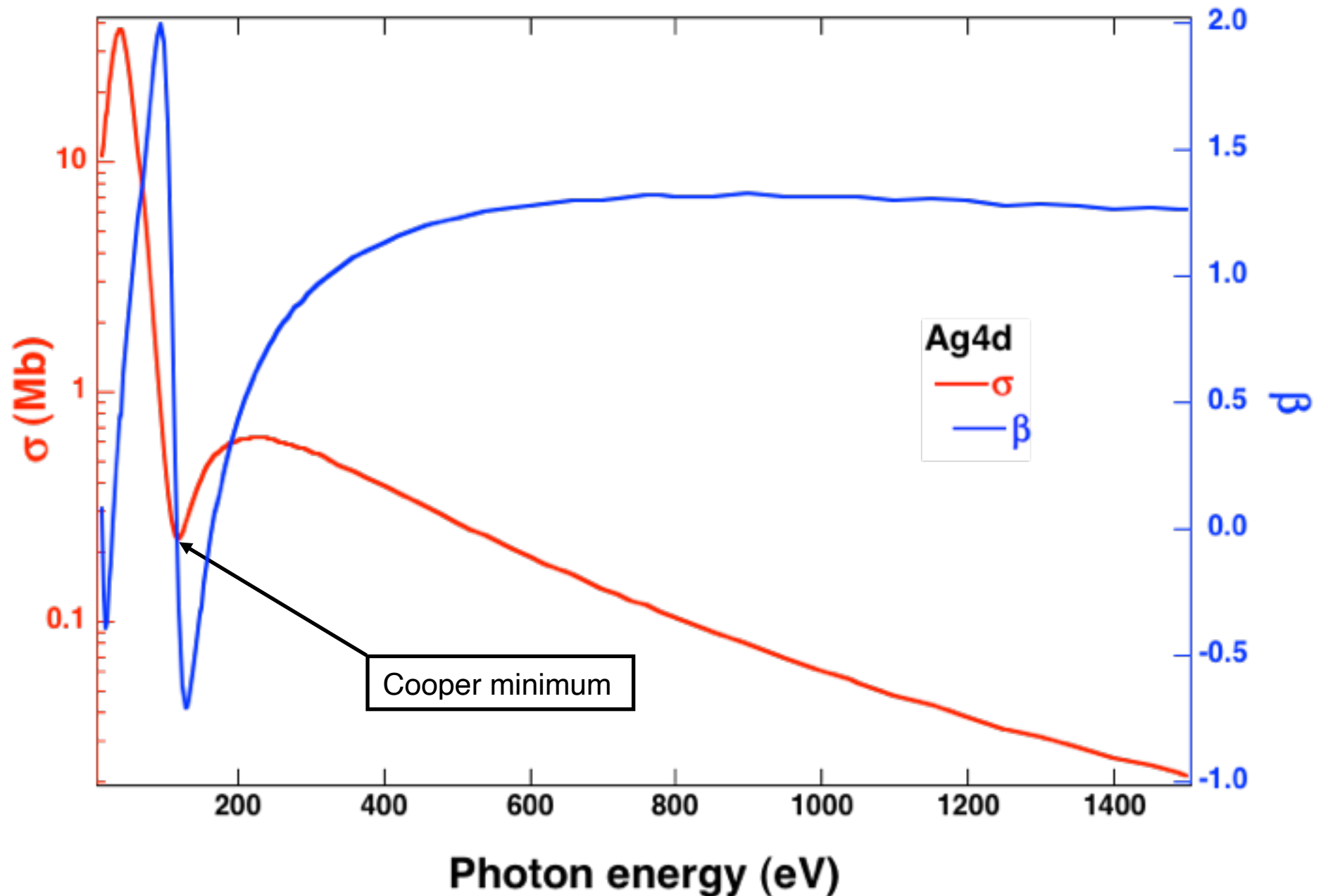
Cooper minimum

The Cooper minimum
is due to a node in the initial state
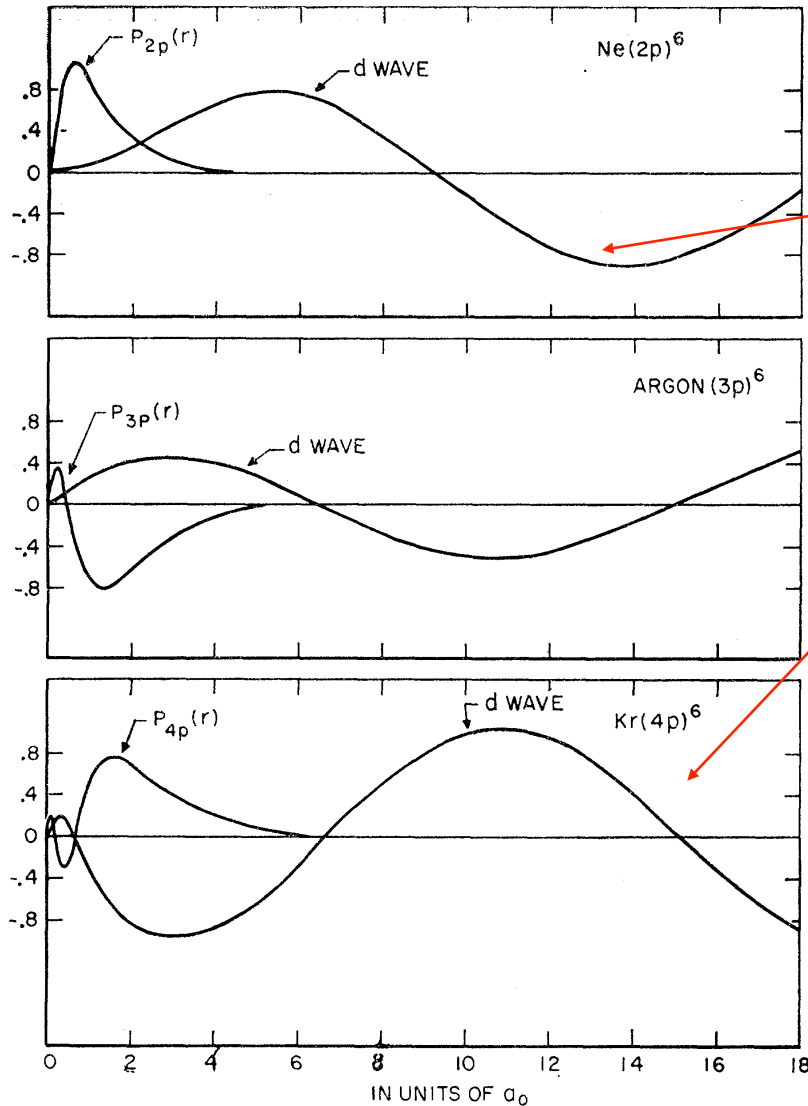
$\Delta l=+1$, $E_k=0$ (i.e. at threshold)

At some kinetic energy the integral will become positive!

FIG. 2. Outer subshell radial wave functions and d waves for $\epsilon=0$ for Ne, Ar, and Kr.

Example: the Ag 4d level
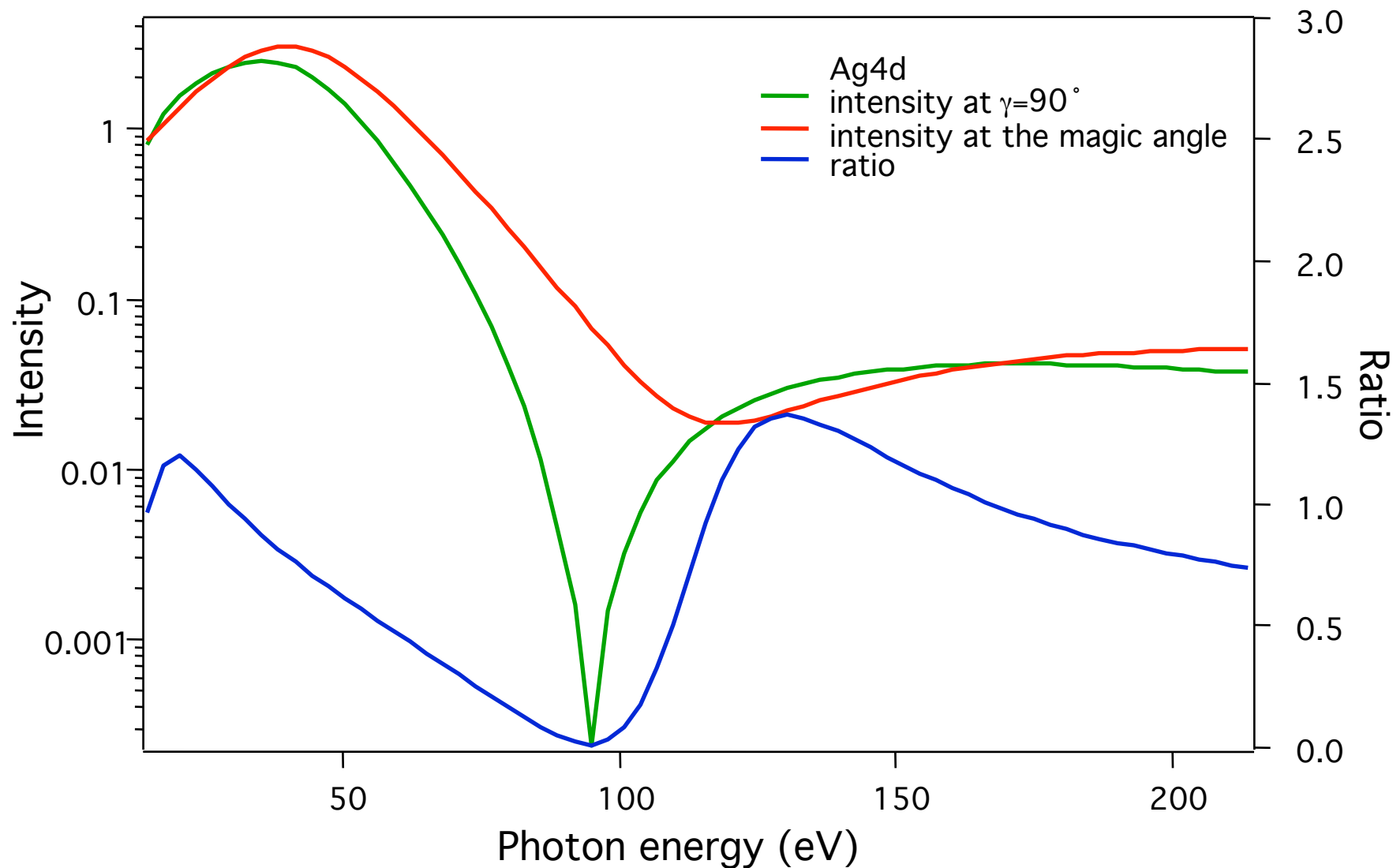
Application of the Cooper minimum effect to alloys
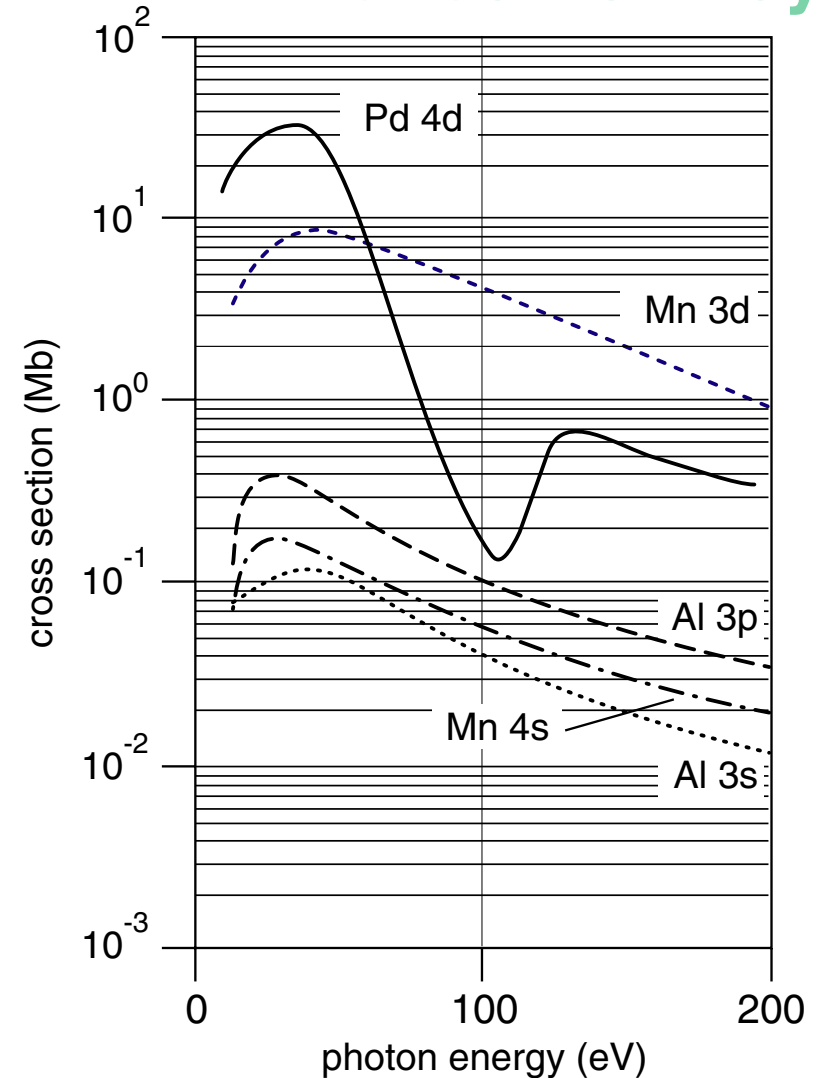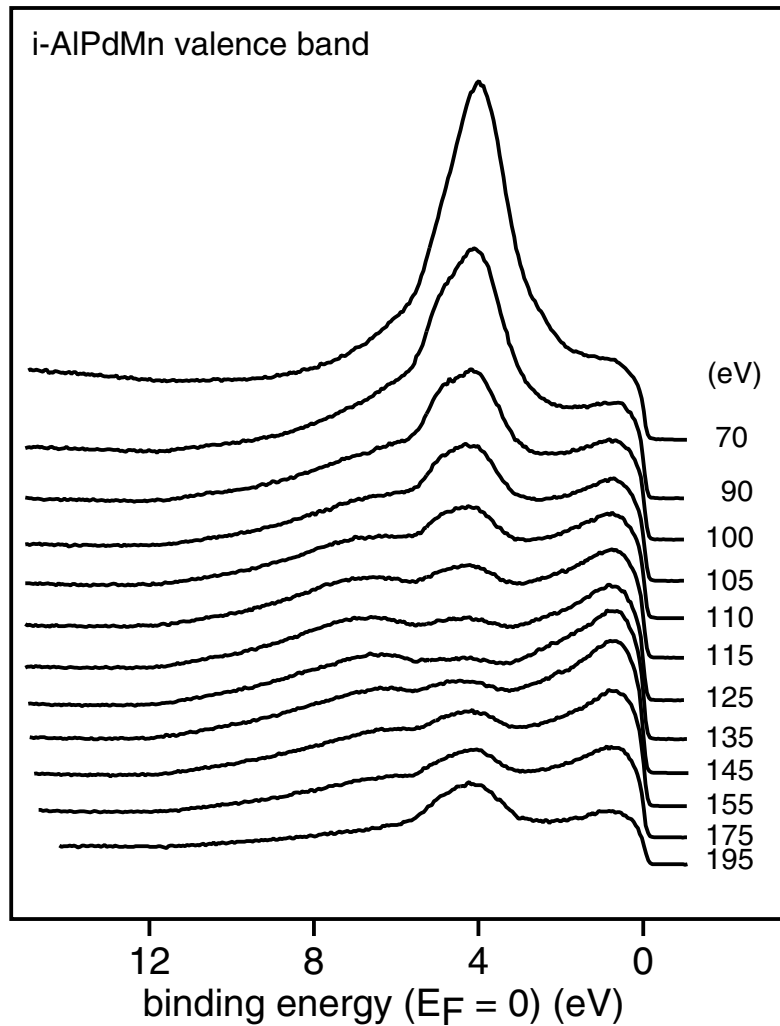
Left: series of normal emission spectra from a freshly cleaved i-Al–Pd–Mn sample recorded at normal emission for photon energies from 70 to 195 eV. The peak which is strongly suppressed at higher photon energies is attributed to emission form the Pd 4d level. Right: atomic photoionization cross sections $\sigma(\bar{}\ h\omega)$ or the Al, Pd and Mn states, calculated within the Hartree–Fock–Slater scheme by Yeh and Lindau showing the strong Cooper minimum in the Pd 4d line

K Horn et al 2006 J. Phys.: Condens. Matter 18 435

Electron mean free path
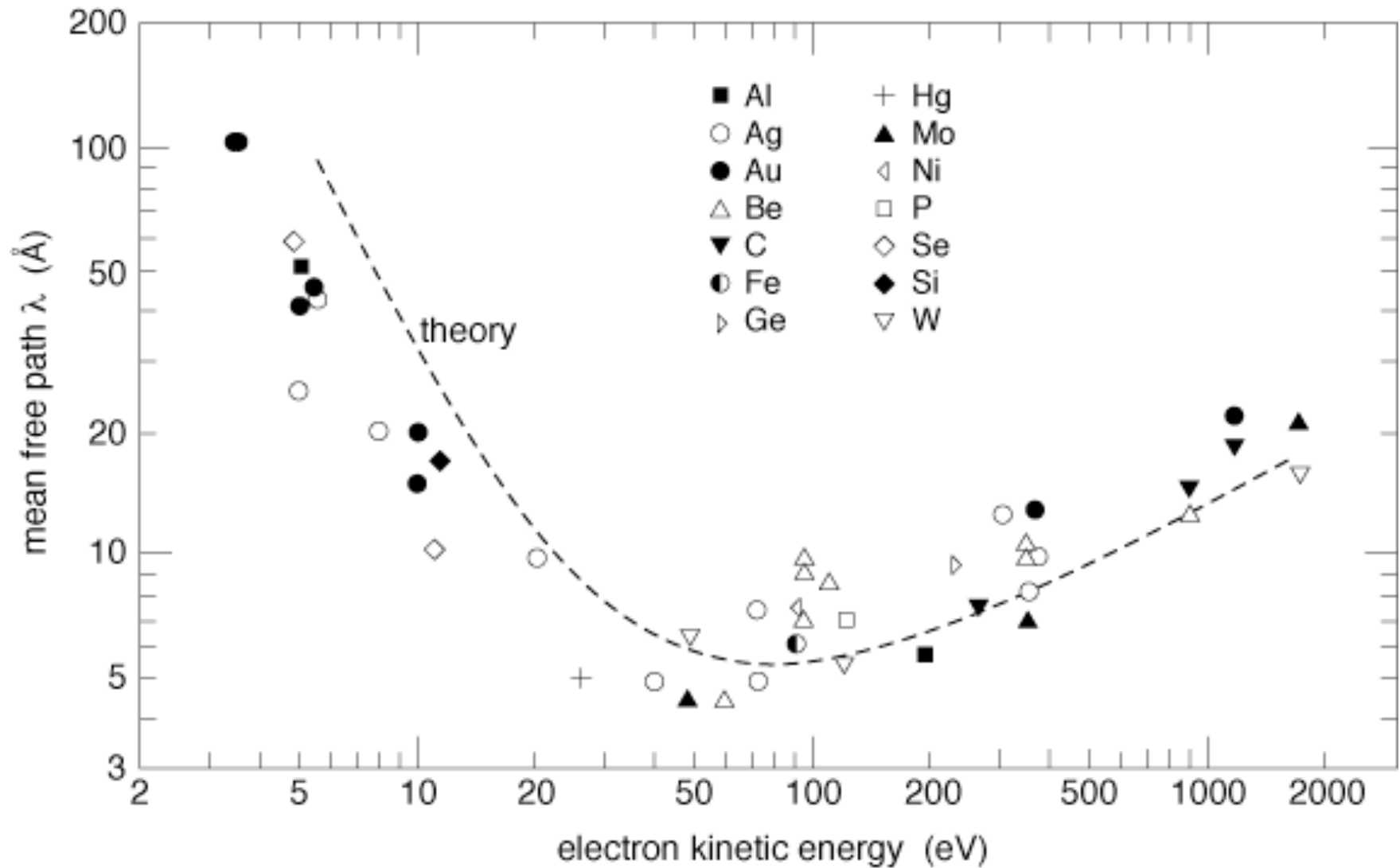
Valence band angle resolved photoemission (ARUPS)

- Bulk and surface states
- Band mapping

WAVE FUNCTIONS AT THE SURFACE

VACUUM | SOLID

ABOVE E_V

f   BULK STATE
e
d   { EVANESCENT FINAL STATE

BELOW E_V

c   BULK STATE
b   SURFACE RESONANCE
a   SURFACE STATE
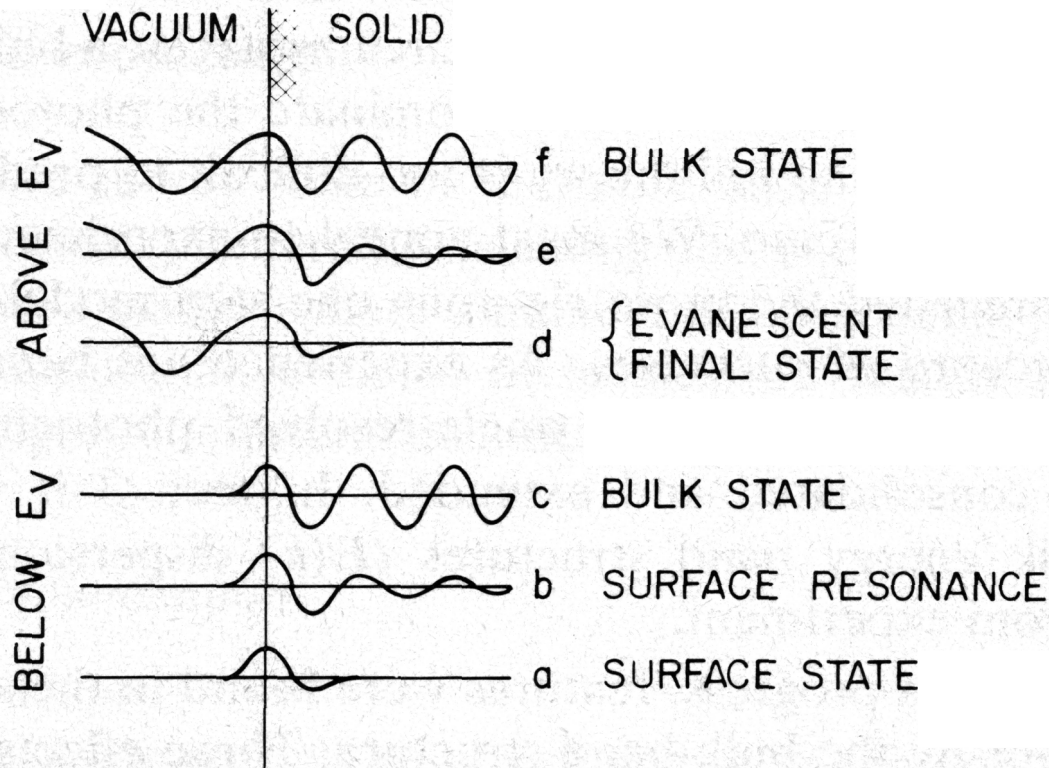
Schematic representation of the wave functions of initial states (a), (b) and (c), and final states (d), (e) and (f), involved in optical transitions giving rise to photoelectron emission. States (c) and (f) correspond to bulk Bloch states hardly modified by the presence of the surface. States (b) and (e) are more strongly evanescent (surface resonances). States (a) and (d) have essentially no amplitude in the interior of the solid and correspond respectively to a true bound surface state and the case of band-gap emission.

Photoexcitation process: Momentum conservation

Photon Momentum $\qquad p = \hbar q = h / \lambda$

Photon Energy $\qquad E = h \nu = hc / \lambda$

Typical photon wavenumber

$$q = 2\pi \frac{E}{hc} = 2\pi \frac{E\,[\text{eV}]}{12400\,[\text{eV} - \text{Å}]}$$

$$= .01 \text{ to } .05 \text{ Å}^{-1} \quad (\text{for } E = 20 \text{ to } 100 \text{ eV})$$

20-100 eV

2-3 Å⁻¹
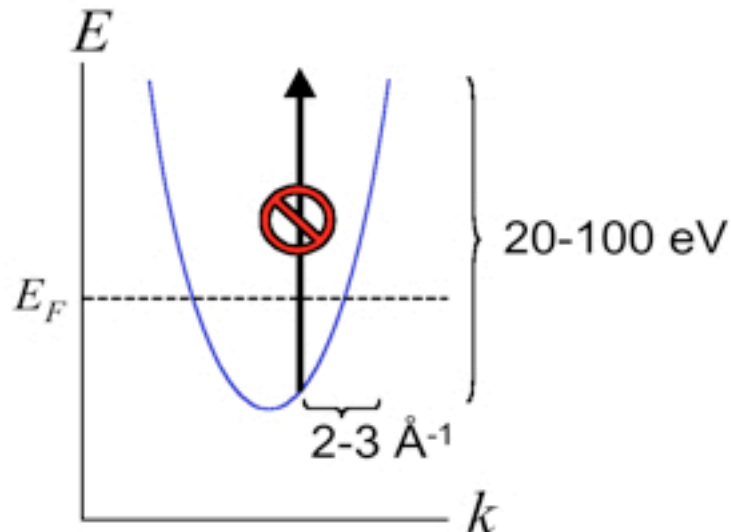
- The photons impart very little momentum in the photoemission process, **i.e. vertical transitions**

- Therefore photon-stimulated transitions are not allowed for free electrons **(energy and momentum conservation laws cannot be satisfied at the same time).**

In order to satisfy both energy and momentum conservation
The role of crystal translational symmetry is crucial
– i.e. no photoemission is allowed from truly free electrons.
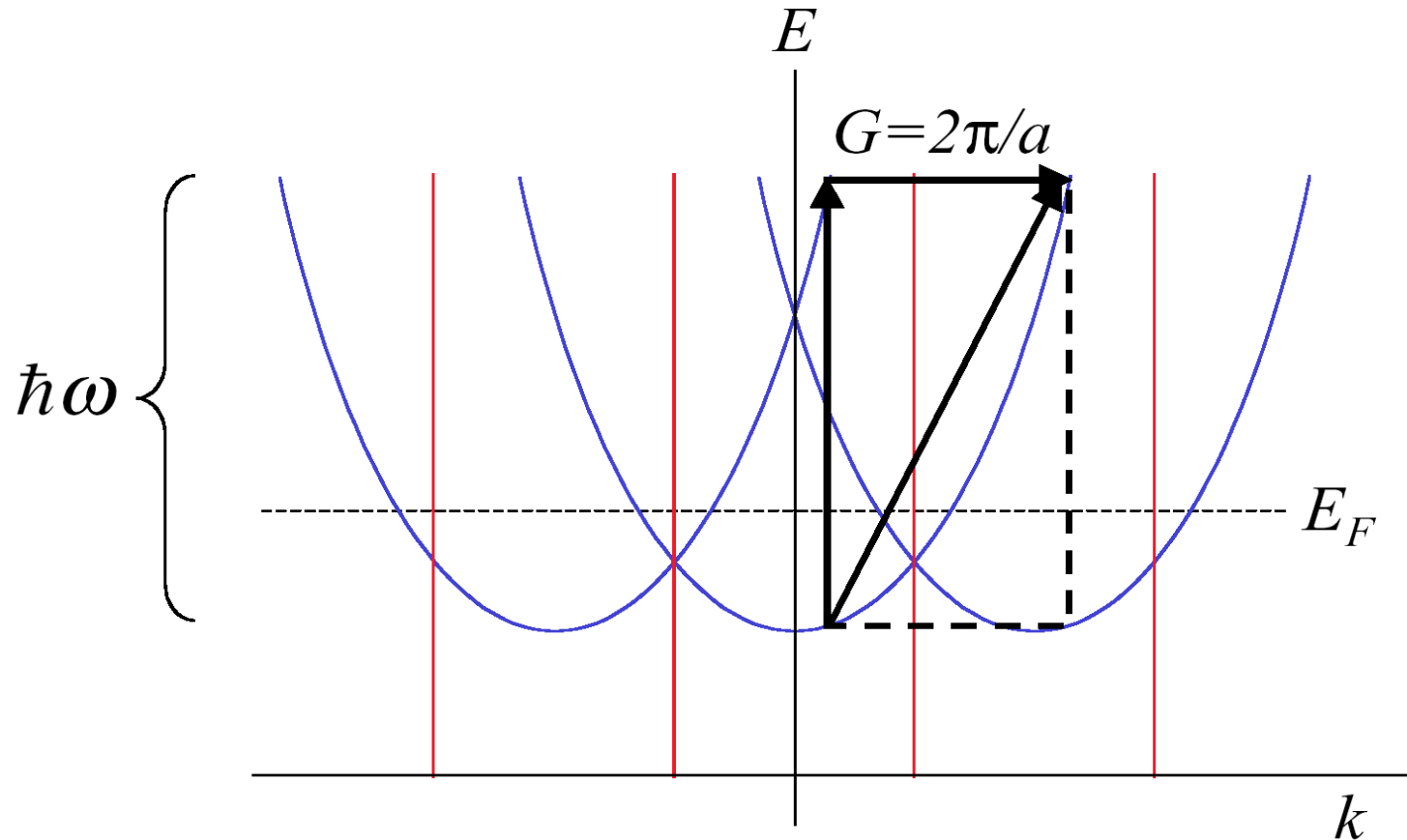
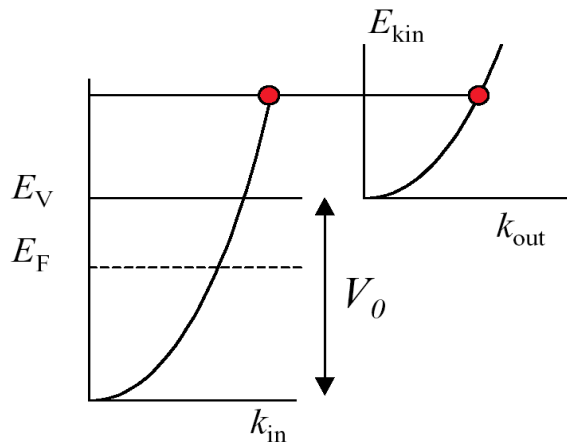$$E_f=E_i+h\nu \ \ \& \ \ \mathbf{k}_f=\mathbf{k}_i+\mathbf{G}$$
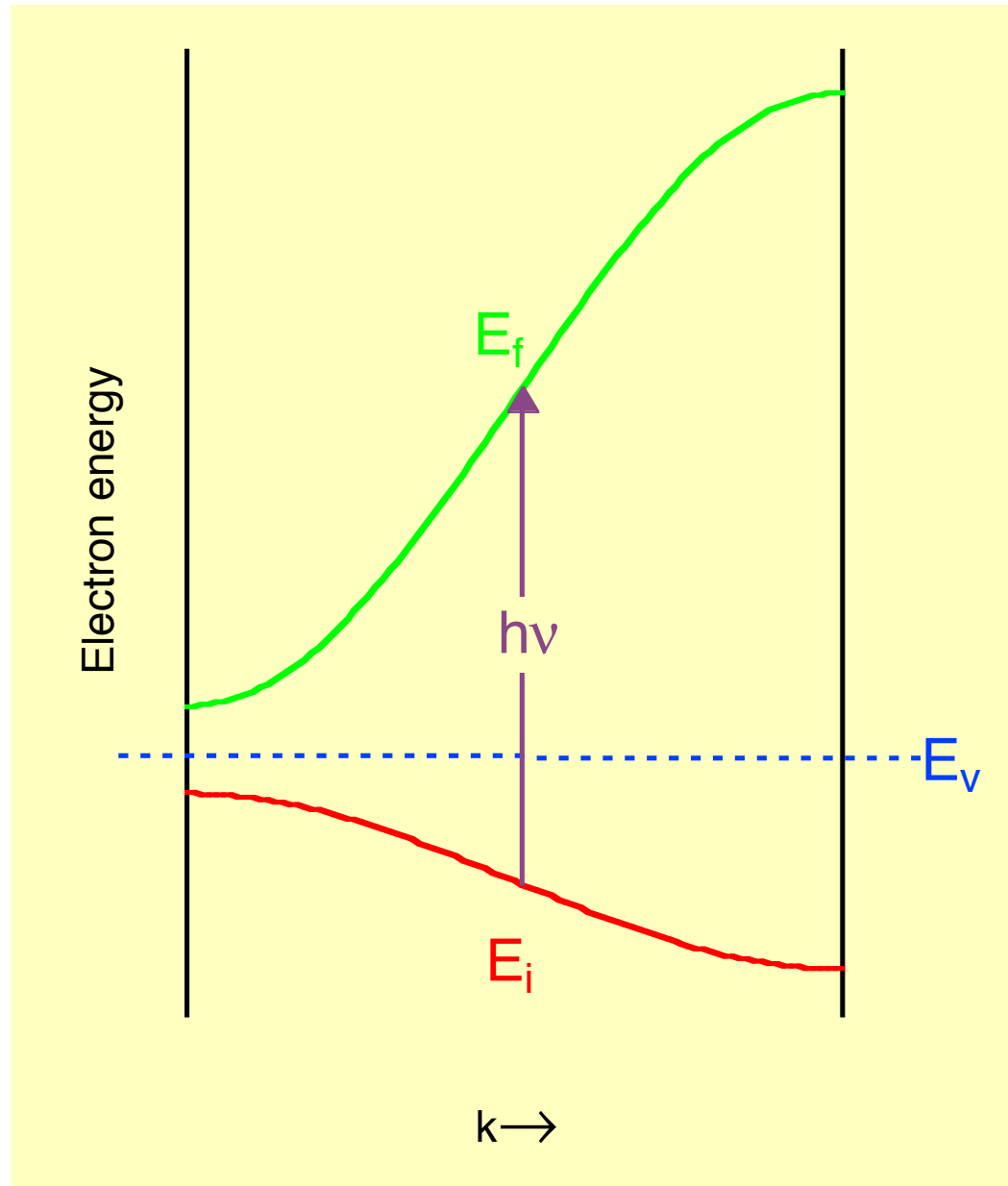
At the surface the crystal symmetry is conserved in the surface plane but is broken perpendicularly to the surface: the component of the electron momentum parallel to the surface plane ($k_{//}$) is conserved, but $k_{\perp}$ is not

The potential barrier at the surface slows the electron in the direction normal to the surface.

V_0=Surface potential step "inner potential"
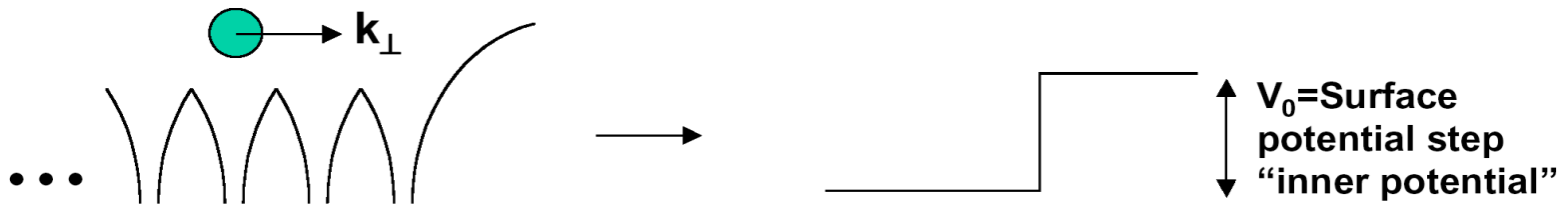
Free-electron final state model

We match the free-electron parabolas inside and outside the solid to obtain the wavevector k inside the solid

Momentum conservation

The surface breaks the translational symmetry along $\hat{n}$

Conserved (i.e. = $\vec{k}_{parallel}$ in the sample)

$\vec{k}_{parallel}$

θ_e

$\vec{k}$

$\vec{k}_{perpendicular}$

ϕ_e

$\hat{n}$
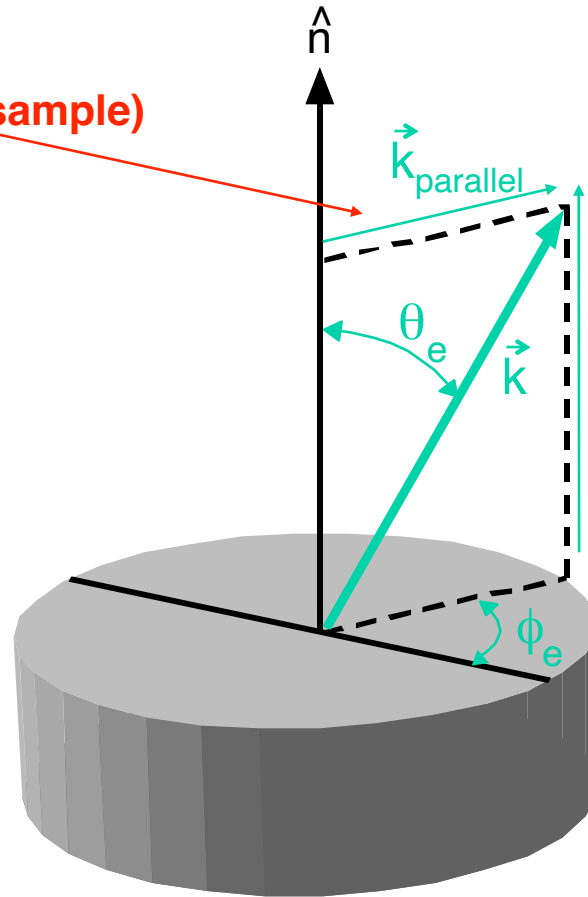
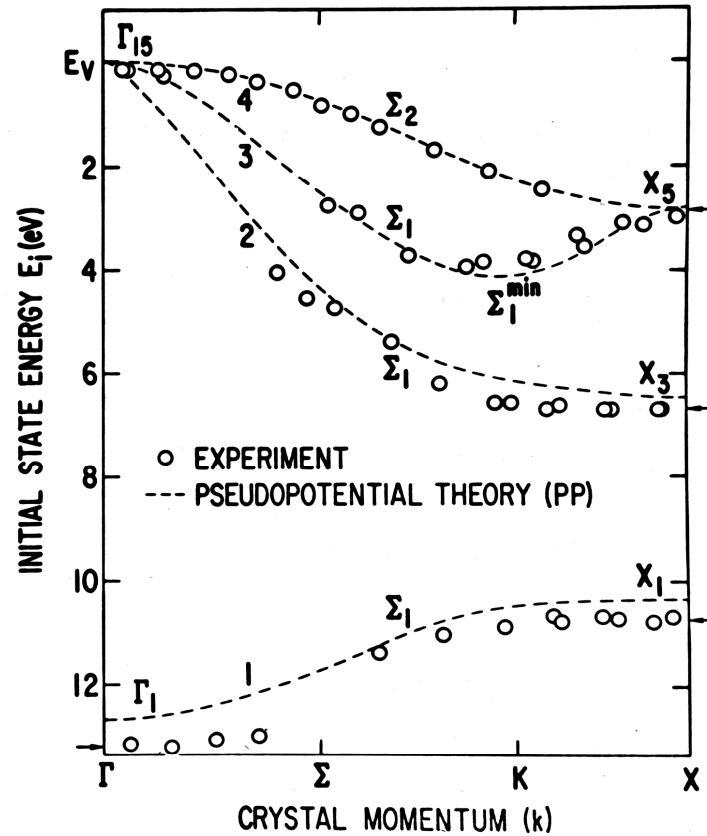$$E_k = \frac{\hbar^2 k^2}{2m}$$

Outgoing electron

NOT Conserved

Oriented single crystal

Band mapping: GaAs

GaAs (110) NORMAL EMISSION SPECTRA
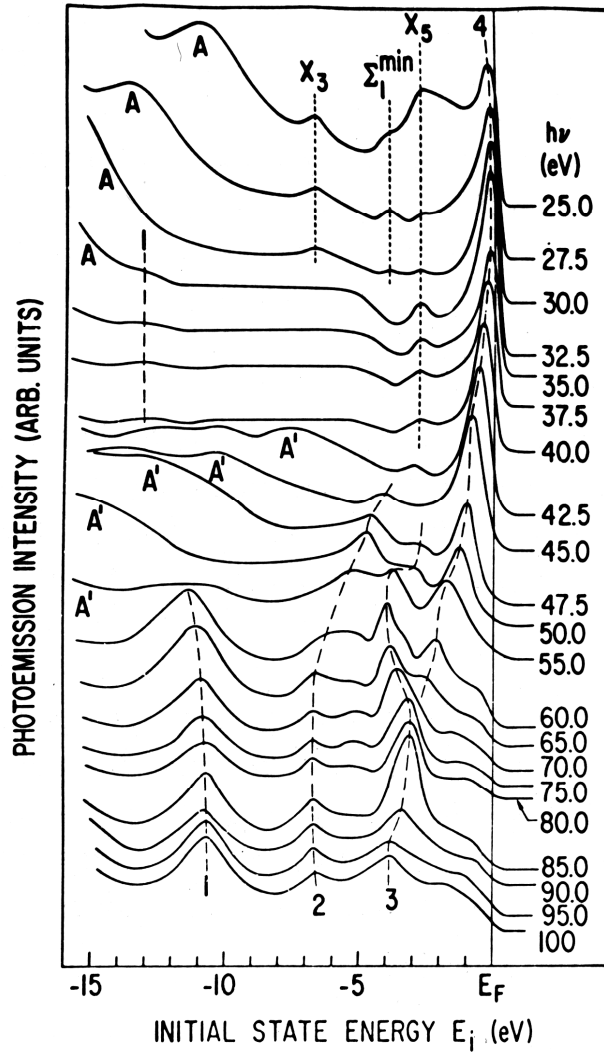
GaAs ENERGY BANDS E(k) ALONG ΓKX

At the surface the crystal symmetry is conserved in the surface plane but is broken perpendicularly to the surface: the component of the electron momentum parallel to the surface plane ($k_{//}$) is conserved, but $k_\perp$ is not
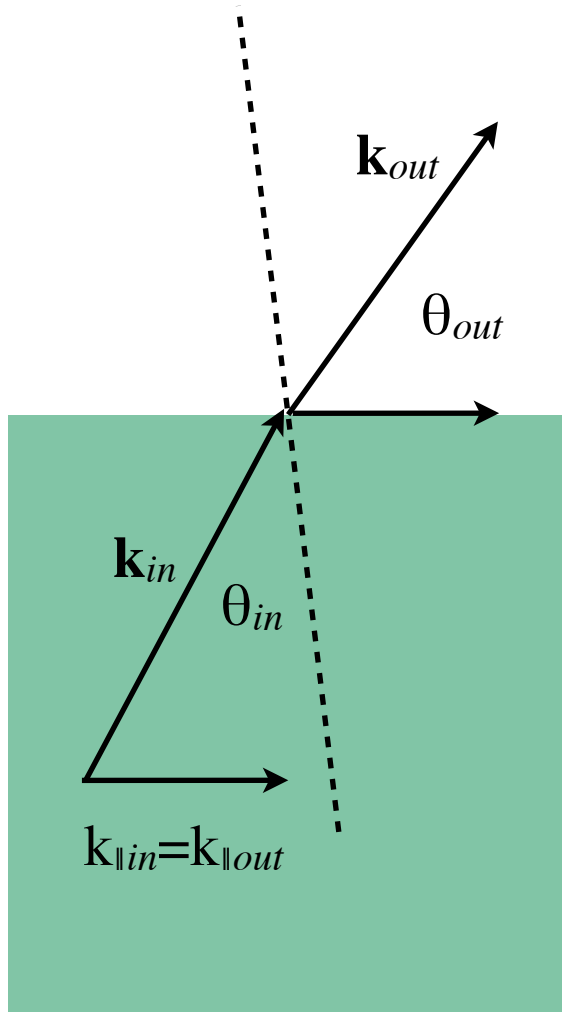
Kinematic relations

$$k_{out} = \sqrt{\frac{2m^*}{\hbar^2} E_{kin}}$$

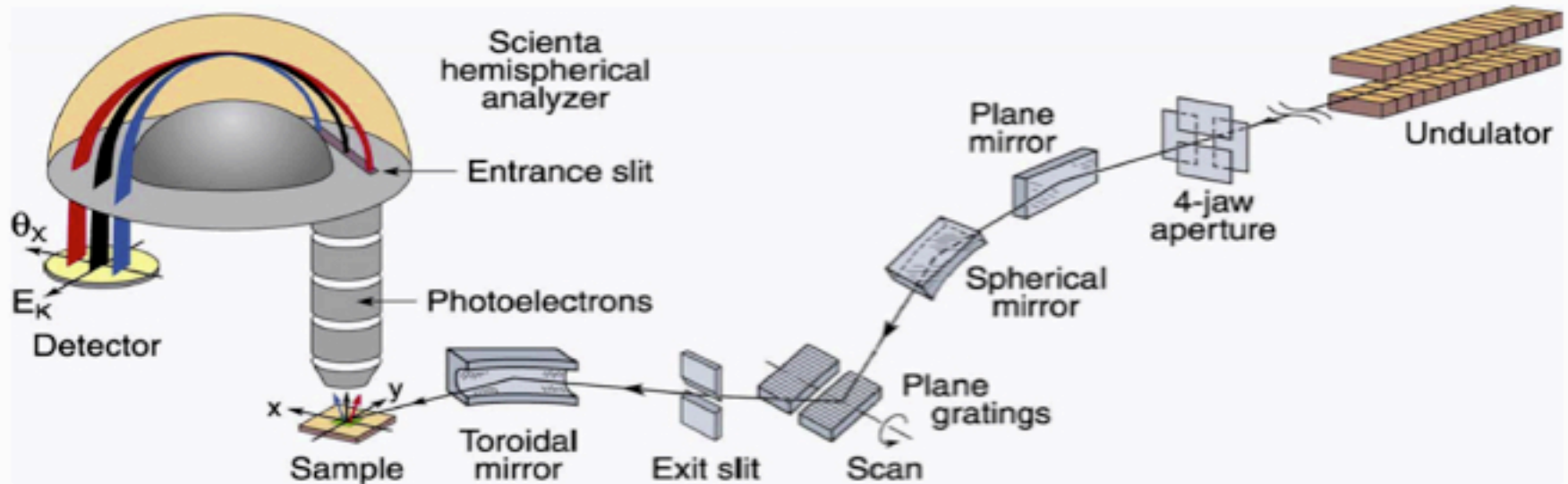$$k_{in} = \sqrt{\frac{2m^*}{\hbar^2}(E_{kin} + V_0)}$$

$$k_{out\|} = k_{in\|} = k_\|$$

"Snell's law"

$$k_\| = \sin\theta_{out}\sqrt{\frac{2m^*}{\hbar^2}E_{kin}} = \sin\theta_{in}\sqrt{\frac{2m^*}{\hbar^2}(E_{kin} + V_0)}$$

Critical angle for emission from bulk states

$$(\sin\theta_{in})_{max} = \sqrt{\frac{E_{kin}}{E_{kin} + V_0}}$$
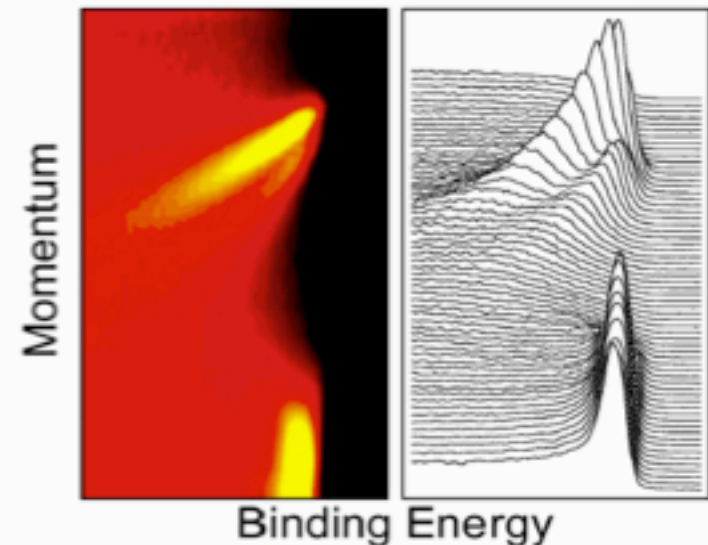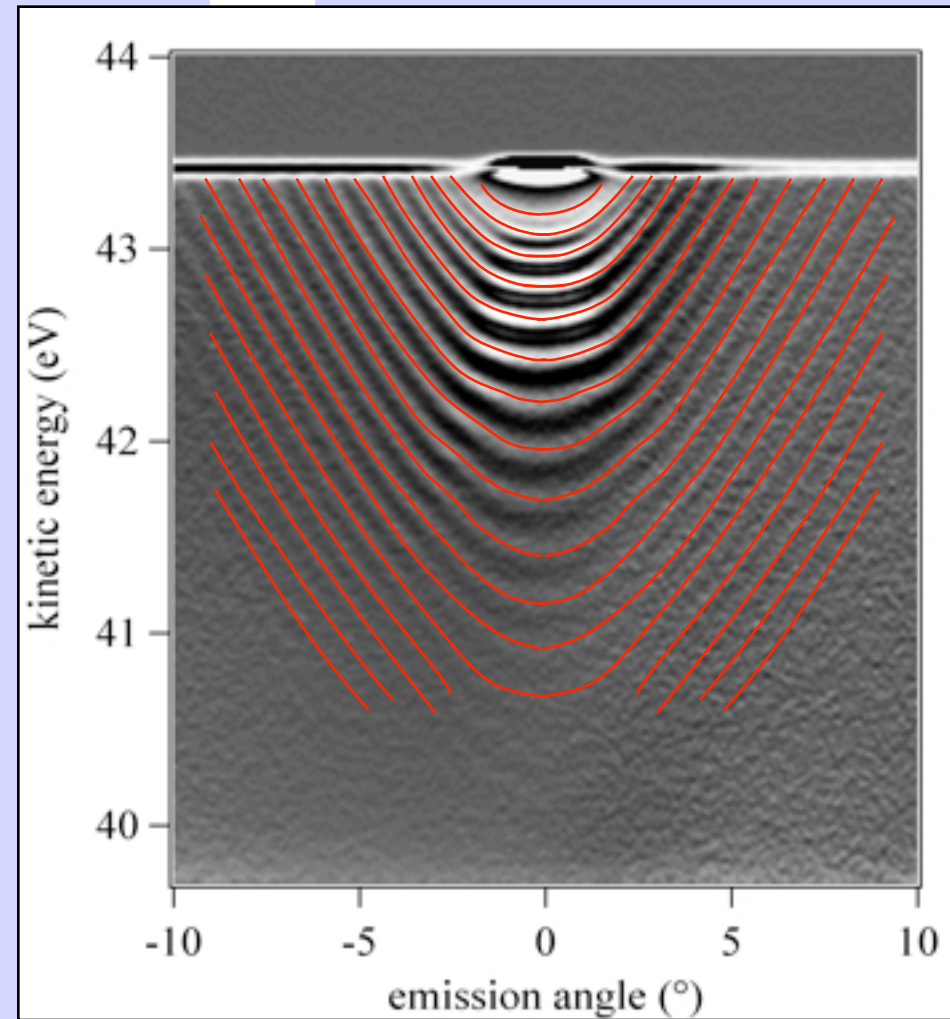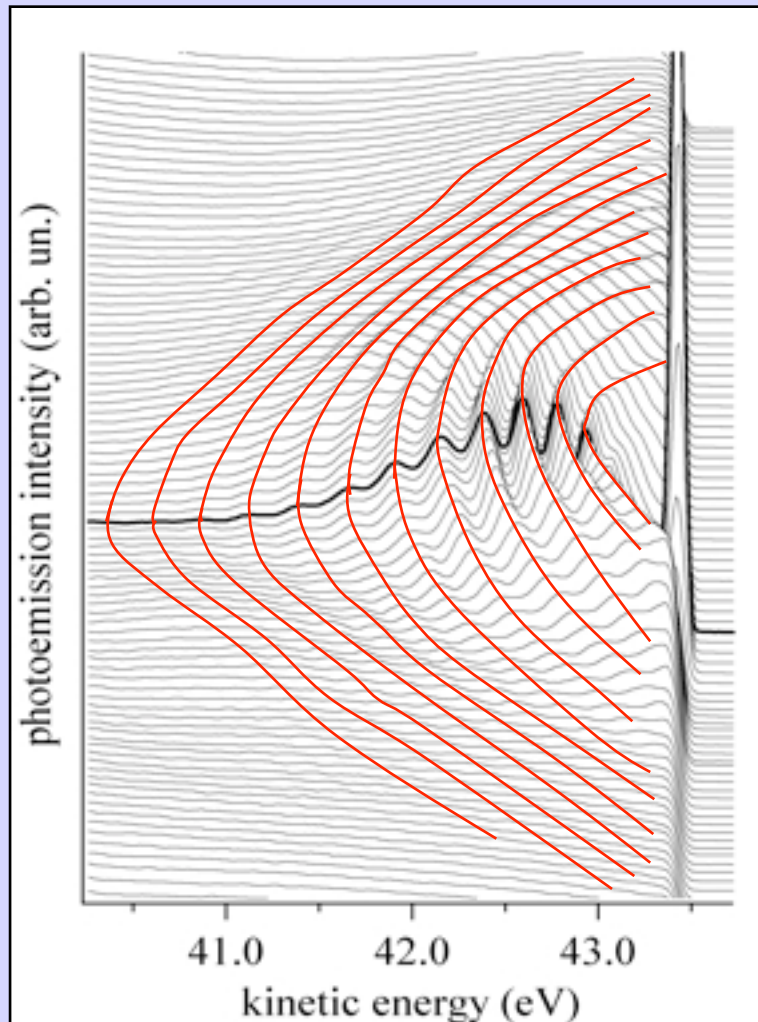
State-of-the-art

courtesy of A. Damascelli

Istituto di Struttura della Materia

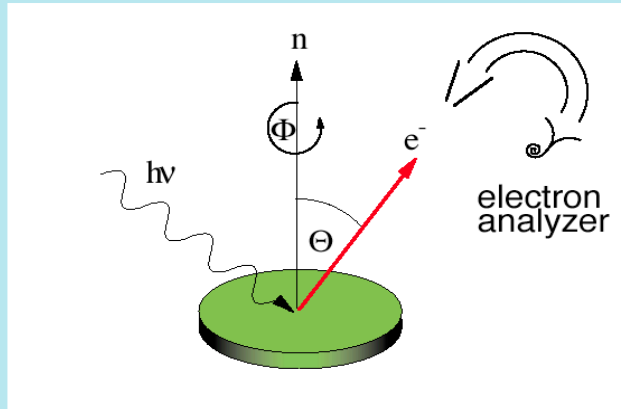Consiglio Nazionale delle Ricerche

elettra

Discrete quantum well states of an atomically flat 150 Å Ag film on Pt(111)

Angle-resolved photoemission from (quasi) 2D systems: a simple picture
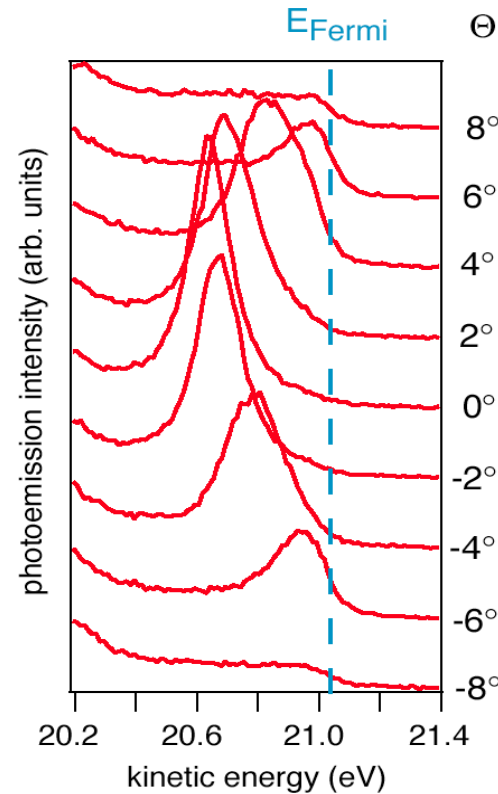
Example: Cu(111) surface state

- measure E_{kin}, Θ, Φ.

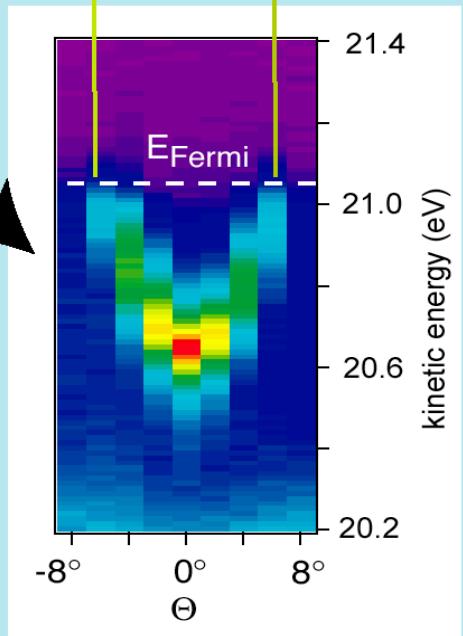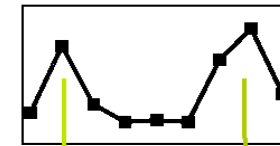$$k_x = \sqrt{\frac{2m}{\hbar^2}} \sin\Theta \cos\Phi \sqrt{E_{kin}}$$

$$k_y = \sqrt{\frac{2m}{\hbar^2}} \sin\Theta \sin\Phi \sqrt{E_{kin}}$$

obtain $E_{bin}(k_x, k_y)$, i.e. the occupied band structure
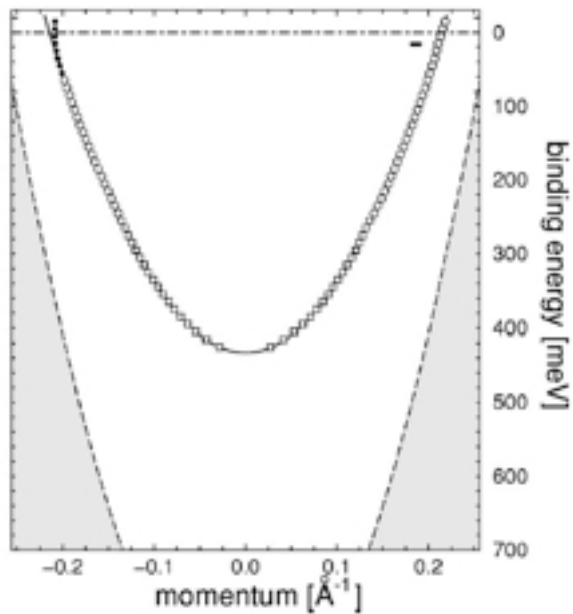
Energy Distribution Curve (EDC)

E_{Fermi} Θ

photoemission intensity (arb. units)

kinetic energy (eV)

Momentum Distribution Curve (MDC)

E_{Fermi}

kinetic energy (eV)

Θ

Courtesy of Ph. Hofmann

Shockley Surface States of Noble Metal (111) Surfaces
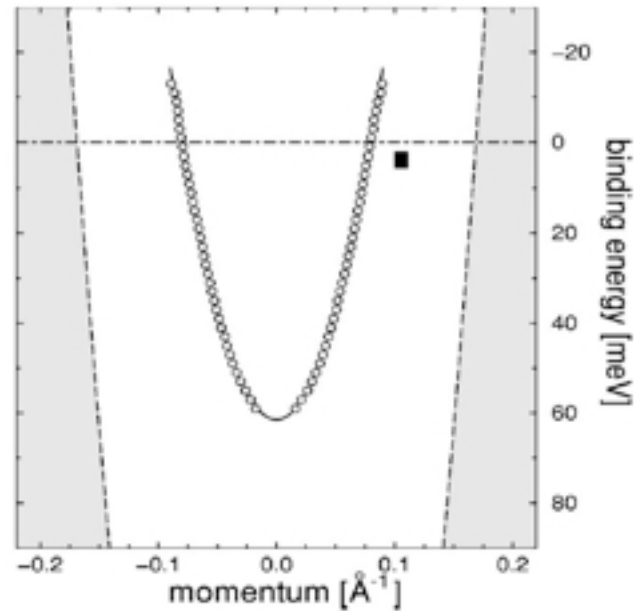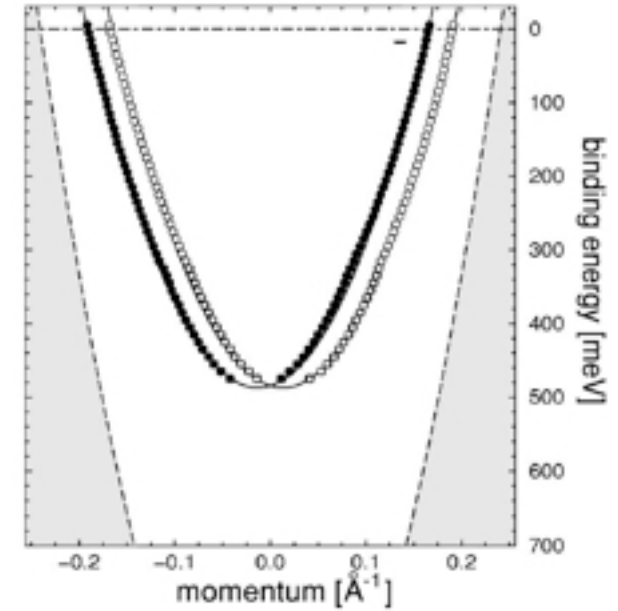
Cu(111)
Z=29

Ag(111)
Z=47

Au(111)
Z=79

Two parabolas: spin-orbit splitting

PES Experiment, Reinert, Nicolay, Ehm, and Hüfner, PRB 63, 115415 (2001)

Bandgap opening in graphene induced by patterned hydrogen adsorption

Richard Balog[1], Bjarke Jørgensen[1], Louis Nilsson[1], Mie Andersen[1], Emile Rienks[2], Marco Bianchi[3],
Mattia Fanetti[4], Erik Lægsgaard[1], Alessandro Baraldi[3,4], Silvano Lizzit[5], Zeljko Sljivancanin[6],
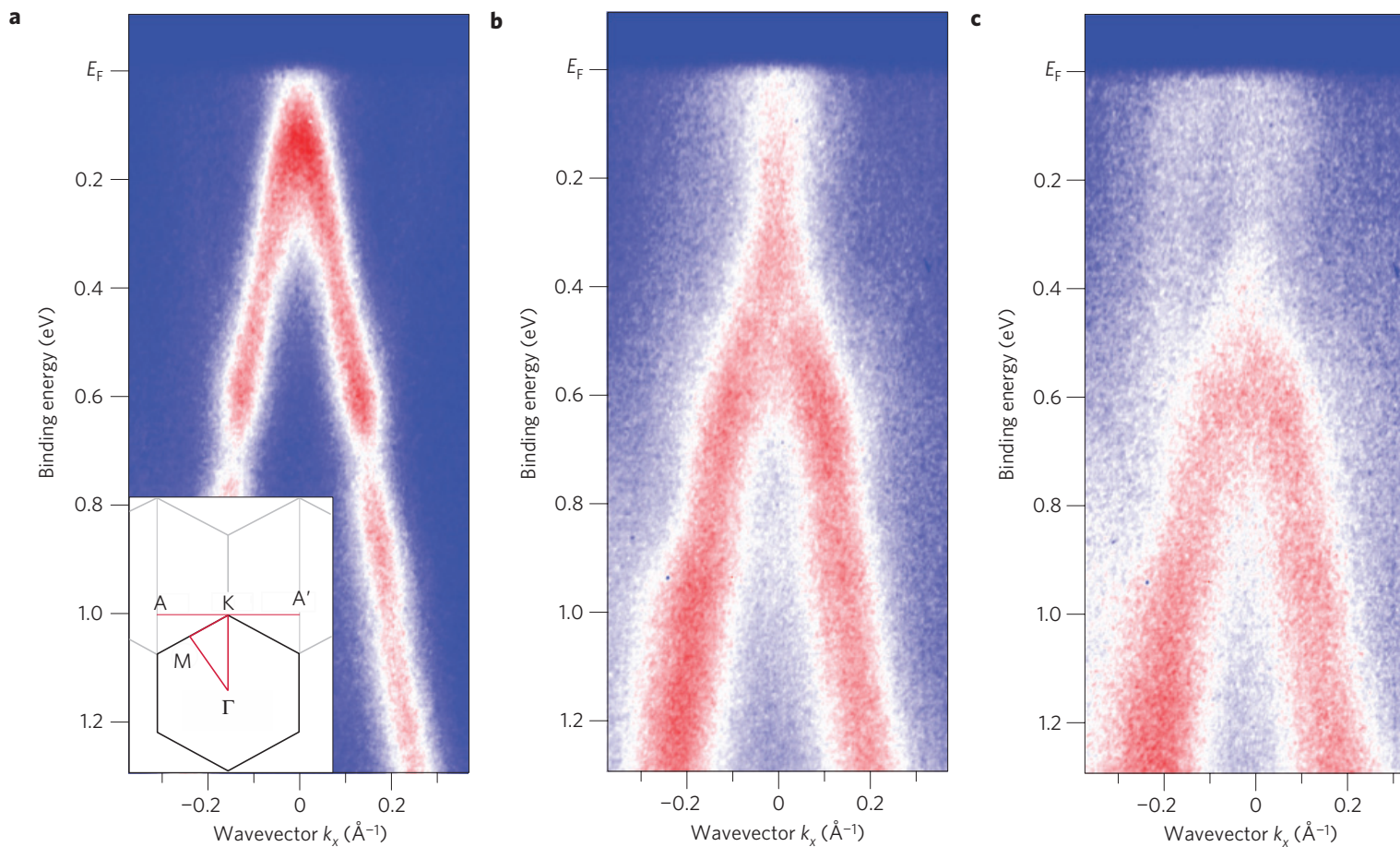Flemming Besenbacher[1], Bjørk Hammer[1], Thomas G. Pedersen[7], Philip Hofmann[2] and Liv Hornekær[1]*

Figure 1 | Observation of a gap opening in hydrogenated graphene. a–c, Photoemission intensity along the A–K–A' direction of the Brillouin zone (see inset) for clean graphene on Ir(111) (**a**), graphene exposed to a 30 s dose of atomic hydrogen (**b**) and graphene exposed to a 50 s dose of atomic hydrogen (**c**).

Bandgap opening in graphene induced by patterned hydrogen adsorption

Richard Balog[1], Bjarke Jørgensen[1], Louis Nilsson[1], Mie Andersen[1], Emile Rienks[2], Marco Bianchi[3],
Mattia Fanetti[4], Erik Lægsgaard[1], Alessandro Baraldi[3,4], Silvano Lizzit[5], Zeljko Sljivancanin[6],
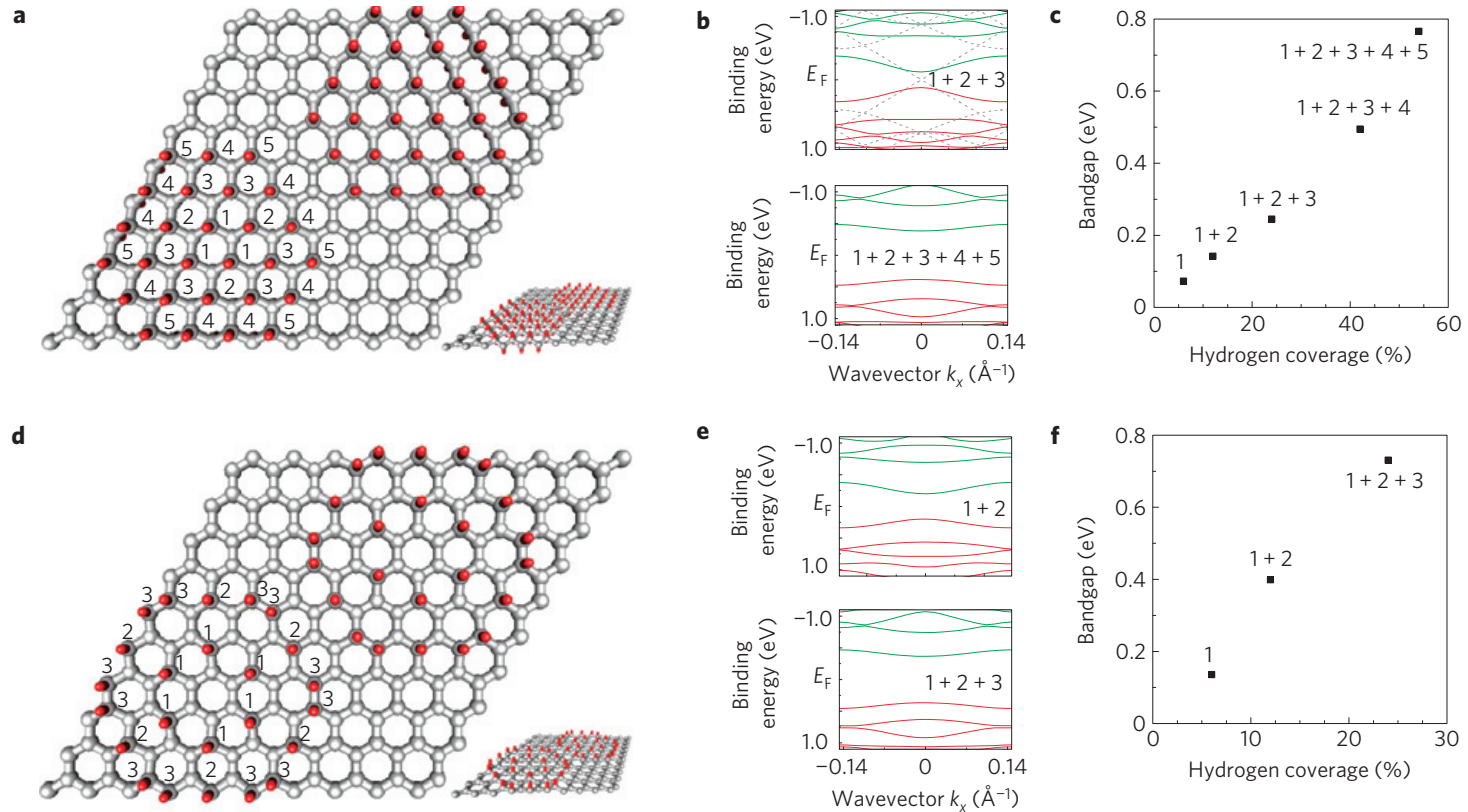Flemming Besenbacher[1], Bjørk Hammer[1], Thomas G. Pedersen[7], Philip Hofmann[2] and Liv Hornekær[1]*

Figure 4 | Hydrogen adsorbate structures, calculated band structures and bandgaps. a, Hydrogen atom adsorbate structures forming graphane islands with hydrogen coverage ranging between 6% and 54% (corresponding to 3%–27% of the top sites) following the Moiré superlattice periodicity. **b**, Band structures for graphane-like islands with medium and high hydrogen coverage. Filled and empty bands are shown in red and green, respectively. For comparison, the band structure of intact graphene is shown in grey (dashed). **c**, Bandgap opening as a function of hydrogen coverage. A maximum of 0.77 eV is reached with 54% coverage (corresponding to 27% top site coverage). **d**, Adsorbate structures composed of increasing amounts of hydrogen pairs in *para* and *ortho* dimer configurations. **e**, Band structures with and without *ortho*-hydrogen dimers. **f**, Bandgap opening as a function of hydrogen coverage. At 23% coverage a bandgap opening as large as 0.73 eV is obtained. In **b**,**c**,**e** and **f**, numbers 1–5 refer to absorbate structures formed by hydrogen atoms at all the positions marked by the corresponding numbers in **a** and **d** respectively.

# Bandgap opening in graphene induced by patterned hydrogen adsorption

Richard Balog[1], Bjarke Jørgensen[1], Louis Nilsson[1], Mie Andersen[1], Emile Rienks[2], Marco Bianchi[3],
Mattia Fanetti[4], Erik Lægsgaard[1], Alessandro Baraldi[3,4], Silvano Lizzit[5], Zeljko Sljivancanin[6],
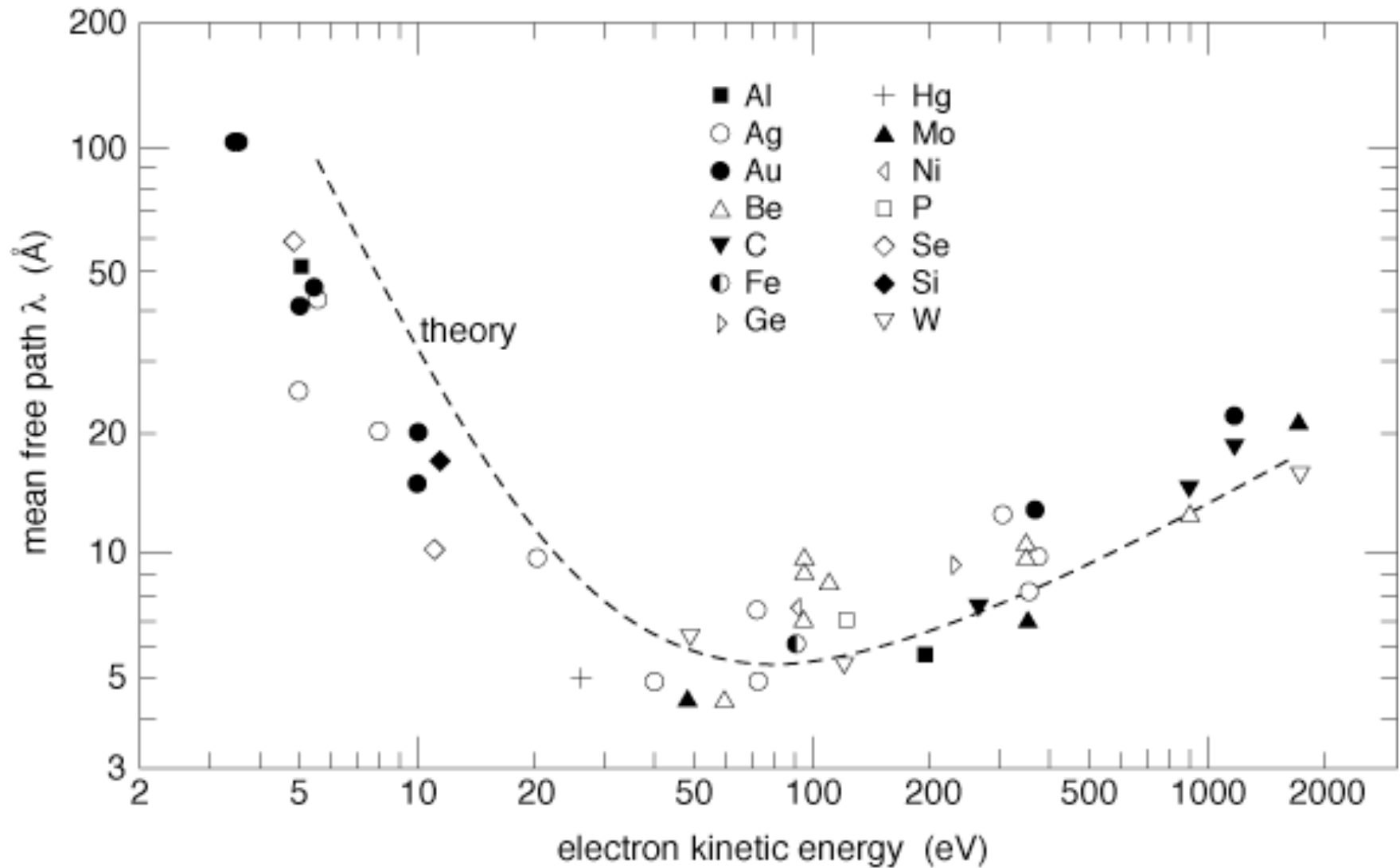Flemming Besenbacher[1], Bjørk Hammer[1], Thomas G. Pedersen[7], Philip Hofmann[2] and Liv Hornekær[1]*
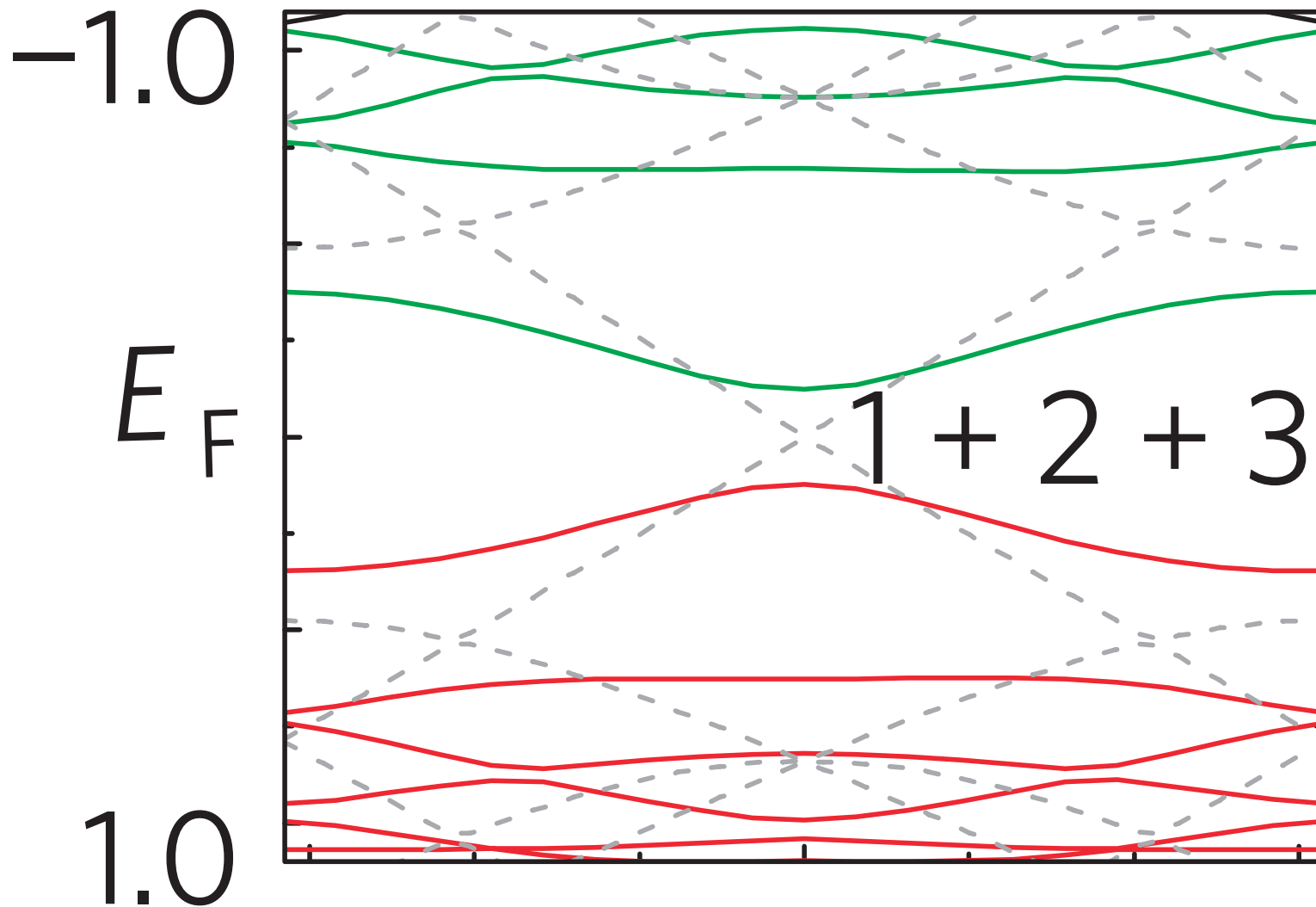
Core level photoemission (XPS or ESCA)

- Element specificity
- Sensitivity to chemical environment
  – the core level shift
- Photoelectron diffraction
- Examples

Surface chemical analysis.
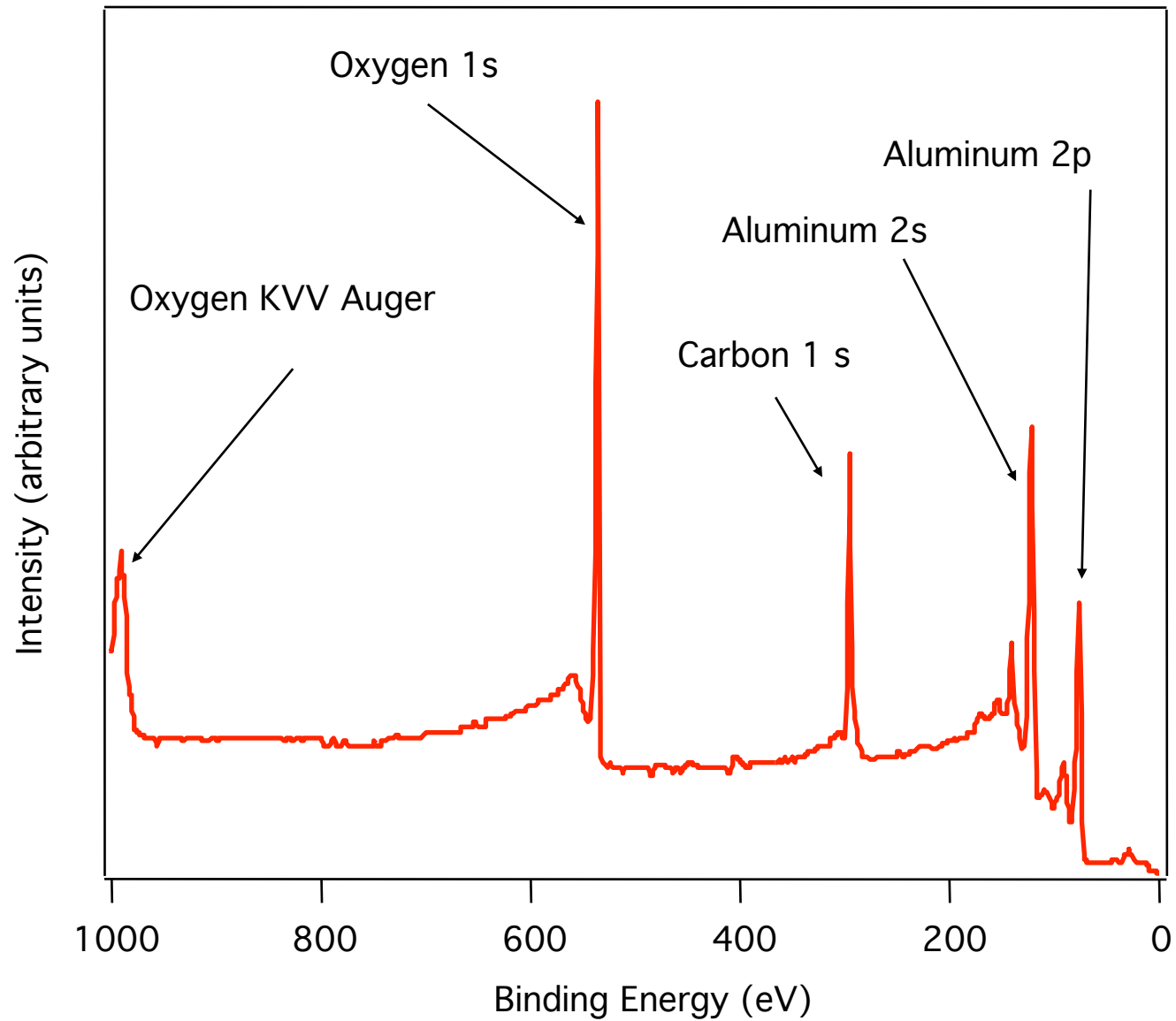
Electron mean free path

Each element has a specific set of accessible core levels

		K 1s	L-I 2s	L-II 2p1/2	L-III 2p3/2	M-I 3s	M-II 3p1/2	M-III 3p3/2	M-IV 3d3/2	M-V 3d5/2
1	H	13.6								
2	He	24.6*								
3	Li	54.7*								
4	Be	111.5*								
5	B	188*								
6	C	284.2*								
7	N	409.9*	37.3*							
8	O	543.1*	41.6*							
9	F	696.7*								
10	Ne	870.2*	48.5*	21.7*	21.6*					
11	Na	1070.8+	63.5+	30.4+	30.5*					
12	Mg	1303.0+	88.6*	49.6+	49.21					
13	Al	1559	117.8*	72.9*	72.5*					
14	Si	1839	149.7*b	99.8*	99.2*					
15	P	2145.5	189*	136*	135*					
16	S	2472	230.9	163.6*	162.5*					
17	Cl	2822	270*	202*	200*					
18	Ar	3205.9*	326.3*	250.6+	248.4*	29.3*	15.9*	15.7*		
19	K	3608.4*	378.6*	297.3*	294.6*	34.8*	18.3*	18.3*		
20	Ca	4038.5*	438.4+	349.7+	346.2+	44.3+	25.4+	25.4+		
21	Sc	4492	498.0*	403.6*	398.7*	51.1*	28.3*	28.3*		
22	Ti	4966	560.9+	460.2+	453.8+	58.7+	32.6+	32.6+		
23	V	5465	626.7+	519.8+	512.1+	66.3+	37.2+	37.2+		
24	Cr	5989	696.0+	583.8+	574.1+	74.1+	42.2+	42.2+		
25	Mn	6539	769.1+	649.9+	638.7+	82.3+	47.2+	47.2+		
26	Fe	7112	844.6+	719.9+	706.8+	91.3+	52.7+	52.7+		
27	Co	7709	925.1+	793.2+	778.1+	101.0+	58.9+	59.9+		
28	Ni	8333	1008.6+	870.0+	852.7+	110.8+	68.0+	66.2+		
29	Cu	8979	1096.7+	952.3+	932.7	122.5+	77.3+	75.1+		
30	Zn	9659	1196.2*	1044.9*	1021.8*	139.8*	91.4*	88.6*	10.2*	10.1*
31	Ga	10367	1299.0*b	1143.2+	1116.4+	159.51	103.5+	100.0+	18.7+	18.7+
32	Ge	11103	1414.6*b	1248.1*b	1217.0*b	180.1*	124.9*	120.8*	29.8*	29.2*
33	As	11867	1527.0*b	1359.1*b	1323.6*b	204.7*	146.2*	141.2*	41.7*	41.7*
34	Se	12658	1652.0*b	1474.3*b	1433.9*b	229.6*	166.5*	160.7*	55.5*	54.6*
35	Br	13474	1782*	1596*	1550*	257*	189*	182*	70*	69*
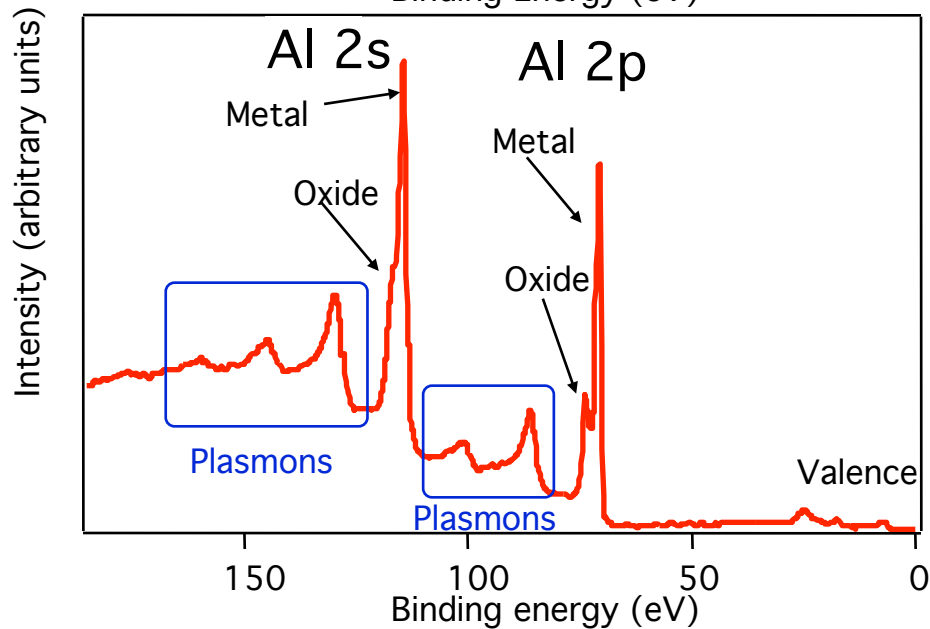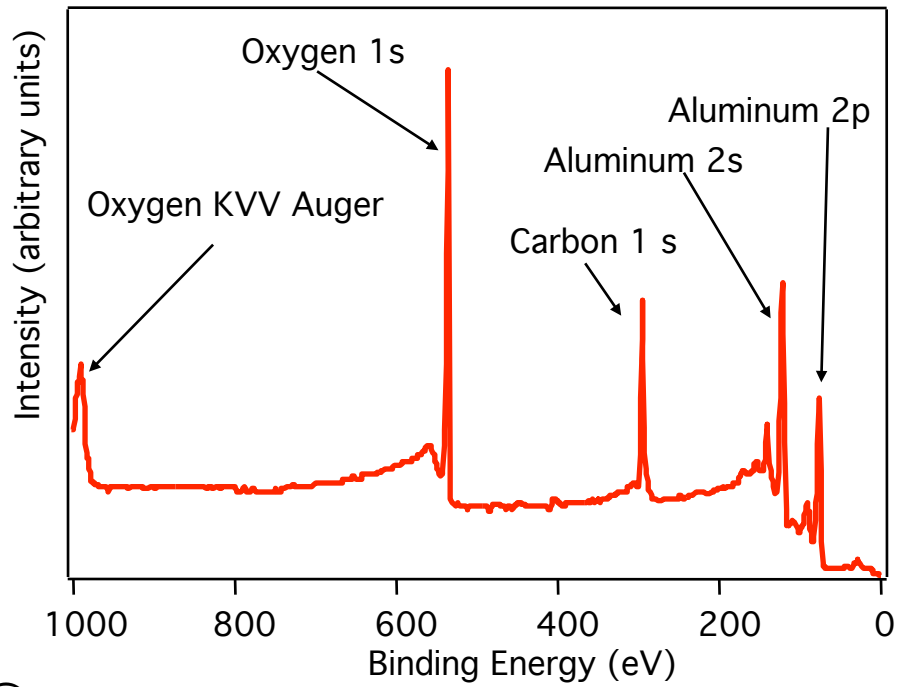
The photoemission spectrum of a "dirty" aluminum sample is dominated by the oxygen 1s level. The core levels of oxidized aluminum show a shift with respect to the metal.
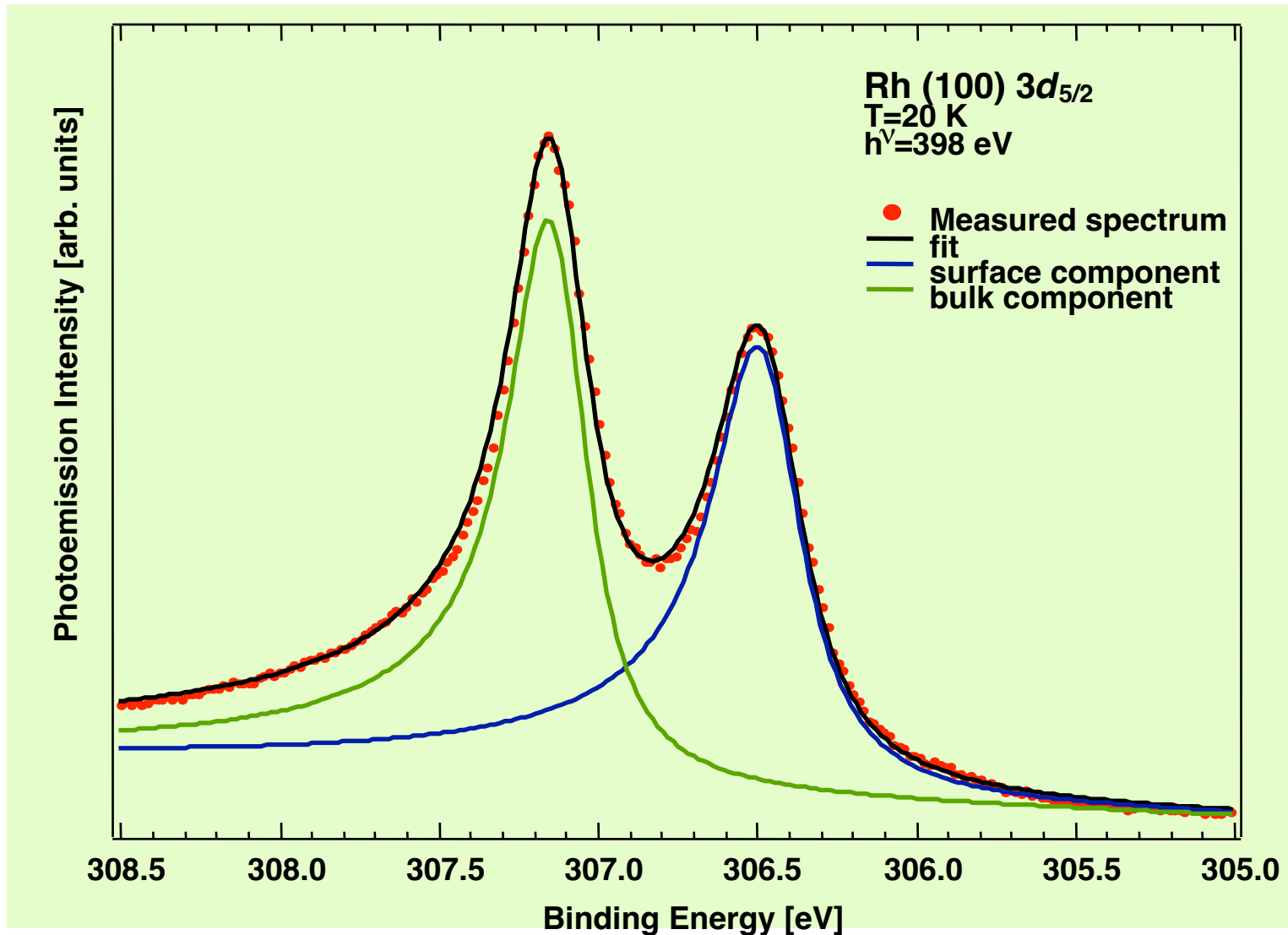
Energy of core level peaks.
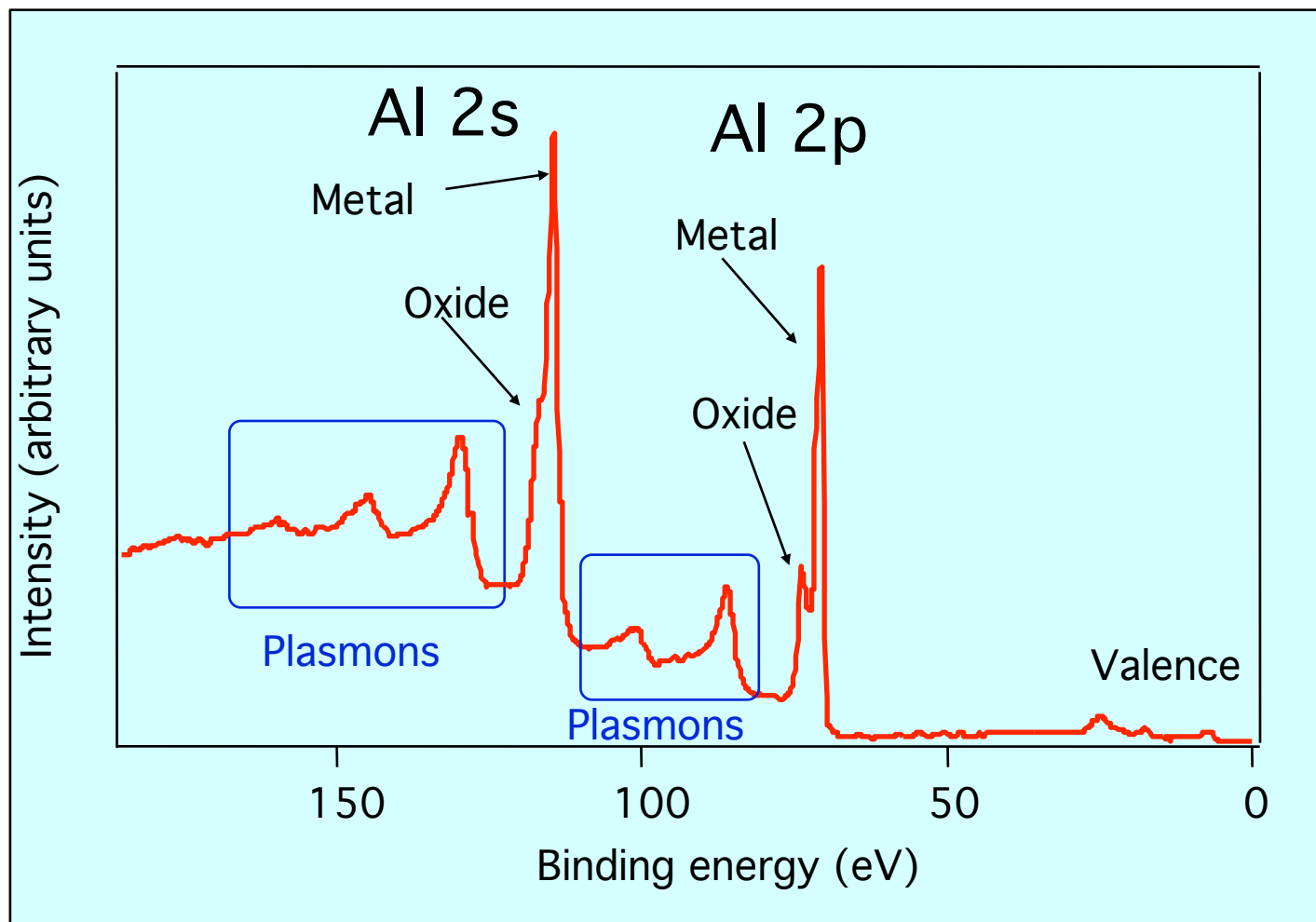
$$E_k = h\nu - E_b + E_a + E_r$$

Koopman (initial state) binding energy

Intraatomic relaxation

Extraatomic relaxation

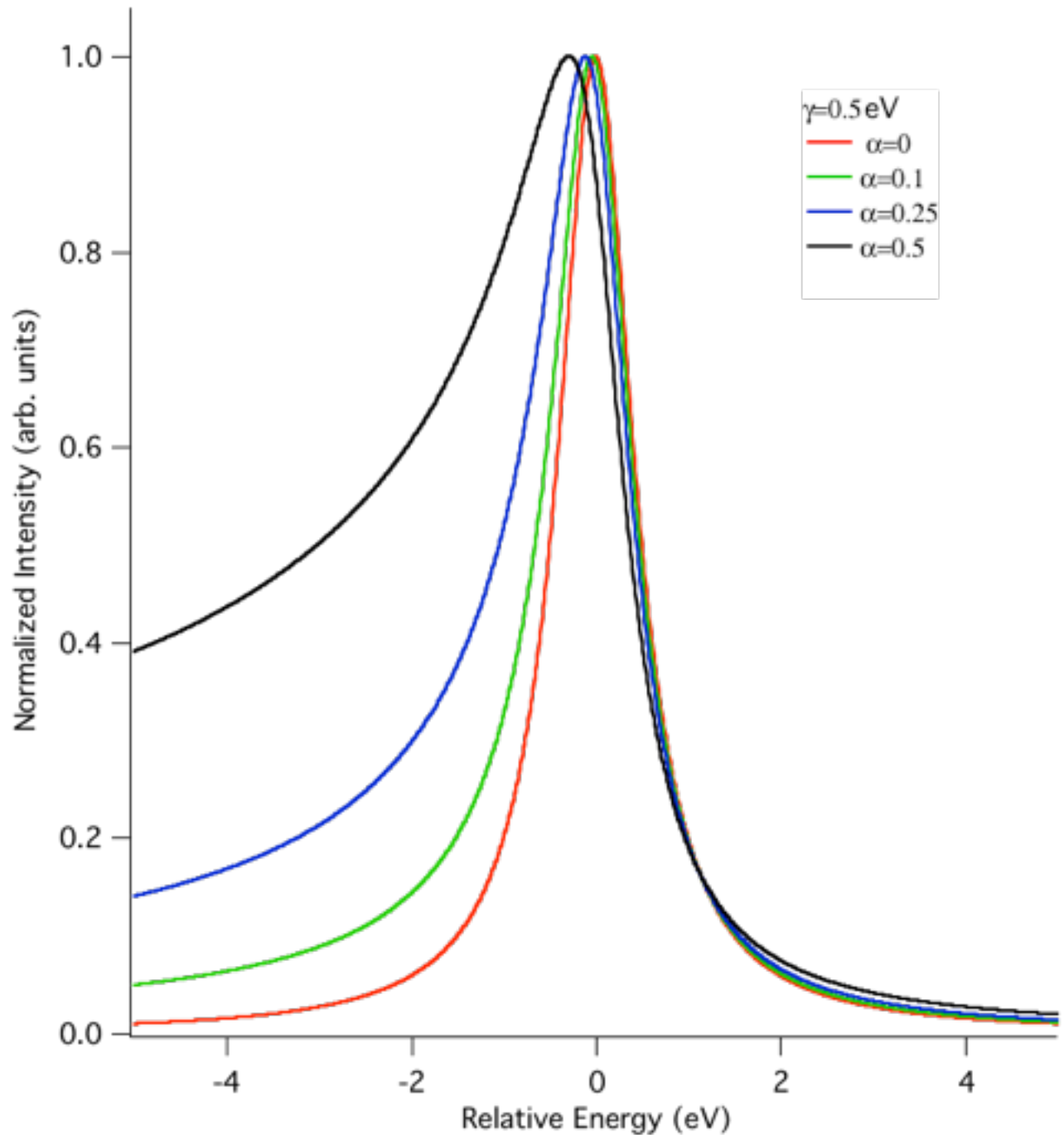# A particular case of core level shift: the *surface* core level shift

The Doniach-Šunjić lineshape
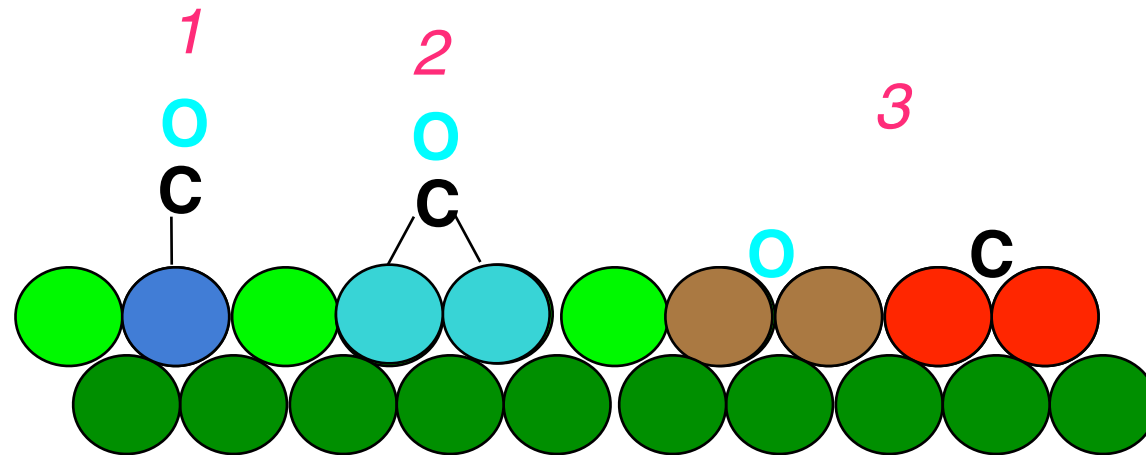
$$Y(E) = \frac{\Gamma(1-\alpha)}{(E^2 + \gamma^2)^{\frac{(1-\alpha)}{2}}} \cos\left[\frac{\pi\alpha}{2} + (1-\alpha)\arctan\left(\frac{E}{\gamma}\right)\right]$$

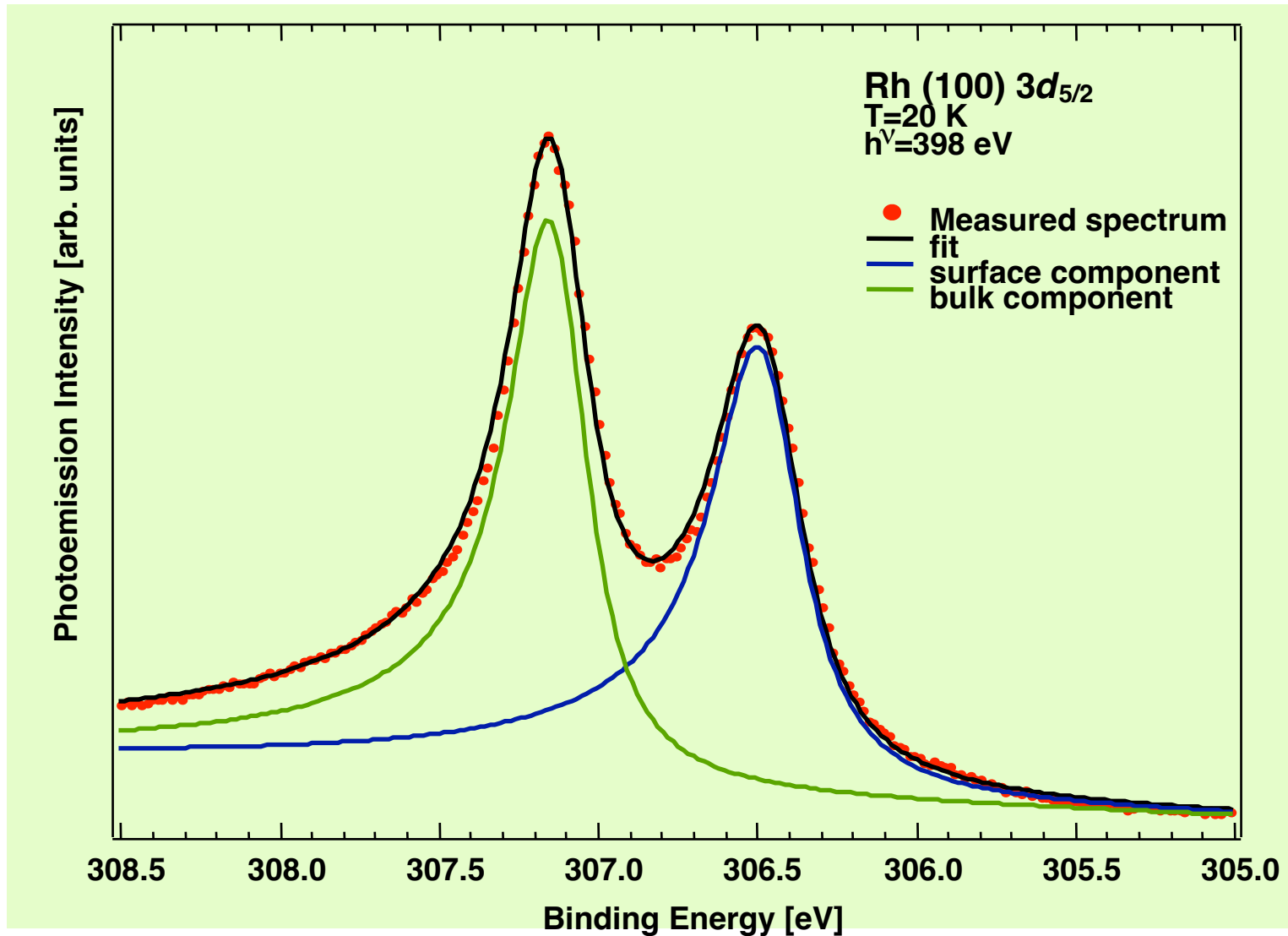**The Doniach-Šunjić lineshape**

J. Phys. C **3**, 285 (1970)

Reactions on surfaces

- Distinguish *1* (CO on top) from *2* (CO on a bridge site) and from *3* (dissociated CO)
- Follow changes from *1* to *2* and/or to *3*

The surface core level shift

Rh (100) $3d_{5/2}$
T=20 K
h^{γ}=398 eV

● Measured spectrum
— fit
— surface component
— bulk component

Identification of adsorbate bonding by changes in the substrate *Surface Core level Shift*

Evolution of the del SCLS of low Miller indices Rh surfaces as a function of O_2 dose
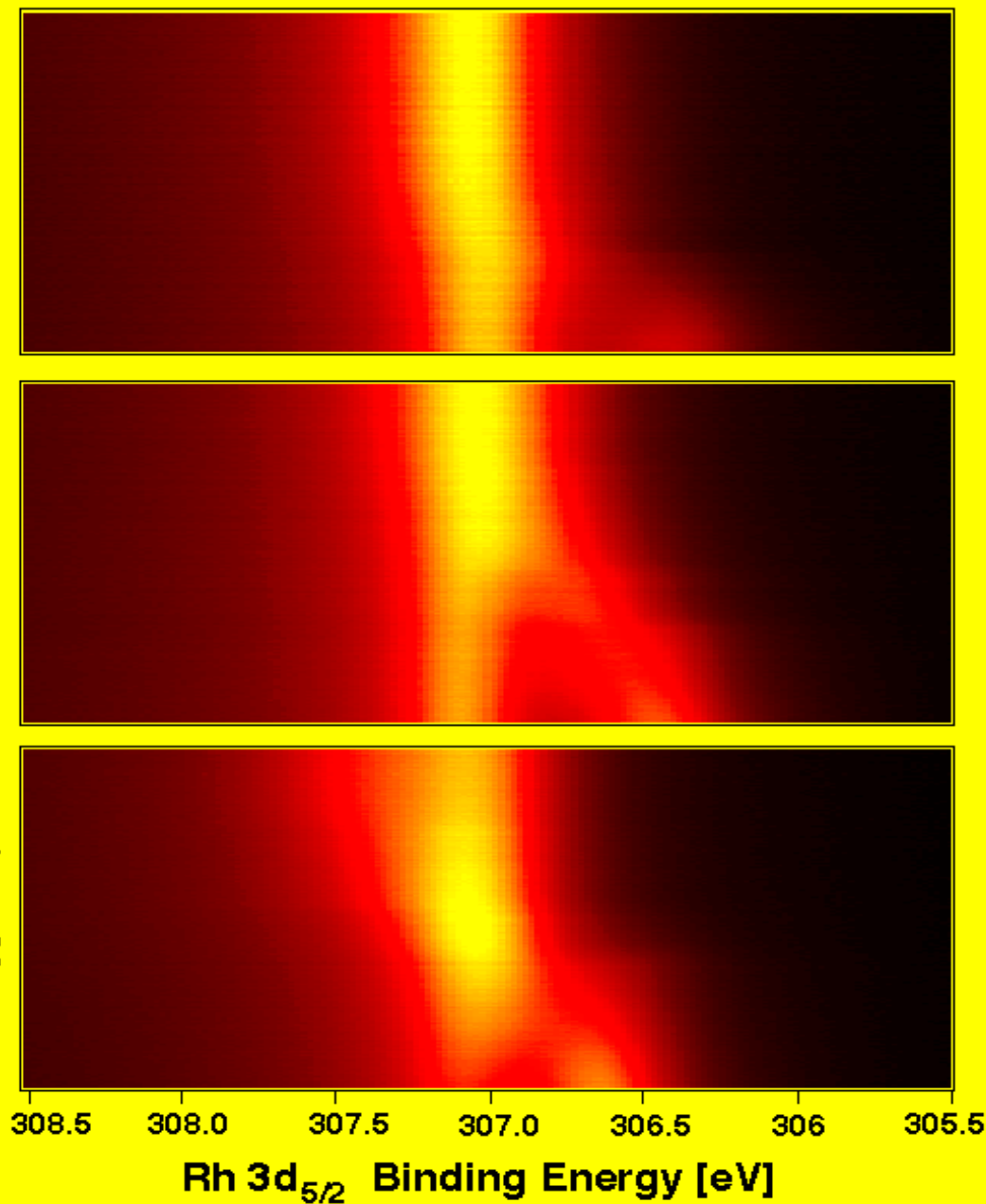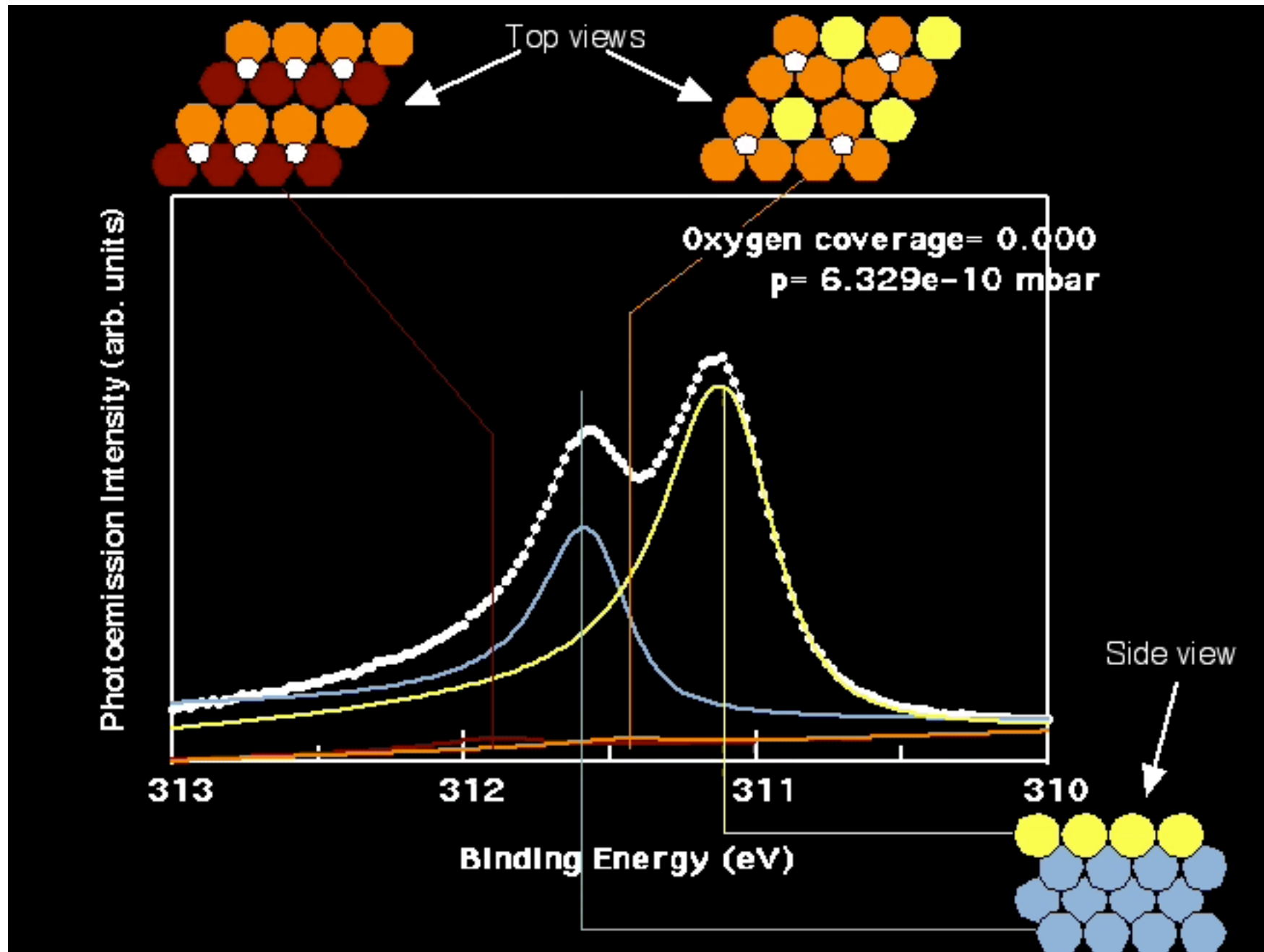
Surface Core Level Shift

Rh surfaces

Rh(110)

Rh(100)

Rh(111)

Oxygen exposure

Rh 3d$_{5/2}$ Binding Energy [eV]

Elettra Sincrotrone Trieste

ELSEVIER
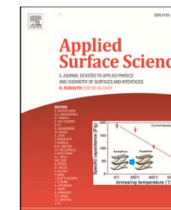
Full Length Article

Tracking interfacial changes of graphene/Ge(110) during in-vacuum annealing

L. Camilli [a,*], M. Galbiati [b], L. Di Gaspare [c], M. De Seta [c,*], I. Píš [d], F. Bondino [d], A. Caporale [a,c], V.-P. Veigang-Radulescu [e], V. Babenko [e], S. Hofmann [e], A. Sodo [c], R. Gunnella [f], L. Persichetti [a,c,*]

a Dipartimento di Fisica, Università di Roma "Tor Vergata", Via Della Ricerca Scientifica, 1-00133 Rome, Italy
b Department of Physics, Technical University of Denmark, 2800 Lyngby, Denmark
c Dipartimento di Scienze, Università Roma Tre, Viale G. Marconi, 446-00146 Rome, Italy
d IOM-CNR Laboratorio TASC, Trieste I-34149, Italy
e Department of Engineering, University of Cambridge, Cambridge CB3 0FA, United Kingdom
f School of Science and Technology Physics Division, University of Camerino, Italy

Combination of XPS, NEXAFS, Raman and STM showing the correlation of structural changes at the graphene/ Ge(110) interface. In particular it was found that defects are formed upon annealing and that they are due to Ge(110) surface reconstruction upon release of H_2

Elettra
Sincrotrone
Trieste
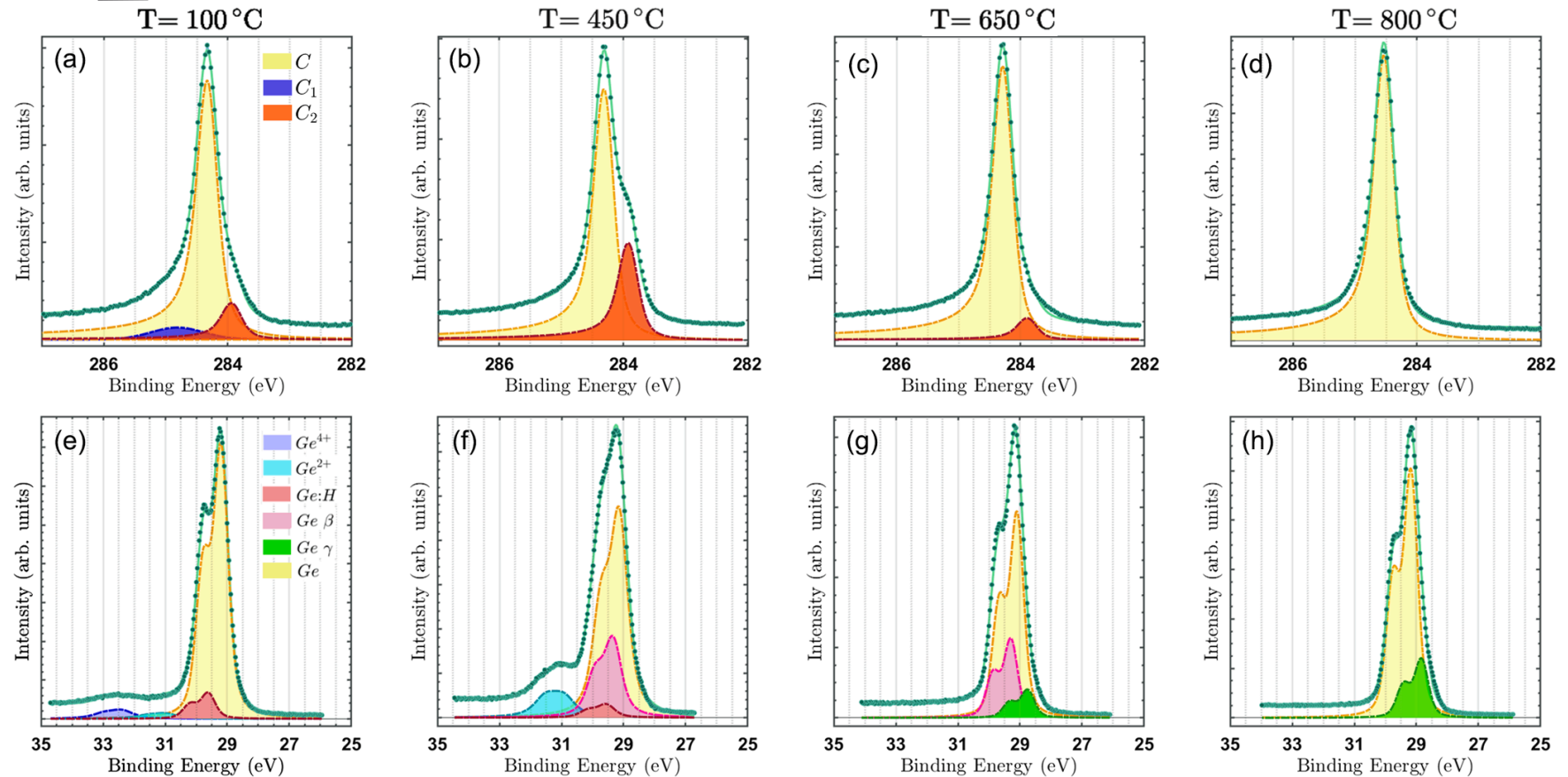
XPS spectra measured at room temperature with a photon energy of 400 eV at emission angle $60°$ as a function of the annealing temperature
C 1s (upper panels) and Ge 3d core levels (lower panels). Experimental datapoints are shown as dots; green continuous lines are the fits to
experimental data obtained with the components displayed as coloured shaded areas.

Photoemission microscopy:
spatial+chemical information

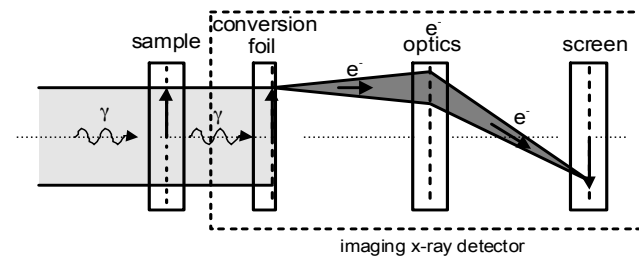# Why Microspectroscopy and Spectromicroscopy?

- elemental resolution:

  quantify composition of sample with lateral resolution

- chemical information:

  characterize chemical environment

- further information on:

  Magnetism
  different type of bonding (e.g. π, σ bonds)
  orbital alignment
  electronic structure

- combination with other microscopy techniques

Concepts to achieve spatial resolution

a)   μ-spot illumination
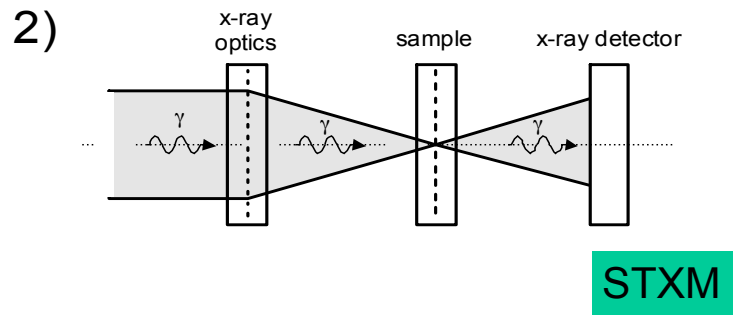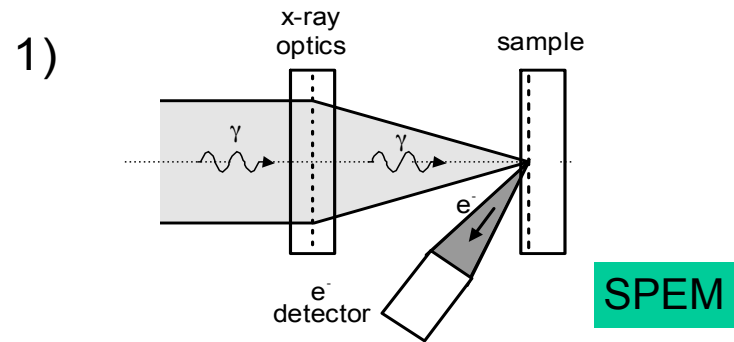
b)   homogeneous illumination + imaging system
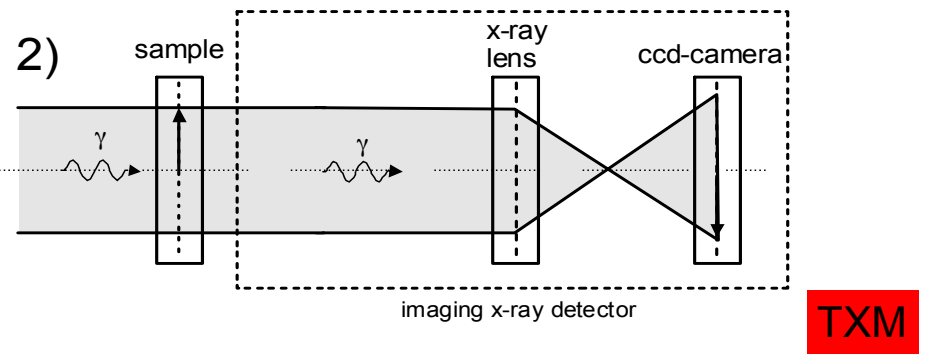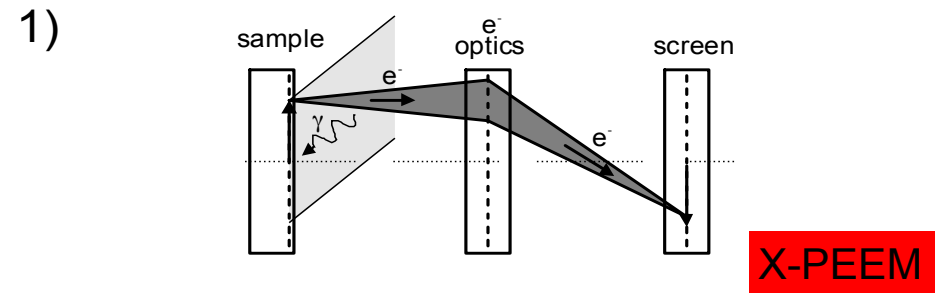
Scanning versus full field imaging transmission microscopy

Scanning

Sample (scanned)

Detector

OSA

ZP

Monochromatic light

Photo-emission detector

Full-field imaging

Sample (fixed)

Aperture

ZP

Monochromatic light

ZP

CCD
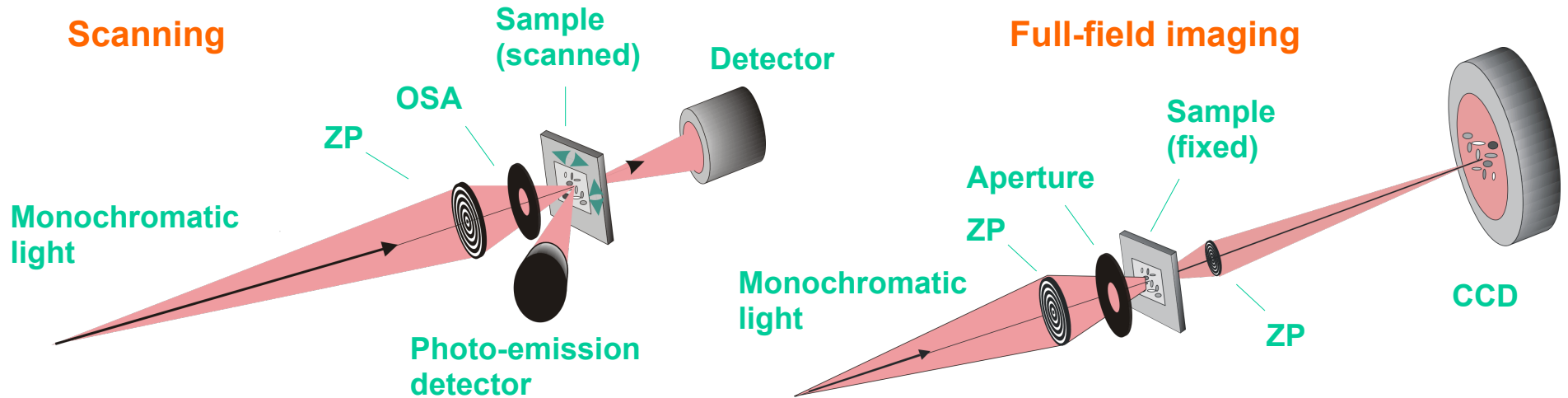
+ versatile detectors can be run simultaneously

+ low demands in the optics setup

+ SPEM possible

- long exposure times

- complex electronics

+ short exposure times

+ access to X-ray tomography in combination with spectro-microscopy

+ highest resolution due to static system

- complex optical alignment

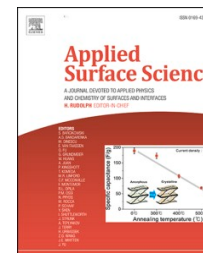# Scanning Photoemission Microscope

sample

y

x

focussing optics

monochromatized x-rays

emitted photoelectrons

hemispherical analyzer

channeltron
or channel-plate

computer

counts/sec

scanning control

Full Length Article

Understanding carbide evolution and surface chemistry during deep cryogenic treatment in high-alloyed ferrous alloy

Patricia Jovičević-Klug [a,b,*], Levi Tegg [c,d], Matic Jovičević-Klug [b], Rahul Parmar [e], Matteo Amati [e], Luca Gregoratti [e], László Almásy [f], Julie M. Cairney [c,d], Bojan Podgornik [a]

[a] Institute of Metals and Technology, Lepi pot 11, 1000 Ljubljana, Slovenia
[b] Max-Planck Institute for Iron Research, Max-Planck-Str. 1, 40237 Düsseldorf, Germany
[c] School of Aerospace, Mechanical and Mechatronic Engineering, The University of Sydney, Camperdown, NSW 2006, Australia
[d] Australian Centre for Microscopy and Microanalysis, The University of Sydney, Camperdown, NSW 2006, Australia
[e] Elettra - Sincrotone Trieste, S.C.p.A., SS14 – km 163.5 in Area Science Park, 34149 Trieste, Italy
[f] Institute for Energy Security and Environmental Safety, Centre for Energy Research, Konkoly-Thege Miklos út. 29-33, 1121 Budapest, Hungary

Elettra SAC September 2023

Giorgio Paolucci: Research Highlights at Elettra

ESCAmicroscopy (Applied Surface Science 610 (2023) 155497)

Elettra
Sincrotrone
Trieste

SPEM color-coded elemental maps of selected areas of (a) the CHT and (b) the DCT sample before (top) and after (bottom) tempering. The white circles indicate the exemplar positions probed for point-analysis with XPS. (c)-(e) XPS chemical spectra of the larger MC (top) and M6C (bottom) carbides before (dark color) and after (red color) tempering, for (c) C1s (d) V2p and (e) Fe3p, Cr3p, V3p and W4f. The data represents the chemical state of both carbide types for both CHT and DCT samples.

Elettra
Sincrotrone
Trieste
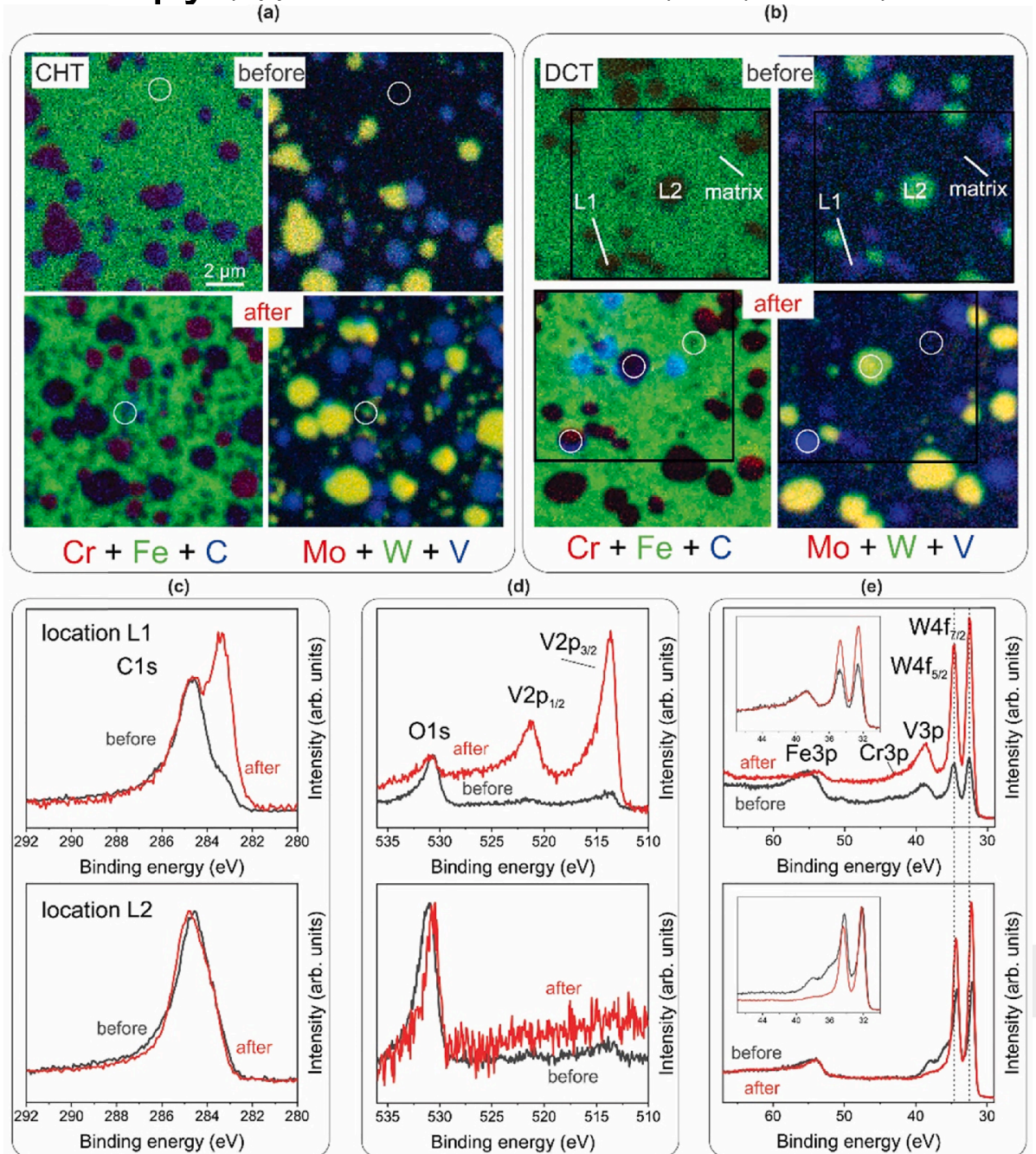
Domain Dependent Fermi Arcs Observed in a Striped Phase Dichalcogenide

Takashi Mizokawa,* Alexei Barinov, Viktor Kandyba, Alessio Giampietri, Ryoya Matsumoto, Yohei Okamoto, Kou Takubo, Koji Miyamoto, Taichi Okuda, Sunseng Pyon, Hiroyuki Ishii, Kazutaka Kudo, Minoru Nohara, and Naurang L. Saini*

SpectroMicroscopy

Solids undergoing symmetry breaking phase transitions commonly exhibit domains of low symmetry phases with various sizes and morphological shapes. Usually, the shapes of these domains are not directly related to the nature of symmetry breaking. Here, an interesting example of a layered dichalcogenide with a triangular lattice is shown, in which symmetry breaking of electronic charge/orbital is accompanied by formation of striped domains and exotic surface states with peculiar spin textures. Using angle-resolved photoemission spectromicroscopy, the mesoscopic striped domains in the layered $IrTe_2$ are observed across the first order phase transition at ≈ 280 K. Under further cooling down to 47 K, the striped domains evolve into trijunction domains with electronic anisotropy in three directions. Each domain harbors quasi 1D surface bands forming fragmented Fermi surfaces (Fermi arcs) with peculiar spin polarization revealed by spin-resolved photoemission spectroscopy. The Fermi arc corresponds to an edge state of the 2D bulk electronic bands truncated at the surface, indicating an interesting interplay between the symmetry breaking, surface electronic structure, and the spin state.

1. Introduction

Domain structures in bistable or polystable electronic systems exhibit various morphological shapes that have been one of the subjects of frontier research in fundamental science of advanced materials. Some fascinating examples include the topological domain textures in multiferroic $YMnO_3$[1,2] and antiferromagnetic Fe_2O_3[3] revealed by electron microscopy and photoemission electron microscopy. Other interesting examples are the antiferromagnetic $Nd_2Ir_2O_7$[4] and multiferroic $BiFeO_3$[5,6] showing domain wall properties discovered, respectively, by scanning microwave impedance microscopy and conductive atomic force microscopy. In systems showing Mott transitions and colossal magnetoresistance, metallic and insulating domains have also been disclosed by photoemission spectromicroscopy.[7,8] In general, mesoscopic domain structures of symmetry-broken electronic systems are not directly related to the nature of the broken symmetry itself but determined by the interfacial energy minimum.

T. Mizokawa, R. Matsumoto, Y. Okamoto
Department of Applied Physics
Waseda University
Shinjuku, Tokyo 169-8555, Japan
E-mail: mizokawa@waseda.jp
A. Barinov, V. Kandyba, A. Giampietri
Sincrotrone Trieste S.C.p.A.
Area Science Park, Basovizza, Trieste 34012, Italy
K. Takubo
Department of Chemistry
Tokyo Institute of Technology
Meguro, Tokyo 152-8551, Japan
K. Miyamoto, T. Okuda
Hiroshima Synchrotron Radiation Center
Hiroshima University
Hiroshima 739-0046, Japan

S. Pyon
Department of Applied Physics
The University of Tokyo
Bunkyo, Tokyo 113-8656, Japan
H. Ishii
Department of Physics
Okayama University
Okayama 700-8530, Japan
K. Kudo
Department of Physics
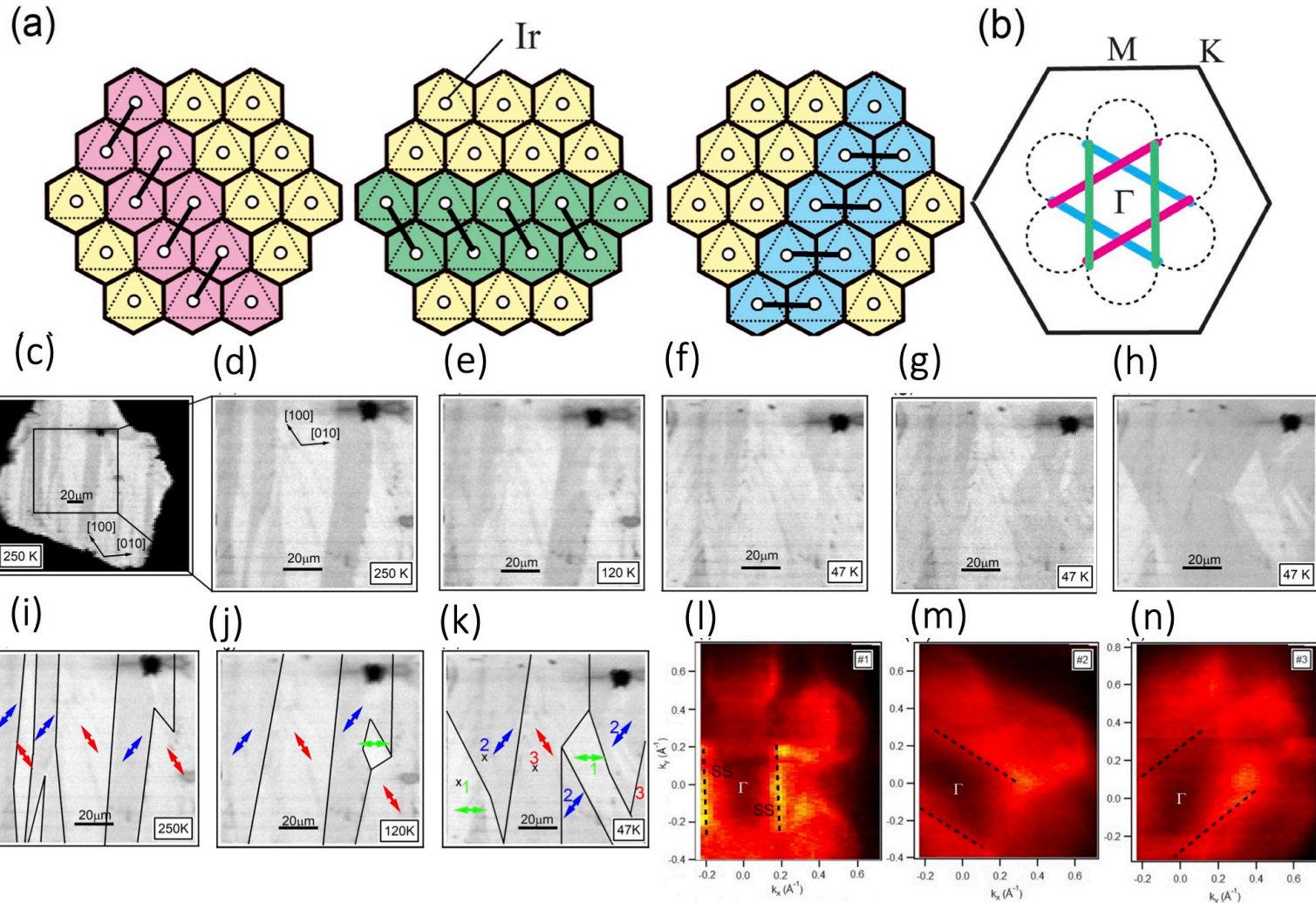Osaka University
Toyonaka, Osaka 560-0043, Japan
M. Nohara
Department of Quantum Matter
Hiroshima University
Hiroshima 739-8530, Japan
N. L. Saini
Department of Physics
Universitá di Roma "La Sapienza,"
Rome 00185, Italy
E-mail: naurang.saini@roma1.infn.it

CERTIFIED MANAGEMENT SYSTEM
CQY CERTIQUALITY
UNI EN ISO 9001:2015
UNI ISO 45001:2018

Elettra SAC September 2023

Giorgio Paolucci: Research Highlights at Elettra

SpectroMicroscopy

(a) Three directions of the striped charge ordering in the IrTe$_2$ layer. (b) Three directions of the Fermi arcs in the Brillouin zone corresponding to the three directions of the striped charge ordering. The dotted curves schematically show the bulk Fermi surfaces. (c) Photoemission intensity image of the wide area at 250 K. (d,e,f) Photoemission intensity image of the selected area at 250 K, 120 K, and 47 K. (g, h) Domain textures at 47 K visualized by different energy windows. All the images were taken at hv=27 eV with linear polarization (horizontal). (i, j, k) Domain textures at 250 K, 120 K, and 47 K. The solid lines indicate domain boundaries. The arrows indicate the directions of charge/orbital stripes. (l, m, n) Fermi surfaces of the three different domains at 47 K. The broken lines indicate Fermi arcs derived from the surface states.

The principle of photoelectron diffraction
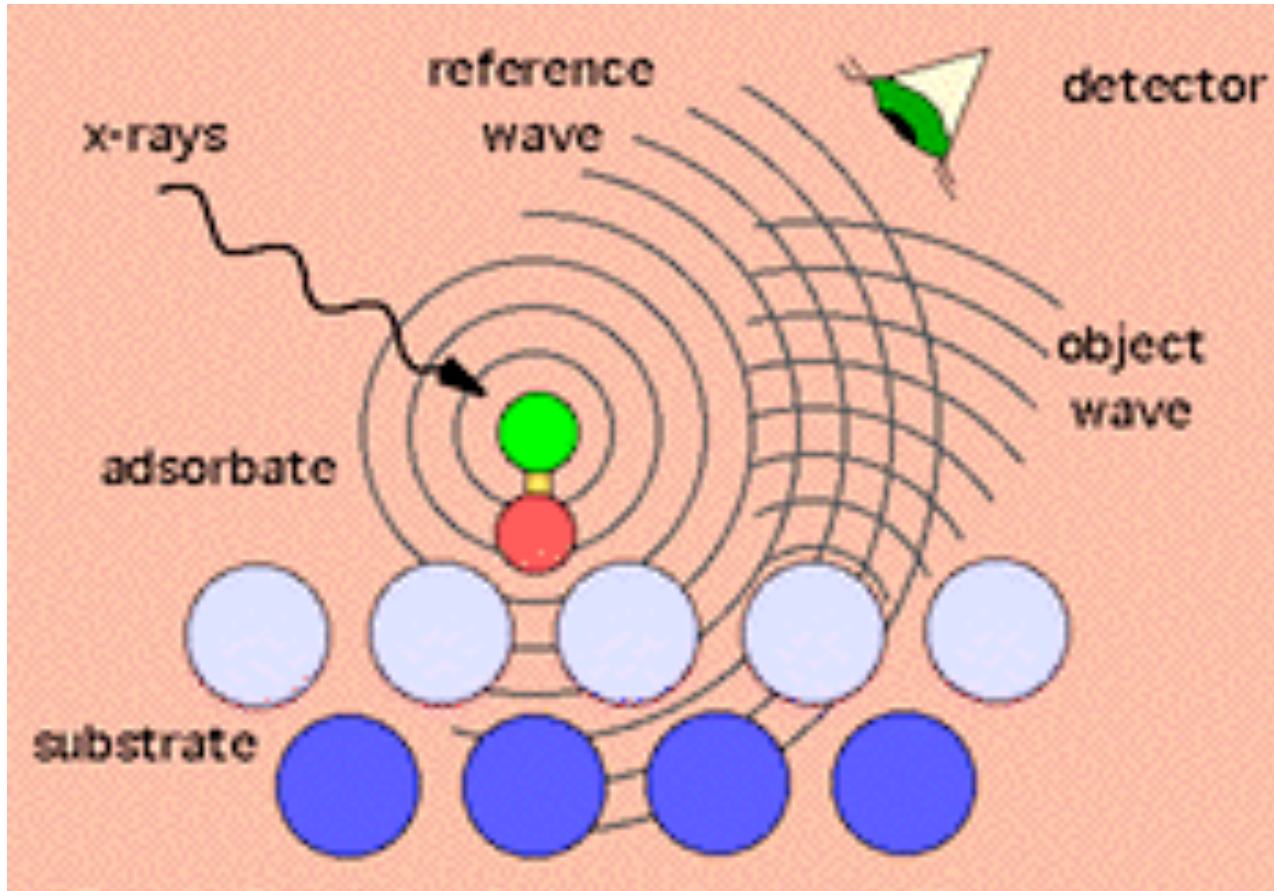
Modulations in the intensity of the photoemitted electron wave are measured. For a given arrangment of atoms, the intensity depends on the photon energy and on the emission angle

Internal wave source
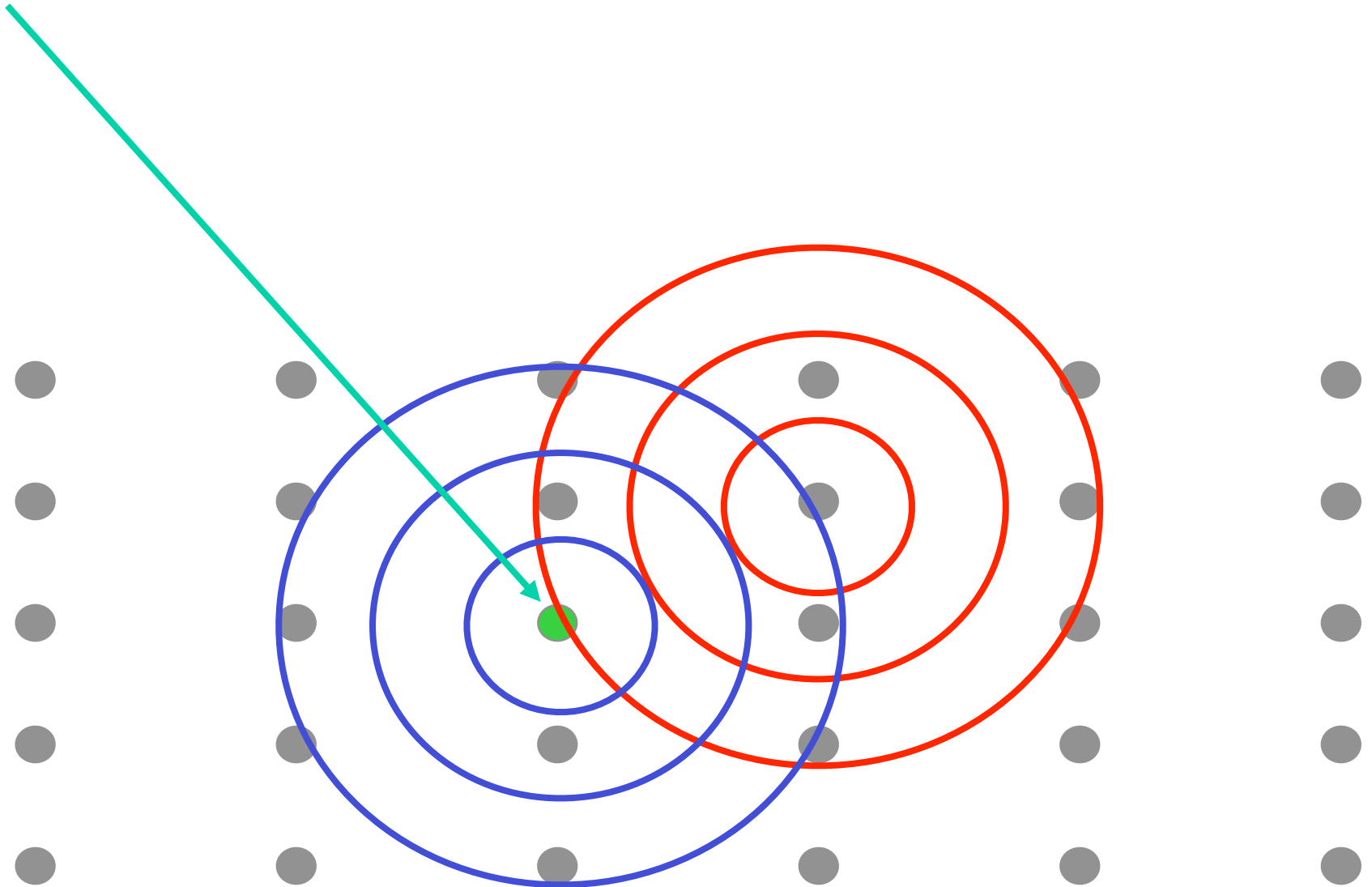
External plane wave source:
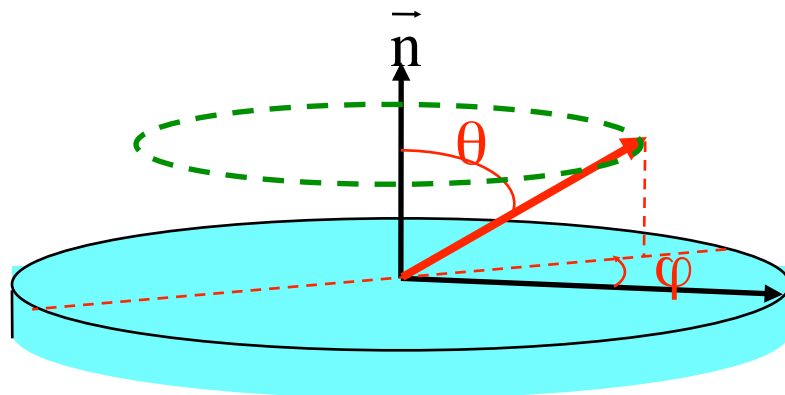**single crystal (long range order)**

Internal spherical wave source:

1) **Measure what happens at the absorber**
   (i.e. absorption)→ short range order

2) **Measure outside the sample**
   (i.e. photoemission) → short range
   order+same orientation at different sites

LP/ RCP/ LCP/ UL
radiation field
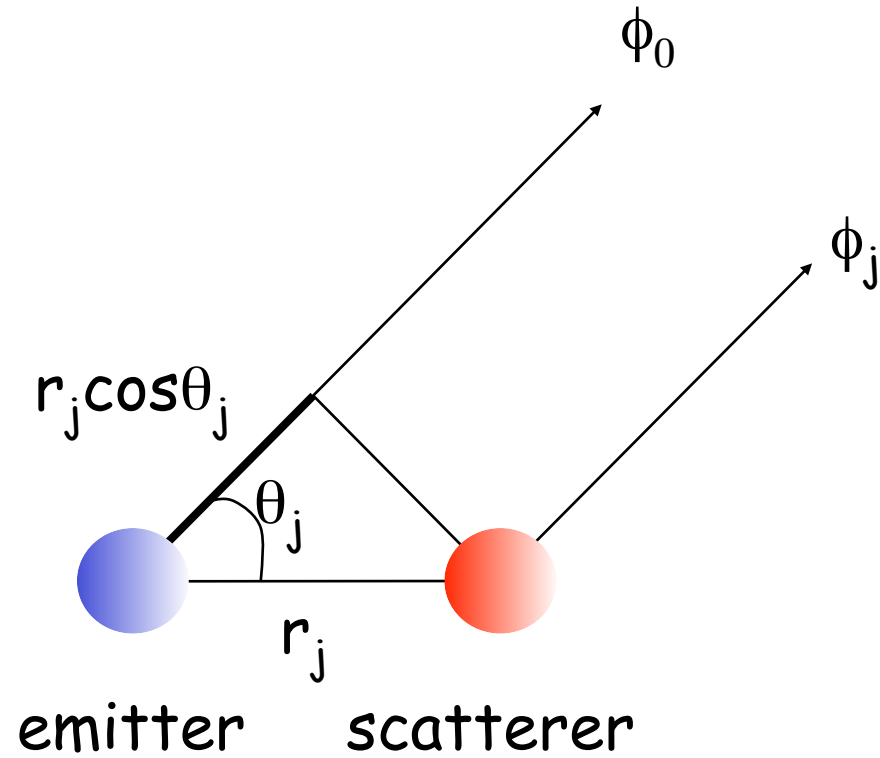
$\vec{\varepsilon}$

Polar scan

angle-resolved
Ω detector

ϕ_0

ϕ_j

E_k

ϕ_k

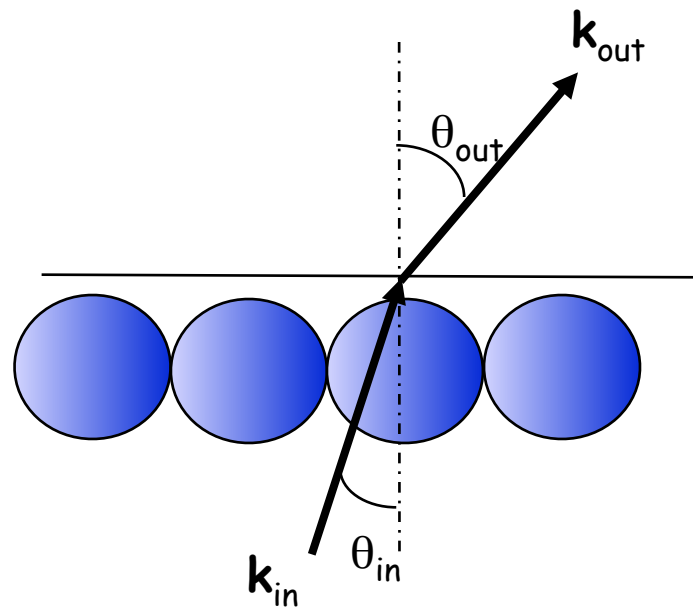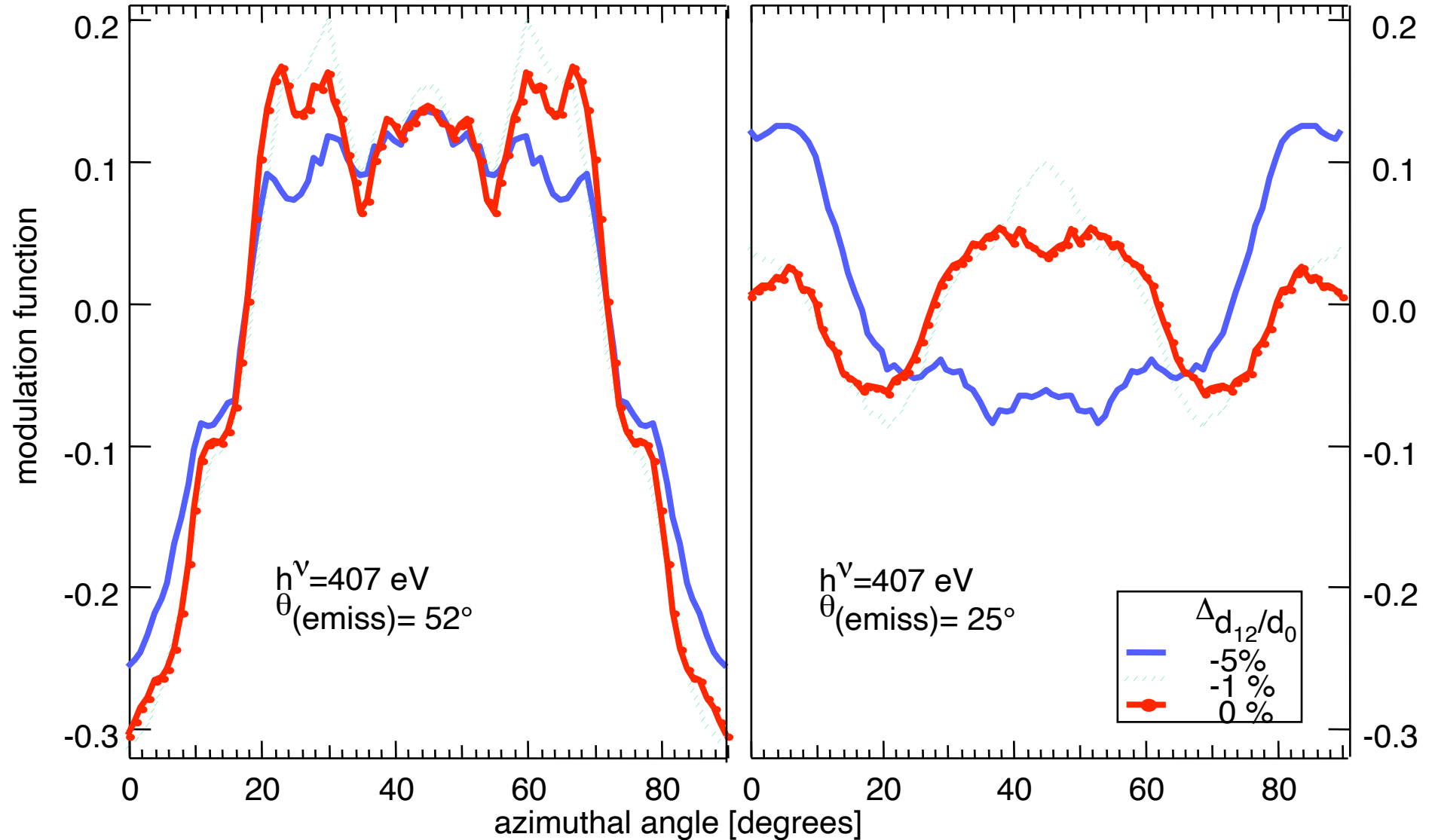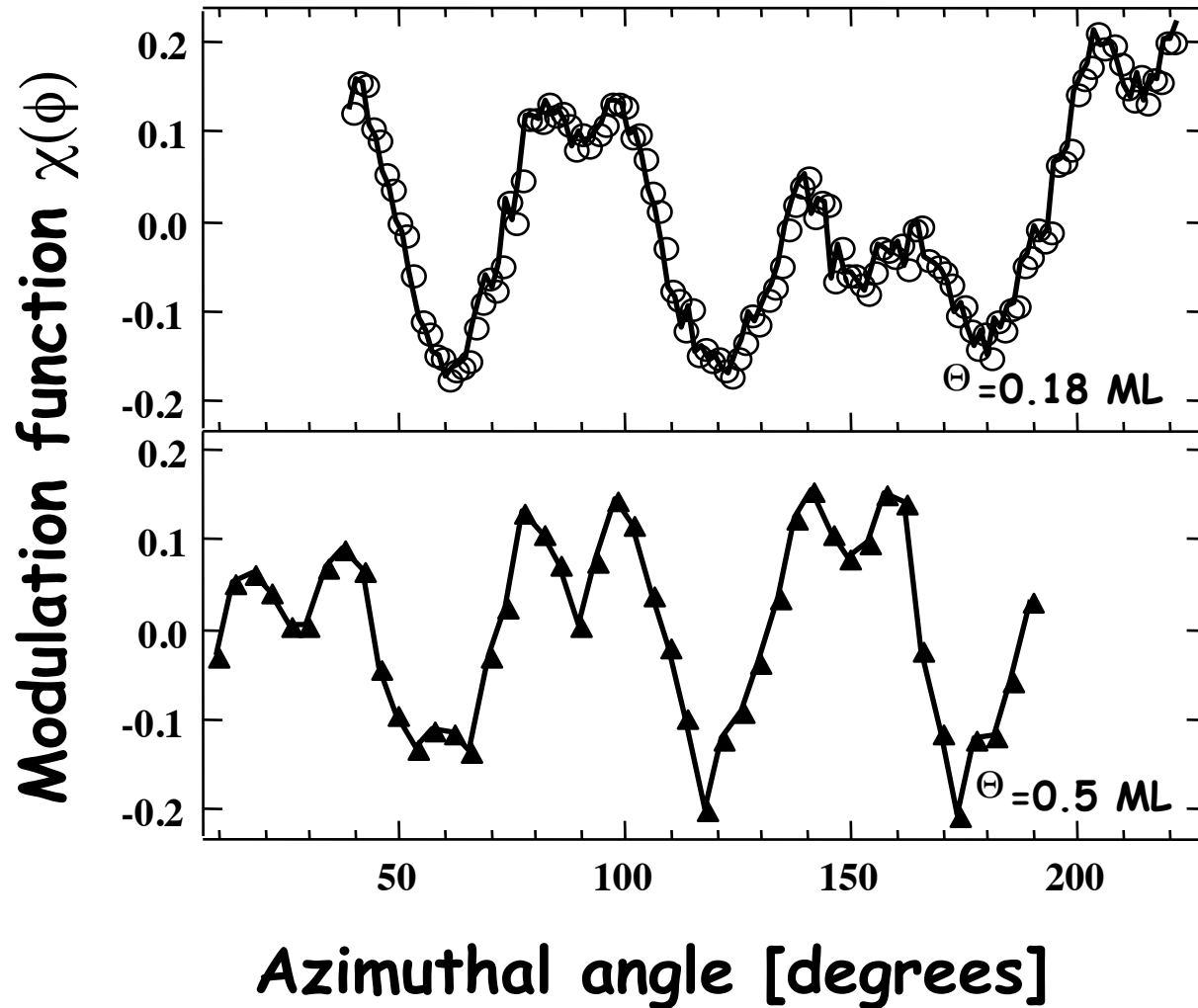Refraction effect
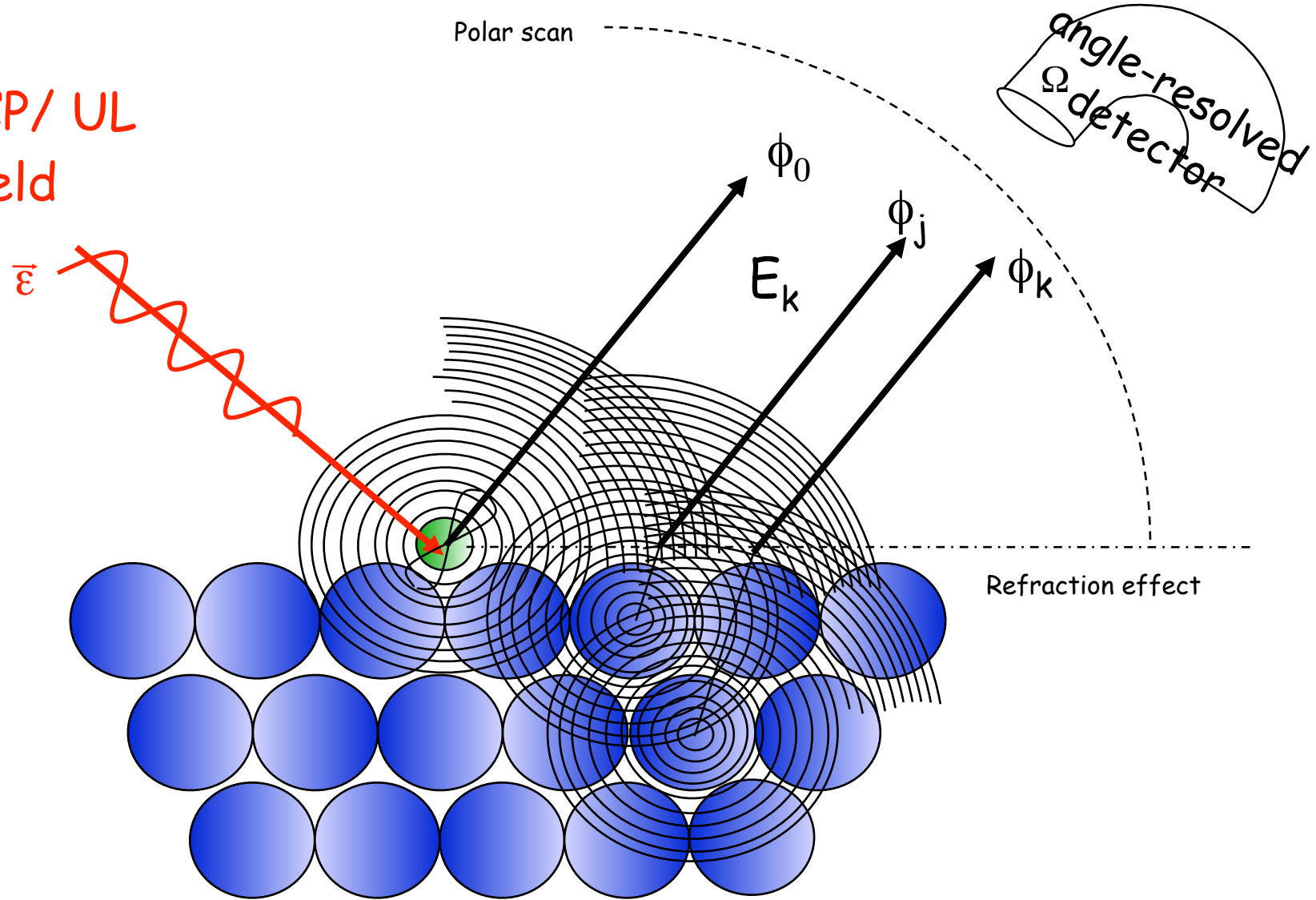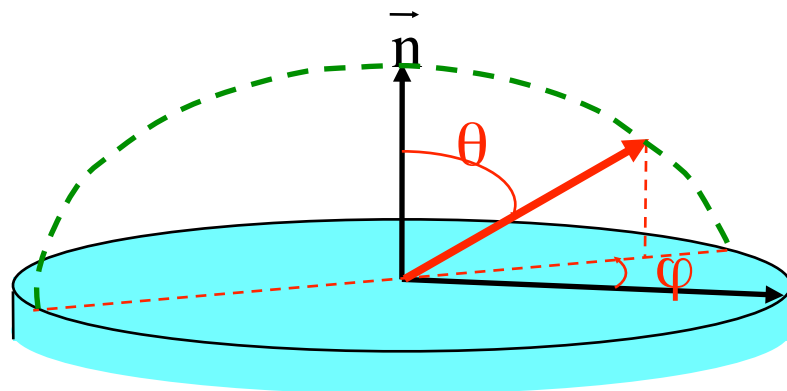
Polar scan

Azimuthal scan

The basic scattering event:

Refraction at the surface

Sensitivity to structural parameters in different measurement conditions: clean Rh(100)

modulation function

azimuthal angle [degrees]

$h^{\nu}=407$ eV
θ(emiss)= 52°

$h^{\nu}=407$ eV
θ(emiss)= 25°

Δ_{d_{12}/d_0}
-5%
-1 %
0 %

"Fingerprinting": CO/Pt(111)

SuperESCA

Elettra
Sincrotrone
Trieste

ACS **APPLIED** MATERIALS
&**INTERFACES**

Research Article

Probing the Atomic Arrangement of Subsurface Dopants in a Silicon Quantum Device Platform

Håkon I. Røst, Ezequiel Tosi, Frode S. Strand, Anna Cecilie Åsland, Paolo Lacovig, Silvano Lizzit, and Justin W. Wells*

Read Online
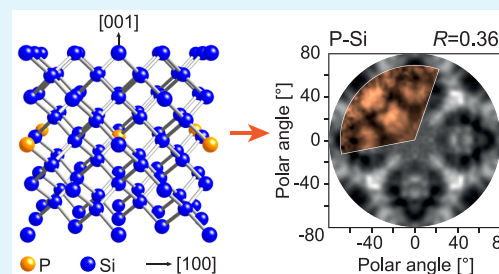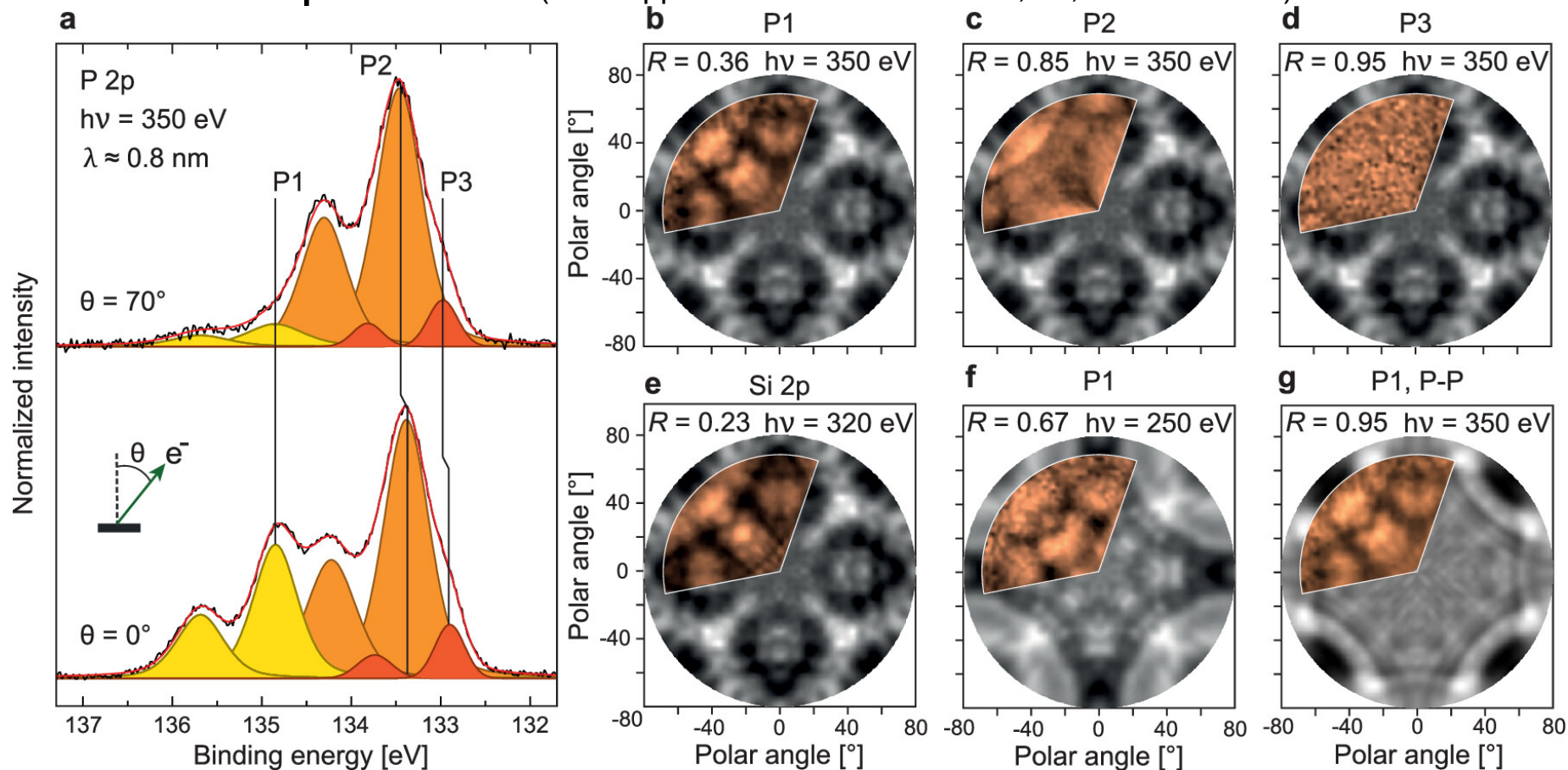
ACCESS | 📊 Metrics & More | 📰 Article Recommendations | 🆂🅸 Supporting Information
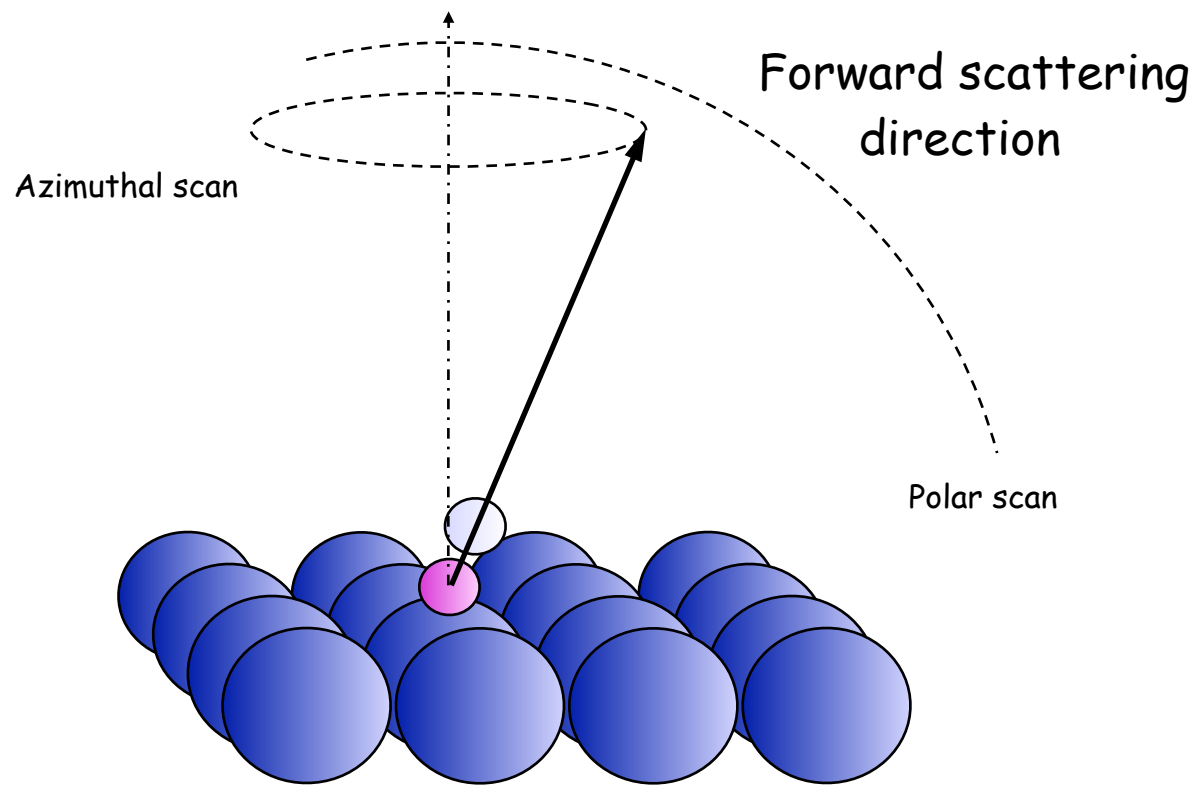
ABSTRACT: High-density structures of subsurface phosphorus dopants in silicon continue to garner interest as a silicon-based quantum computer platform; however, a much-needed confirmation of their dopant arrangement has been lacking. In this work, we take advantage of the chemical specificity of X-ray photoelectron diffraction to obtain the precise structural configuration of P dopants in subsurface Si:P δ-layers. The growth of δ-layer systems with different levels of doping is carefully studied and verified using X-ray photoelectron spectroscopy and low-energy electron diffraction. Subsequent diffraction measurements reveal that in all cases, the subsurface dopants primarily substitute with Si atoms from the host material. Furthermore, no signs of carrier-inhibiting P−P dimerization can be observed. Our observations not only settle a nearly decade-long debate about the dopant arrangement but also demonstrate how X-ray photoelectron diffraction is surprisingly well suited for studying subsurface dopant structure. This work thus provides valuable input for an updated understanding of the behavior of Si:P δ-layers and the modeling of their derived quantum devices.

KEYWORDS: *delta-layers, quantum electronic devices, quantum computing, photoemission, photoelectron diffraction*
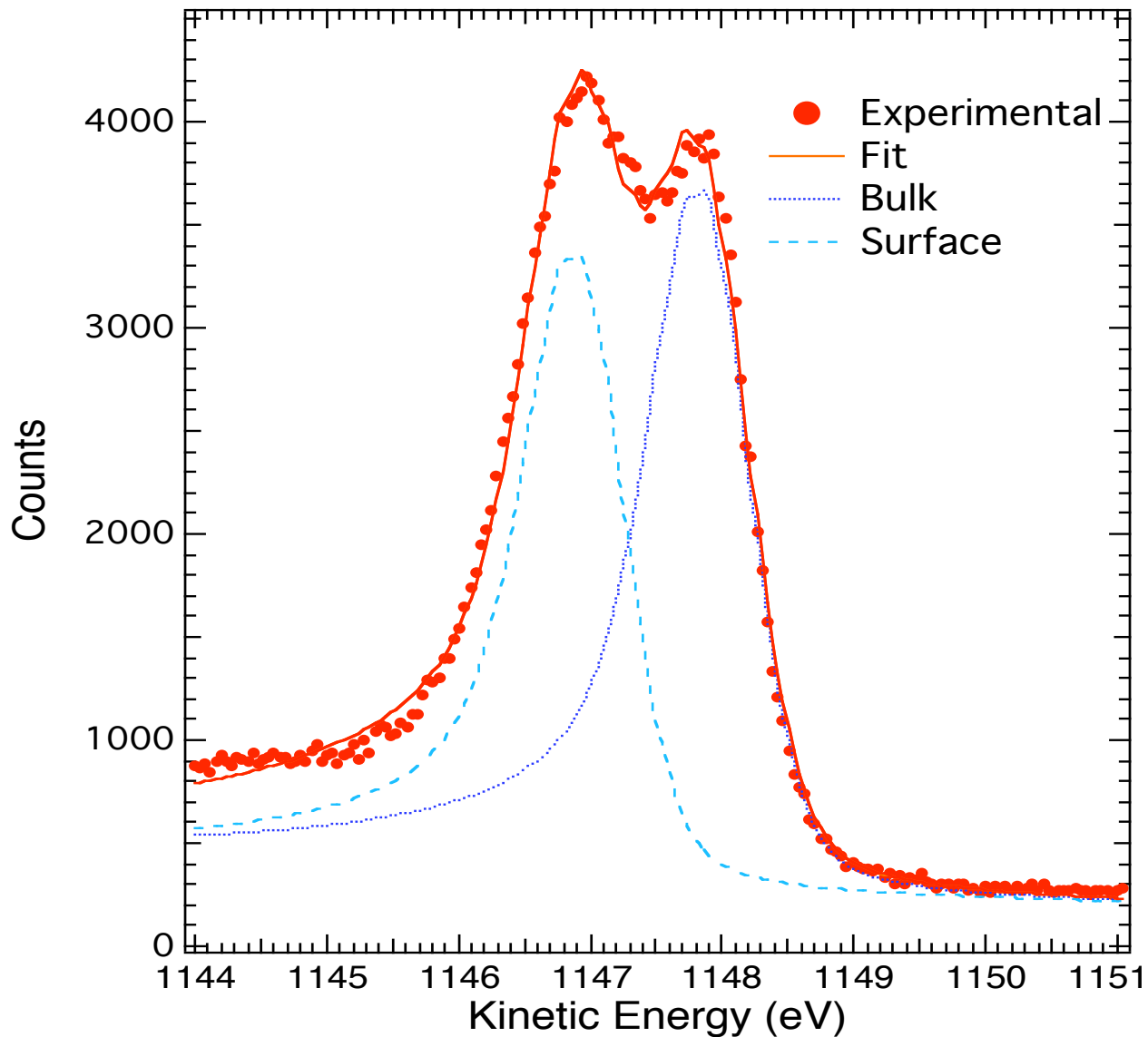
CERTIFIED
MANAGEMENT
SYSTEM

CQY
CERTIQUALITY

UNI EN ISO **9001:2015**
UNI ISO **45001:2018**

Elettra SAC September 2023

Giorgio Paolucci: Research Highlights at Elettra

Angle-dependent photoelectron spectroscopy from a "double-dosed", Si-encapsulated δ-layer. (a) XPS of the P 2p peak, measured with hν = 350 eV at normal (θ = 0°) and grazing (θ = 70°) emission and an integrated half-angle acceptance of ≤5°. P1 comes from P in the δ-layer, P2 and P3 from P near the Si surface. Both spectra have been scaled to the intensity of P2. (b–d) The measured (orange) and calculated (grey) XPD patterns for the peaks P1–P3 from the double-dosed δ-layer system shown in (a). (e) The measured and calculated XPD from the corresponding Si 2p core level. (f) The measured XPD from P1 at hν = 250 eV, compared with XPD simulations of P–Si bonding (i.e., substitutional doping) within the δ-layer. (g) The measured XPD of P1 at hν = 350 eV from (b), compared with XPD simulations of P–P bonding (i.e., dimerization) within the δ-layer.
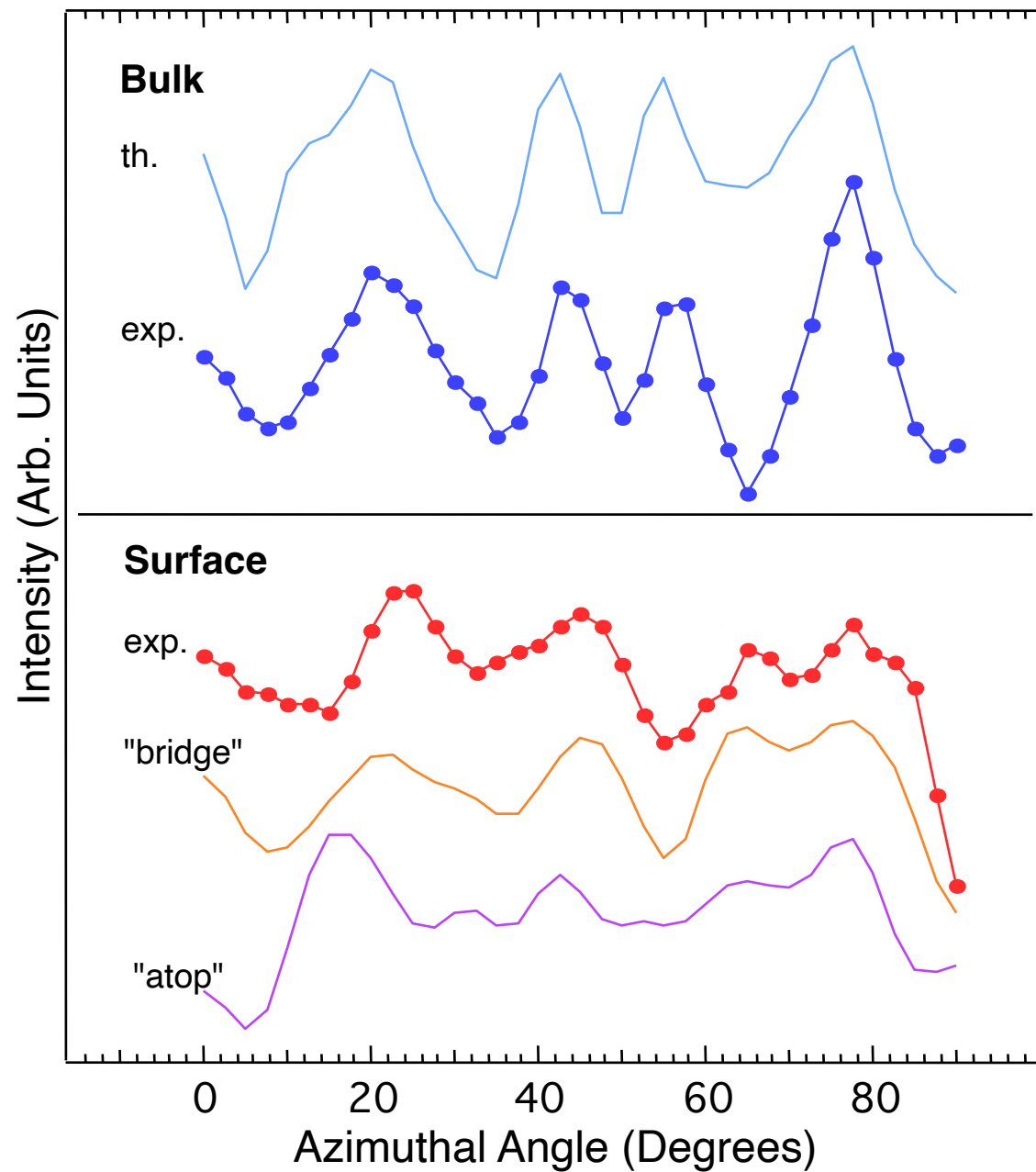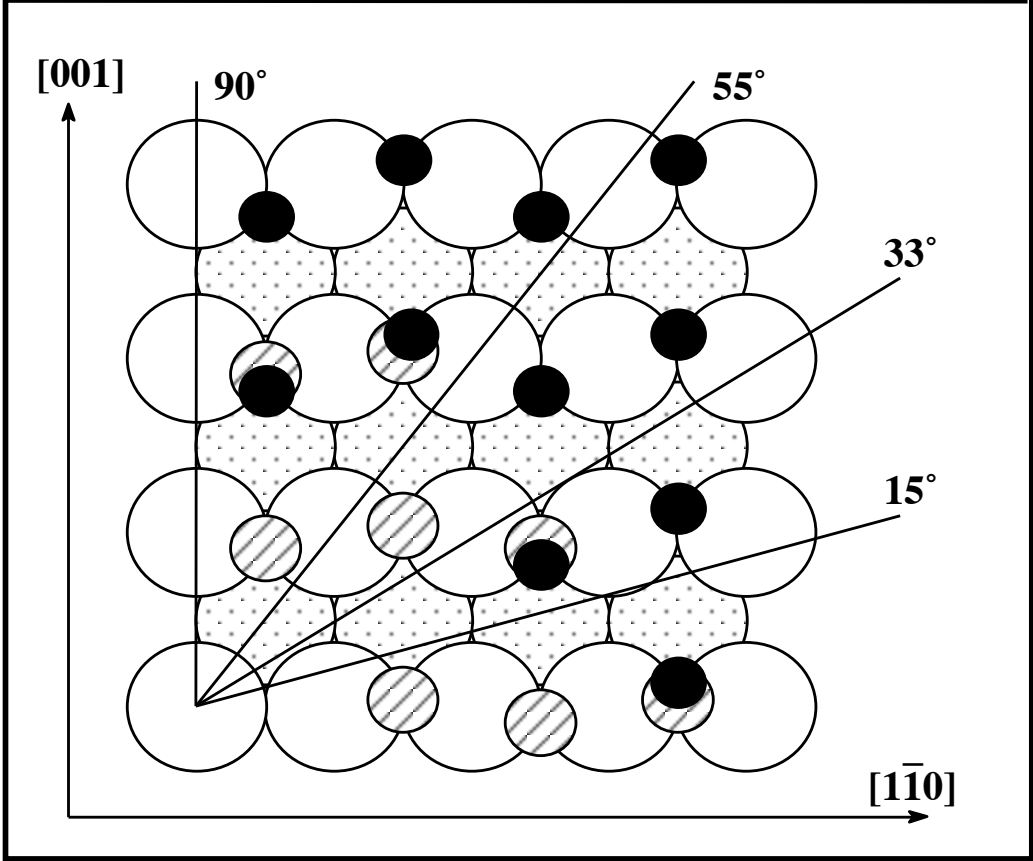
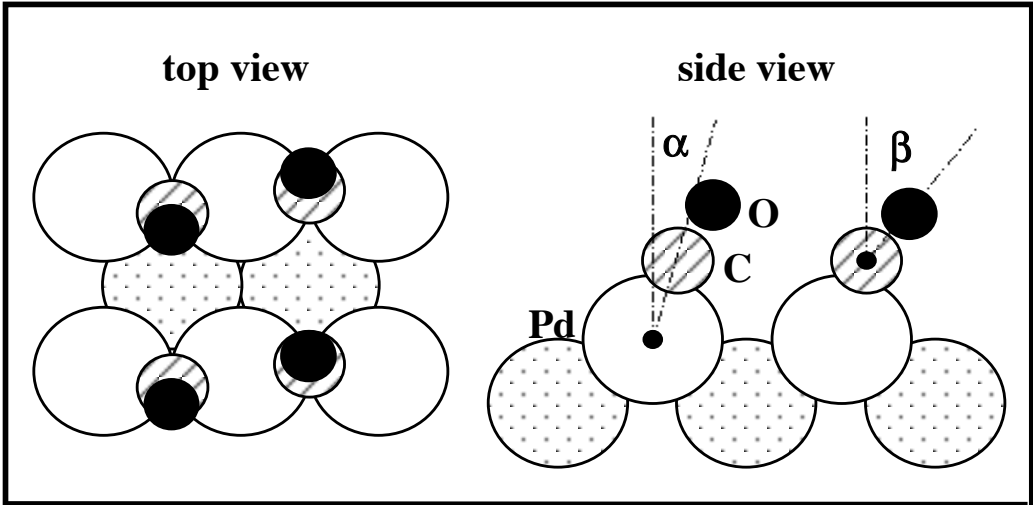CERTIFIED MANAGEMENT SYSTEM
CQY CERTIQUALITY
UNI EN ISO 9001:2015
UNI ISO 45001:2018

Forward scattering
direction

Azimuthal scan

Polar scan

Chemical shift
photoelectron diffraction

SCLS induced by CO on Pd(110)

top view

side view

α

β

O

C

Pd

[001]

90°

55°

33°

15°

[1Ī0]

- Basics
  - Photoelectric effect
  - Sources and electron analyzers
  - A bit of quantum mechanics
  - Photoemission cross section&Cooper minimum
- Valence band angle resolved photoemission
  - momentum conservation
  - band mapping
- Core level photoemission
  - Element specificity
  - Sensitivity to chemical environment
  - Photoelectron diffraction
  - Time evolution
  - Microscopy